# Carbon Capture Methods Utilizing Organosulfur Compounds

by

Joseph H. Rheinhardt

A Dissertation Presented in Partial Fulfillment
of the Requirements for the Degree
Doctor of Philosophy

Approved November 2017 by the
Graduate Supervisory Committee:

Daniel A. Buttry, Chair
C. Austen Angell
Andrew V. G. Chizmeshya

ARIZONA STATE UNIVERSITY

May 2018

ABSTRACT

The US National Academy of Sciences and The Royal Society have recently released a detailed report on the causes and effects of global climate change.[1] This report states that the Earth's climate is rapidly changing due to human activity. Specifically, the burning of fossil fuels to satisfy the energy demands of rising global population has resulted in unprecedented levels of greenhouse gasses in the atmosphere. These high levels of greenhouse gasses are serving to warm the surface of the planet resulting in extreme weather events. Thus, controlling the atmospheric $CO_2$ level is motivating a great deal of scientific research in the area of carbon capture and storage (CCS).

Despite the great strides being made in the areas of alternative energy and solar-energy conversion, consumption of fossil fuels for energy generation will likely continue into the foreseeable future. This is primarily motivated by economic factors inasmuch as fossil fuels are a proven resource base with robust harvesting and distribution infrastructure.[2] Presently, there are more than 8,000 stationary $CO_2$ emission sources with an annual output of 13,466 megatons of $CO_2$ per year.[2] In this context, development of systems that ameliorate the output of greenhouse gasses from stationary $CO_2$ sources, such as coal and natural gas burning power plants, is urgently needed.

In this document the utility of sulfur nucleophiles for CCS schemes is explored. The main thrust of the research has been utilizing electrogenerated sulfur nucleophiles to capture $CO_2$, which can be electrochemically recovered from the resulting thiocarbonates while concomitantly regenerating the masked capture agent. Further, a temperature swing $CO_2$ capture scheme that employs benzylthiolate as the $CO_2$ sorbent is proposed and methods of manipulating the release temperature and kinetics were investigated.

These reports represent the first application of organosulfur compounds toward CCS technologies and there are a number of newly reported compounds. The appendix deviates from the theme of the first four chapters to describe the functionalization of poly(2,6-dimethyl-1,4-phenylene oxide) with ferrocene moieties by the copper catalyzed azide-alkyne coupling reaction. This material is discussed within the context of anion recognition and sensing applications.

For my family

ACKNOWLEDGMENTS

First and foremost I must thank my advisory committee, especially my advisor Professor Daniel Buttry. Professors Buttry, Angell, and Chizmeshya are all exceptional scientists with quick minds and their advice and mentorship has been invaluable during my degree program. I entered Arizona State University mid-degree and Professor Buttry was kind enough to welcome me into his group. During my four years in his laboratory he has been a true role model and has taught me how to be a responsible and ethical scientist. Professor Buttry's breadth and depth of knowledge, his commitment to education, and his calm and patient demeanor make me very proud to be one of his students and I am thankful for our relationship. I must also thank my undergraduate advisor, Professor Dennis Peters of Indiana University, who passed his love of chemistry and of education on to me. I would not be here today if he had not welcomed me into his laboratory nearly a decade ago.

I would also like to thank the National Science Foundation Graduate Research Fellowship program. I am very honored and grateful to have received this award, which has provided funding throughout my degree.

Lastly, I must also thank my family. First, my mother-in-law Karen Mann, who I love very much, who has unreservedly welcomed me into her family, and without whose support this degree would not have been possible. My father Jeff and stepmother Brenda whose love and support have buoyed me during the more difficult moments. My father seems to always know the perfect piece of advice to give at the exact right moment. My brother- and sister-in-law, Guy Ortolano and Jenny Mann, both of who are extraordinarily gifted scholars, whose kindness and generosity are beyond reproach, and

whose friendship I value a great deal. My father-in-law John Mann and his wife Tama Baldwin whose encouragement and interest in my work has kept me motivated to finish. My daughter, Anna Faye, who has brought me incredible joy, and who melts away the stress of the workday with a simple “daddy!” and a hug. Finally, my wife Annika Mann, an exceptional scholar, a loving partner, and a generous person who has a seemingly inexhaustible reservoir of patience and grace. She is the person who I admire most and who I try to emulate, but always seem to come up short.

Thank you, all.

TABLE OF CONTENTS

Page

LIST OF TABLES

Table Page

LIST OF FIGURES

Figure Page



---

Figure Page

Figure Page



---

Figure Page

LIST OF SCHEMES



---

CHAPTER 1

**Assessing the Origins and Effects of Atmospheric $CO_2$ on Mean Global Surface Temperature.**

As described by Arrhenius in 1896, stable atmospheric carbon dioxide levels are essential for maintaining the Earth's energy balance.[3] In an effort to understand the environmental conditions that triggered the last ice age, Arrhenius conducted an exacting numerical calculation to quantitatively assess the role that heat-absorbing gasses in the atmosphere have on the mean global surface temperature. Based upon his calculations, Arrhenius proposed that halving the atmospheric $CO_2$ concentration would result in a 4–5 $^{o}$C decrease in the average surface temperature across Europe. In an effort to explore whether such large charges in atmospheric $CO_2$ concentration were possible, Arrhenius partnered with Avrid Högbom, who had previously formulated estimates of how geochemical processes such as volcano eruptions and $CO_2$ uptake by the oceans affected atmospheric $CO_2$ concentration, and by extension the Earth's climate.[4] Högbom and Arrhenius found that doubling the atmospheric $CO_2$ would likely result in a 5–6 $^{o}$C increase in mean global surface temperature.[5] Rather presciently, Arrhenius and Högbom addressed the role that human activity, specifically the burning of coal, could have on the mean global surface temperature. They correctly concluded that anthropogenic $CO_2$ emissions could indeed affect the climate; however, they drastically underestimated the amount of $CO_2$ that humans were capable of producing.

Beginning in the early 1980's the Goddard Institute for Space Studies (GISS) began producing data that showed the mean global surface temperature is rising and that the increase will continue into the 21$^{st}$ century.[6] The most recent GISS data shows that

there has been a nearly 1 $^{o}$C increase in global surface temperature since 1951.[7] Furthermore, The US National Academy of Sciences, The Royal Society, and the Intergovernmental Panel on Climate Change have all recently released detailed reports on the causes and effects of global climate change.[8] Succinctly put, these reports confirm the work of Arrhenius and Högbom as to the causes of climate change—the Earth's climate is rapidly changing due to increased atmospheric $CO_2$ concentration. By examining both amount of atmospheric $CO_2$ and the isotopic ratio of atmospheric carbon at observation posts in Alaska, California, Hawaii, Christmas Island, Samoa, and the South Pole[9] Charles Keeling et al. have determined not only that the increase in atmospheric $CO_2$ concentration is due to human activity, but also that there is a strong correlation between the year-to-year increase in atmospheric $CO_2$ and the amount of fossil fuels burned during the preceding year(s).[10] The human contribution to the rising atmospheric $CO_2$ concentration is summarized by the ubiquitous Keeling curve, which plots atmospheric $CO_2$ concentration by year in parts per million (ppm). At the inception of Keeling's experiment in the late 1950's, the mean atmospheric $CO_2$ concentration was 315 ppm; it has risen to 407 ppm as of July 2017. Lastly, in 2010 a review of papers published by 1,300 climate scientist showed that 97% of them accept the anthropogenic origin of rising global surface temperatures as fact.[11] In other words, there is an abundance of scientific data that definitively show anthropogenic $CO_2$ in the atmosphere is most directly a result of the burning of fossil fuels to satisfy the energy demands of rising global population. Furthermore, there is broad consensus that this increase in atmospheric $CO_2$ is serving to warm the surface of the planet resulting in extreme weather events, droughts, and melting of Artic sea ice.

In 2011 an estimated 34 billion tons of waste $CO_2$ were generated worldwide, with the top five emitters being China (29%), the United States (16%), the European Union (11%), India (6%), and the Russian Federation (5%).[12] It is important to note that although China accounts for nearly one third of the total global $CO_2$ emissions, US per capita emissions are more than double that of China at nearly 17 tons $CO_2$ per US citizen (compared to 7.2 tons $CO_2$ per Chinese citizen). Presently, there are more than 8,000 stationary $CO_2$ emission sources with an annual output of 13,466 megatons of $CO_2$ per year.[13] The main sources of $CO_2$ pollution are from fossil fuel combustion, flaring of waste gas during oil production, and cement production, with coal-fired power plants being the largest stationary point-source $CO_2$ emitters.[14] Domestically, $CO_2$ emissions for both electricity and non-electricity energy generation from fossil fuel consumption accounted for 5.63 Gigatons of anthropogenic $CO_2$.[15] If catastrophic climate change is to be avoided, new technologies that mitigate $CO_2$ emissions from energy-generating facilities and that capture $CO_2$ directly from air are urgently needed.

**Strategies for Reducing $CO_2$ Emissions.**

Technologies presently being developed to reduce $CO_2$ emissions can be divided into three general categories: Pre-combustion decarbonization, during-combustion or oxy-fuel combustion, and post-combustion $CO_2$ capture. Although the present account concerns itself with a novel post-combustion capture strategy, a brief overview of both pre-combustion decarbonization and oxy-fuel combustion highlighting the relative advantages and disadvantages of each method is prudent. Pre-combustion decarbonization has the advantage of being able to accommodate high $CO_2$ levels and separation is facile as compared to the other two methods. The general paradigm for pre-

combustion $CO_2$ separation is shown in Equations 1–3.[16] Briefly, the fuel is either subjected to steam reforming (Eq. 1) or it is gasified (Eq. 2) to produce syngas (a mixture of $H_2$ and CO), which is subsequently mixed with water vapor in the water–gas shift reaction (Eq. 3) to produce $H_2$ and $CO_2$. The $CO_2$ is then separated prior to combustion leaving water as the sole combustion product. Large-scale implementation of pre-combustion decarbonization is presently unrealistic because both gasification and steam reforming are challenging and costly, with both requiring substantial initial capital investment.[17]

$$C_xH_y + x\,H_2O \rightarrow x\,CO + \left(x + \frac{y}{2}\right) H_2 \quad (1)$$

$$C_xH_y + \frac{x}{2}\,O_2 \rightarrow x\,CO + \frac{y}{2}H_2 \quad (2)$$

$$CO + H_2O \rightarrow CO_2 + H_2 \quad (3)$$

During-combustion or oxy-fuel combustion employs pure oxygen or oxygen-enriched air as the combustion medium. Oxy-fuel processes produce flue gas that is much lower in total volume as compared to combustion in air. Further, these methods yield flue gas that is composed of up to 98% $CO_2$ after water vapor is removed, which significantly lowers the cost of $CO_2$ separation.[18] Oxy-fuel combustion suffers from the high cost of pure $O_2$ production, high levels of $NO_x$ formation, and the need for improved oxyfuel boilers.[19]

In any discussion of post-combustion $CO_2$ capture technologies, there are several important points to consider when evaluating potential $CO_2$ separation strategies.[20] First, any process that employs a commodity chemical as a once-through capture agent is going to suffer from a problem of scale. That is, $CO_2$ is generated in such vast quantities that

the capture agent will be quickly exhausted if it is not able to be recycled. Along this line, for any capture process to be widely applicable it must contain a regenerative step to recover the capture agent, employ a membrane or membrane-like material for separation, or the capture chemical will have to be produced in quantities that exceed the current manufacturing capacity of the entire chemical industry.[21] Second, any process that consumes $CO_2$ as a reactant to produce a non-fuel commodity chemical will quickly overwhelm the global demand for said chemical. In other words, capture processes that are inextricably coupled to a chemical transformation of $CO_2$ into a non-fuel commodity chemical will necessarily require a strategy for storing the excess product. Although this second point should not be given any consideration with respect to market implications, the long-term storage of the $CO_2$ capture product must be taken seriously from a waste disposal standpoint, especially if the product is unstable or requires special handling.

Post-combustion $CO_2$ capture technologies that are presently being developed can be broadly thought of as being either physisorption or chemisorption processes. Chemisorption is adsorption in which $CO_2$ is sequestered via the formation of chemical bonds. Physisorption processes, on the other hand, are aimed at $CO_2$ capture where no significant change in the electronic structure of the involved species occurs.[22] One of the simplest cases that exemplifies the physisorption of $CO_2$ is simply bubbling the gas into water or another solvent where it reaches an equilibrium concentration depending upon the Henry's law constant for said medium. The gas can then be expelled from the medium by heating. Although there is a large body of work pertaining to physisorption processes, many of which show great promise for selective $CO_2$ capture, our work has been on a chemisorptive process and that will remain the focus throughout this document.

**The Chemistry of $CO_2$.**

Before giving several examples of the more well-studied $CO_2$ chemisorption technologies, it is important to appreciate the chemistry of $CO_2$. In its ground state, $CO_2$ is a 22-electron, linear molecule belonging to the $D_{\infty h}$ point group that is a gas at standard temperature and pressure. Although $CO_2$ is nonpolar, as shown in Figure 1, it contains two polar C–O bonds, and thus possesses characteristics of a polar species with two sites that behave quite differently. As the polarity of $CO_2$ indicates, the carbon atom is

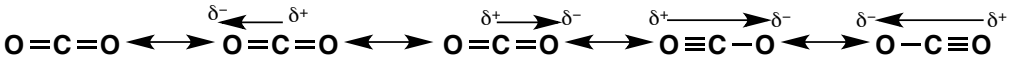


**Figure 1:** Polarity and resonance structures of linear $CO_2$.

electrophilic while the oxygen atoms are nucleophilic, with the electrophilicity of carbon being greater than the nucleophilicity of each O—thus, $CO_2$ prevalently behaves as an electrophile.[23] Further information about the behavior of $CO_2$ can be gleaned by examining its molecular orbital (MO) structure (Figure 2).[24] The HOMO is a degenerate set of non-bonding orbitals having $e_{1g}$ symmetry, while the LUMO is a degenerate set of $\pi$ orbitals having $e_{1u}$ symmetry. Examination of the MO diagram provides an explanation for why the direct reduction of $CO_2$ occurs at a very negative potential of –2.9 V vs. SCE. Population of the LUMO with a single electron induces a concomitant Jahn-Teller distortion where the symmetry of $CO_2$ decreases from $D_{\infty h}$ to $C_{2V}$. By extending this argument in an effort to better understand and conceive of new $CO_2$ capture technologies based upon chemisorption, facile binding $CO_2$ at the electrophilic carbon is possible only when using quite potent nucleophiles, which are required to induce the same reduction in local symmetry.

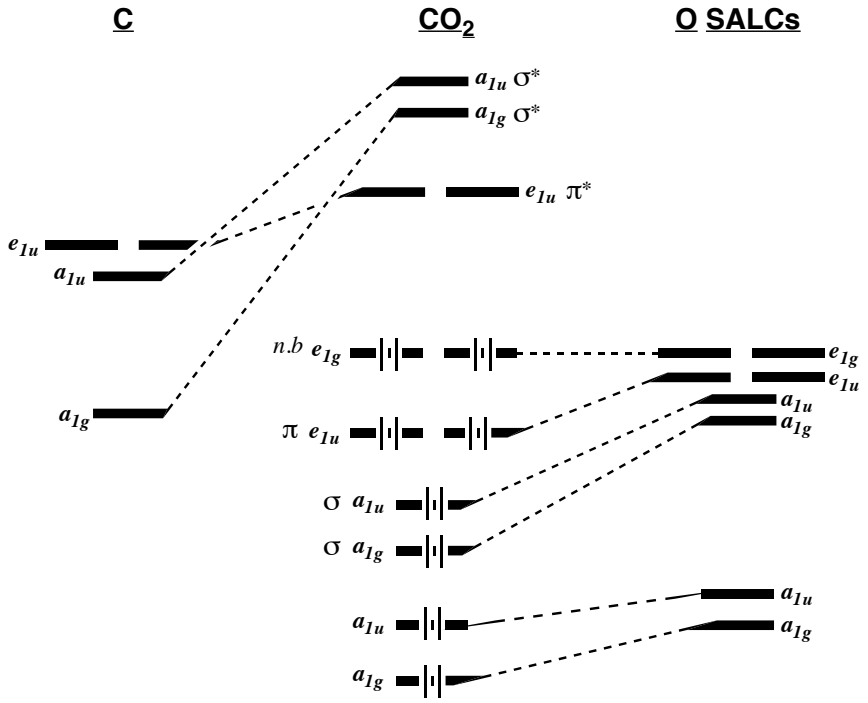


**Figure 2:** Molecular orbital diagram of $D_{\infty h}$ $CO_2$.

**Post-Combustion $CO_2$ Capture and Sequestration.**

There is a great deal of effort presently focused upon so-called end-of-pipe capture strategies, in which an existing coal or natural gas burning power plant is retrofitted with a capture stage at the flue gas output. Another category of post-combustion technologies that are gaining traction are direct air capture (DAC) methods. Direct air capture for the purposes of climate change mitigation was first proposed in 1999 by Lackner and has grown to be defined as any method of direct $CO_2$ extraction from ambient air.[25] One of the key benefits to DAC methods over their end-of-pipe counterparts is that there is no requirement that DAC facilities be located in close proximity to point source emitters, thus providing an avenue for wide-scale implementation of capture strategies that are sensitive to high concentrations of

contaminants such as $SO_x$, $NO_x$, and mercury. Additionally, DAC methods can mitigate emissions from distributed sources, which account for 60% of all anthropogenic $CO_2$.[26] Since there is a great deal of overlap in the chemistries of DAC methods and end-of-pipe methods a brief discussion of the more mature DAC methods is presented here.

The vast majority of DAC technologies that are presently being developed are sorbent-based. These methods can employ a diverse array of materials including zeolites, metal-organic frameworks (MOFs), activated carbons, supported amines, or aqueous hydroxides.[27] Direct air capture technologies that utilize aqueous hydroxides have received considerable attention due to their low cost and to the high binding affinity of hydroxide with $CO_2$. Two such manifestations are the Kraft process[28] and the spray tower method developed by Keith.[29] Briefly, the Kraft process, which has been used in paper manufacturing since the late 1800's, uses NaOH as the $CO_2$ sorbent to generate sodium carbonate.[30] The next step is causticization of $Na_2CO_3$ with $Ca(OH)_2$ in which NaOH is regenerated with concomitant precipitation of $CaCO_3$. The precipitate is transferred to a kiln for calcination where $CO_2$ is released, leaving lime. Resultant CaO undergoes hydration in a slaker, regenerating the $Ca(OH)_2$ needed for the causticization step. Spray towers also employ aqueous hydroxide as the $CO_2$ capture material, and have key advantages over packed towers or open pools. Specifically, the spray provides a larger surface area to maximize the amount of air that contacts the capture liquid. Additionally, the cost to implement a spray tower system is much less than that for large packed towers. The Kraft process and the spray tower method suffer from significant energy losses due to the poor efficiency of the causticization step in the case of the

former, and drop coalescence in case of the latter, both of which will need to be ameliorated before either can be implemented at the necessary scale.

A particularly promising DAC method that utilizes hydroxide ions as the $CO_2$ sorbent was reported by Shi et al. in 2016.[31] In this iteration, hydroxide ions are nano-confined in an ion exchange resin that has ammonium moieties covalently attached to the polymer backbone. Shi hypothesized that $CO_2$ capture and release is facile due to the decrease in water activity in the nanostructured pores of the resin. The proposed $CO_2$ capture reaction is summarized in Equation 4. When the number of water molecules

$$\left[CO_3^{2-} \cdot nH_2O\right] \rightleftharpoons \left[HCO_3^- \cdot m_1H_2O\right] + \left[HO^- \cdot m_2H_2O\right] + (n - m_1 - m_2 - 1)H_2O \quad (4)$$

$$\left[CO_3^{2-} \cdot nH_2O\right] + H^+ \rightleftharpoons [HCO_3^- \cdot m_1H_2O] \quad (5)$$

$$2\left[HCO_3^- \cdot m_1H_2O\right] + H^+ \rightleftharpoons \left[CO_3^{2-} \cdot nH_2O\right] + CO_2 + (m_1 - n - 1)H_2O \quad (6)$$

is small, the reaction equilibrium shifts to the right due to the law of mass action. The hydroxide ions thus produced, in what Shi terms the "dry state," are the active $CO_2$ binders. When the humidity is increased, the reaction equilibrium shifts to the left thus instigating $CO_2$ release by the decomposition of carbonate ions as shown in Equations 5 and 6. The authors note that inside the matrix the ratio of carbonate to water may be as high as 1:1, which facilitates significant driving force for the change in equilibrium owing to changes in the degree of ion hydration. To verify their hypothesis, Shi et al. utilized molecular dynamics simulations and found that the nano-confinement of the reactants is of paramount importance to this system's function. Specifically, the simulations showed that the free energy of Equation 4 is negative when the number of water molecules is less than 7. The free energy rapidly reaches a plateau value of 15 kcal

$mol^{-1}$ when the number of water molecules is increased to 60. These conditions are impossible to achieve in saturated $Na_2CO_3$ solution, where the ratio of carbonate ions to water is 20:1. That is, it is impossible to achieve the dry state without the aid of the resin or another intervening medium.

Another class of materials that show great promise for selective $CO_2$ capture are metal organic frameworks (MOF). Metal organic frameworks are porous, crystalline materials with broad structural and chemical diversity.[32] They show many advantageous properties for $CO_2$ separation including high thermal and chemical stabilities, large void volumes, and low density. Furthermore, they have been shown to absorb $CO_2$ by both physisorption and chemisorption. A particularly compelling example of the latter is the MOF MMEN-Mg2(dobdc), which is a magnesium-containing framework where the $CO_2$ capture moiety is *N,N'*-dimethylethylenediamine (MMEN).[33] Long et al. have demonstrated that MMEN-Mg2(dobdc) is capable of taking up large amounts of $CO_2$ at very low partial pressures, that the material can be cycled by heating, and that increased humidity does not result in decreased performance. Furthermore, using X-ray diffraction, they were able to elucidate the mechanism of $CO_2$ capture, wherein the nitrogen of the tethered MMEN attacks the carbon of $CO_2$ and concomitantly loses a proton to a neighboring MMEN.[34] The resulting carbamate is stabilized by substitution of the Mg–N bond with an Mg–O bond. Long et al. went on to show how the $CO_2$ adsorption behavior of this MOF changes both when Mg is replaced with a variety of metal ions, and when MMEN is replaced with a number of amines, thus illustrating the high degree of control over $CO_2$ capture properties this particular class of compounds affords.

Similar to metal organic frameworks, ionic liquids (IL) also exhibit both physisorption and chemisorption of $CO_2$. Ionic liquids are liquid salts that are liquid at low temperature (informally agreed upon as below 100 $^oC$) and that are composed wholly of ions. Similar to MOFs, there is an enormous amount of chemical space with respect to ionic liquid design. Thus, an exhaustive review of the billions of possible ILs is not feasible. The interested reader is directed to the ILThermo Ionic Liquid database,[35] and to a number of reviews that discuss both first-principles and theoretical approaches to making task-specific ionic liquid (TSIL) design more tractable.[36] With respect to physisorption, Lei et al. have written an excellent review of gas solubility in ionic liquids in which they have devoted a great deal of discussion to gasses that are present in flue gas, especially $CO_2$.[37] Lei notes that while there is ample evidence supporting the hypothesis that the ionic liquid anion is the primary factor that governs $CO_2$ physisorption, there is some evidence to suggest that alkyl chain length on the cation plays a significant role as well. Furthermore cation and/or anion fluorination, cation bromination, branched alkyl chains on the cation, and the inclusion of ester or carbonyl groups on the cation have all been shown to affect the Henry's law constants for $CO_2$ in ILs, which typically range from 30 to 200 bar. To add another layer of complexity to how $CO_2$ physisorption in ILs is understood, there have been several studies of IL mixtures, either with other ILs or with organic solvents, that show $CO_2$ solubility is sensitive both to the identity and to the mole fractions of the ILs and solvents involved.[38] Indeed, this is a very active area of research and physisorption of $CO_2$ in ILs is a promising remediation strategy.

**Chemisorption of $CO_2$ in Task-Specific Ionic Liquids.**

Chemisorption of $CO_2$ in ionic liquids is of particular pedagogical utility toward understanding $CO_2$ capture by electrogenerated sulfur nucleophiles in ionic liquids that will be discussed in later chapters. Thus, it is prudent to examine several cases of $CO_2$ chemisorption in ILs facilitated by a nucleophilic site on either the IL anion or the IL cation that functions as the $CO_2$ binding site. The first report of a task-specific IL for $CO_2$ chemisorption was published in 2002 by Davis et al. who appended a propyl amine functionality to an imidazolium cation.[39] Carbon dioxide capture proceeds by the pendant amine nitrogen on the cation attacking the electrophilic carbon of $CO_2$, thus generating a zwitterionic ammonium carbamate moiety. A neighboring amine then deprotonates the ammonium carbamate, leaving a 1:1 mixture of ammonium–imidazolium dications and zwitterionic imidazolium–carbamates. The reaction stoichiometry theoretically limits this TSIL to capturing 0.5 mol $CO_2$/IL, which was confirmed experimentally by monitoring the molar ratio of $CO_2$ to TSIL over three hours. In addition to evaluating the effectiveness of TSILs for $CO_2$ capture by examining the molar ratio, gravimetric capacity—defined as the wt% of moles $CO_2$ captured per moles of TSIL—is also an important metric to consider. In this case, the gravimetric capacity of Davis' TSIL was around 7%. Finally, since the $CO_2$ sorbent must be able to be recycled in order for any carbon capture technology to be implemented at the necessary scale, it is important to note that $CO_2$ recovery was achieved by heating this TSIL to 80–100 $^{o}$C under vacuum for several hours.

An example of a task-specific ionic liquid in which anionic nitrogen nucleophiles serve a dual role as both the $CO_2$ sorbent and the IL anion was reported in 2014 by Seo

and coworkers.[40] In this report, nitrogen-containing aprotic heterocyclic anions were paired with tetraalkylphosphonium cations and each of the resultant ILs were evaluated as to their $CO_2$ absorption capacity. In contrast to the work of Davis, each IL investigated by Seo was, in theory, capable of binding one $CO_2$ mole per mole of IL. It was inferred that ILs comprised of anions that did not reach unity $CO_2$ capacity did not form stable carbamates upon exposure to $CO_2$. The absorption isotherms that the authors collected showed that ILs with indazolide and benzimidazolide anions had strong chemical binding toward $CO_2$, with reaction enthalpies ranging between –54 to –48 kJ $mol^{-1}$. Seo further determined that three anions, 2-methylthio-benzimidazolide, 3-trifluoromethyl-pyrazolide, and 1,2,3-triazolide did not approach the expected stoichiometry of 1:1, reaching only 0.7, 0.6, and 0.3 mol $CO_2$/IL at a pressure of 1 bar $CO_2$, respectively. These three anions had reaction enthalpies of between –44 to –37 kJ $mol^{-1}$, suggesting that there is a narrow range of reaction enthalpies where the $CO_2$ binding transitions from strong to weak.

In their follow-up publication, Seo et al. described a series of ionic liquids that changed phase from solid to liquid upon exposure to $CO_2$.[41] These so-called phase-change ionic liquids (PCIL) all had anionic nitrogen $CO_2$ capture sites in the form benzimidazolide, pyrrolide, or pyrazolide anions, and had either tetraethyl- or tetrabutylphosphonium cations. The authors make the case that these media will have significant energetic advantages over other $CO_2$ capture processes in that the enthalpy of fusion will act to decrease the thermal energy necessary to decarboxylate the IL anion and regenerate the active $CO_2$ capture species; that is, Heat Load for Regeneration = $\Delta H_{rxn} - \Delta H_{fus}$. The absorption isotherm of the tetraethylphosphonium benzimidazolide

PCIL exhibits a step-change indicating that only a small change in pressure or temperature is necessary to release $CO_2$, thus regenerating the capture medium. Since the regeneration step is typically the most energy-intensive in the reported $CO_2$ capture technologies, this is an attractive feature of PCILs. That said, to fully decarboxylate the model system, tetraethylphosphonium benzimidazolide, it was necessary to heat the PCIL to 70 $^{o}$C under vacuum. Another key finding from this report is that the physical properties, specifically the melting point, of the carboxylated IL are sensitive to the alkyl chain length on the cation. That is, the tetrabutylphosphonium-based PCILs have lower melting points than their tetraethylphosphonium analogs. Finally, Seo et al. confirm the findings from their previous publication—that the reaction enthalpy for the $CO_2$ capture reaction can be tuned by changing the identity of, or the substituents on, the IL anion.

To more fully explore the chemical space of task-specific ionic liquids for $CO_2$ sequestration, we now turn away from ionic liquids containing nitrogen nucleophiles and examine cases where an alkoxide serves both as the TSIL anion and as the $CO_2$ capture nucleophile. In their 2010 publication, Wang et al. report that phenol, α–(trifluoromethyl)benzyl alcohol (TFBA), trifluoroethanol (TFE), and hexafluoropentanediol (HFPD) can be paired with a superbase,[42] and that the resulting acid–base reaction yields TSILs that are competent for $CO_2$ capture.[43] While the TSILs that contain the conjugate bases of TFBA, TFE, and HFPD as the anion all show $CO_2$ capture at, or slightly above their theoretical limits, the phenoxide-based permutations show $CO_2$ capture slightly below 0.5 moles of $CO_2$ captured per mole of TSIL, or roughly half that expected by the reaction stoichiometry. This result was confirmed in a 2011 study by the same authors in which the $CO_2$ capture medium was made by pairing

phenoxide anions with trihexyl-(tetradecyl)phosphonium cations.[44] Experimental results show that the absorption capacity for this TSIL is 0.5 mol $CO_2$/mol TSIL, and the theoretical absorption enthalpy is 46.7 kJ $mol^{-1}$. These data suggest that phenoxide is a lackluster $CO_2$ capture species as compared to some of the reported nitrogen anion TSILs, having an absorption enthalpy between the strong- and weak-binding limits established by Seo.[40]

Manipulation of the $CO_2$ absorption characteristics, particularly the absorption enthalpy, of phenoxide-based task-specific ionic liquids was shown to be quite facile. In order to establish a set of criteria to aid in the design of TSILs for $CO_2$ capture, Wang examined the relationship between the absorption enthalpy and the basicity of the ionic liquid anions.[44] The authors found that anions whose conjugate acids have higher $pK_a$ have both higher $CO_2$ capacity and absorption enthalpy without concomitant increases in viscosity, which would hinder the absorption kinetics. Although the trihexyl-(tetrdecyl)phosphonium phenoxide ionic liquid did not fit the trend (the $pK_a$ of phenol in DMSO suggested that the absorption capacity would be higher than reported), the paradigm that Wang established in this initial report was employed to guide follow-up phenoxide-based ionic liquid $CO_2$ capture strategies. To wit, Wang et al. studied eighteen different trihexyl(tetradecyl)phosphonium phenoxide ionic liquids where they appended the phenoxide with various electron-donating (EDG) and electron-withdrawing (EWG) groups.[45] The authors again found that the $CO_2$ absorption capacity increased with an increase in the pKa of the phenoxide conjugate acids (see footnote).[46] The authors also employed density functional theory (DFT) calculations and found that the more negative the Mulliken charge on the oxygen atom of the phenoxide anion, the more

negative the absorption enthalpy i.e. the stronger the $CO_2$ binding. For example, 4-methoxyphenoxide has a Mulliken charge of –0.7062 on the oxygen atom and an absorption enthalpy of –51.4 kJ $mol^{-1}$; whereas 4-nitrophenoxide has a Mulliken charge of –0.6187 on the oxygen atom and an absorption enthalpy of –17.1 kJ $mol^{-1}$. Thus, Wang illustrates that it is possible to transition between the strong- and weak-binding (or no binding, as in the case of 4-nitrophenoxide) motifs by varying the substituents on the ionic liquid anion.

In the context of the preceding discussion where the $pK_a$ of the ionic liquid anion conjugate acid is correlated to the $CO_2$ absorption properties, it is worthwhile to more closely examine the role of strongly basic ionic liquid anions. Specifically, it can be readily assumed that more basic ionic liquid anions have the potential to participate in unwanted side reactions. An example of this phenomenon was reported by Gohndrone et al. who examined $CO_2$ capture in phosphonium 2-cyanopyrrolide ionic liquids.[47] Using a combination of spectroscopic and computational data, Gohndrone found that, in addition to attacking the electrophilic carbon of $CO_2$, 2-cyanopyrrolide is a strong enough base to deprotonate the α-carbon on the butyl(triethyl)phosphonium cation at elevated temperature. Resulting phosphonium ylides then went on to attack $CO_2$ producing a zwitterionic carboxylate, which was characterized by both IR and NMR. The authors argue that carboxylate stabilizes the zwitterion, and they provide Møller–Plesset calcuations to support their claim. Importantly, Gohndrone does not observe this same behavior when the IL cation is trihexyl(tetradecyl)phosphonium, and hypothesizes that the bulk of the alkyl chains on the cation effectively restrict access to the α-carbon. In a follow-up article by the same group, phenoxide anions are paired with

trihexyl(tetradecyl)phosphonium cations and the $CO_2$ absorption mechanism is characterized by both IR and NMR spectroscopies.[48] In this case, the bulky phosphonium cation was able to be deprotonated at the α-carbon and $CO_2$ absorption proceeds through the phosphonium ylide as described in their previous publication. In both cases, the possibility of deprotonation at the β-carbon in a Hoffman-type elimination reaction is not examined. Despite this omission, the possibility of strongly basic anions participating in this type of chemistry should not be ignored. In this case, the Hoffman elimination reaction would yield a phosphine, which as been shown to be a $CO_2$ capture agent in studies where tris(mesityl)phosphine acts as the Lewis base in frustrated Lewis pairs for $CO_2$ reduction.[49] In either case, it is clear that one must consider cation–anion interactions when designing TSILs for $CO_2$ capture.

A particularly salient example of the importance of cation–anion interactions in TSILs for $CO_2$ capture can be seen in cases where imidazolium is the IL cation. In these cases, several groups have found that the imidazolium cation is the precursor to *N*-heterocyclic carbenes (NHC), which are carbon nucleophiles that have been shown to attack the electrophilic carbon of $CO_2$. The reactivity of NHCs toward $CO_2$ was first investigated by a number of groups in the late 1990's and early 2000's. These early reports were not geared toward $CO_2$ capture, per se. Rather, they sought to either fully characterize the imidazolium carboxylates,[50] or to asses the role of imidazolium carboxylates both in catalytic olefin metathesis[51] and in group transfer reactions.[52] Further, several papers from the Louie group around the same time detailed the synthesis and characterization of a wide array of imidazolium carboxylates on which they performed thermal gravimetric analysis (TGA) in order to fully understand how the

imidazolium substituents affect the decarboxylation temperature.[53] Their findings show that the steric bulk of the *N*-substituent(s) is of primary importance, more so than electronic structure, with NHCs that have bulkier substituents on the nitrogen atoms exhibiting lower decarboxylation temperatures. It was in the context of these studies that in 2005 Maginn postulated that the absorption of $CO_2$ in 1-butyl-3-methylimidazolium acetate may proceed via carboxylation of the imidazolium cation.[54]

Following these initial reports, in 2011 Gurau et al. published their article regarding the chemisorption of carbon dioxide in 1,3-dialkylimidazolium acetate ionic liquids, where they provided substantial evidence of the imidazolium carboxylate in the ionic liquid.[55] There have been numerous subsequent studies that have endeavored to understand the mechanism of $CO_2$ absorption by imidazolium-based ionic liquids.[56] Brennecke and coworkers have proposed that there are two distinct pathways for $CO_2$ chemisorption in imidazolium ILs.[56d] The first is the rather obvious case where the IL anion acts as a nucleophile and attacks the electrophilic carbon of $CO_2$. The second is the combined process where the imidazolium is deprotonated at the bridgehead carbon by the IL anion, and the resultant NHC attacks the $CO_2$ carbon. There is general agreement that in acetate-based ionic liquids the carbene is generated by deprotonation of the bridgehead carbon by the acetate ion. Indeed, in these ILs the product acetic acid has been identified by IR, NMR, and Raman spectroscopies.[56b] Although there is still some question as to how the competing interactions between anion–cation, anion–$CO_2$, and cation–$CO_2$ affect the overall absorption capacity in these materials,[57] it is abundantly clear that in imidazolium-based ionic liquids nucleophilic attack by NHCs account for at least some of the $CO_2$ uptake. This was further confirmed in a series of articles from the Feroci

laboratory that show imidazolium TSILs with anions that lack a basic site—specifically tetrafluoroborate—may be utilized for $CO_2$ capture where the NHC is generated electrochemically at 60 $^{o}$C.[58] Despite the general agreement that NHCs in imidazolium ionic liquids are competent for $CO_2$ capture, there are lingering questions as to their efficacy. Specifically, in a very recent article by Mei et al. it was shown that $CO_2$ absorption in imidazolium ILs can be improved by suppressing NHC formation.[59] In other words, the authors propose that interference by NHCs has a deleterious effect on the $CO_2$ absorption capacity in imidazolium ILs, and designing systems in which $CO_2$ is attacked solely by the ionic liquid anion is beneficial.

**Carbon Dioxide Chemisorption by Monoethanolamine.**

Of the chemisorptive post-combustion methods for $CO_2$ capture that have been reported, there is only one that has been implemented on the pilot scale: chemical absorption using monoethanolamine (MEA). Flue gas scrubbing by aqueous MEA has been shown to capture and release $CO_2$ with a minimum of initial expense.[13a, 13c] Furthermore, utilizing amine scrubbing it is possible to capture 90% of the $CO_2$ from flue gas.[60] However, recovering high-purity $CO_2$ is costly and requires replenishing or replacing the capture agent. Achieving this degree of $CO_2$ capture results in a 21% power loss (170 kJ mol $CO_2^{-1}$), which translates to a 44% increase in generating cost per MWh.[60] Though this may seem to be an insurmountable economic barrier to implementing amine scrubbing at scale, recent polling has shown that the average U.S. citizen will accept a 13% increase in electricity cost to support a national clean energy standard.[61] One final cost-based impediment to MEA scrubbing is the parasitic loss of the amine capture agent, which can amount to as much as 2 kg per ton $CO_2$.[13a, 13c]

Along that line, and of greater importance than the economic obstacles, are the barriers to implementation at scale due to the environmental impacts of amine-based capture methods. Research in this area is incomplete; however, one can a priori identify a number of potential environmentally harmful outcomes to large-scale amine scrubbing. Of primary concern is the potential for what are termed "fugitive emissions" that could be deleterious to human health and to the environment.[62] Fugitive emissions is the term given to the release of process fluids and materials, untreated flue gas, treated gas that contains unidentified compounds, adsorption solvents, corrosion inhibitors, degradation products, and chemical additives whose impacts to human health and environment are not fully understood.[62] In addition to fugitive emissions, since reclaiming the capture species requires heating, there is the potential for a large amount of recovered waste during the reclamation step due to unwanted side reactions. Since it is appropriate to view $CO_2$ remediation in the context waste management, capture technologies that generate waste products that require special handling and/or storage would be counterproductive. Finally, there is a strong likelihood that amine sorbents could lead to highly toxic nitrosamines being formed in the atmosphere from either the emitted amine or degraded amine products.[63]

**Summary and Dissertation Outline.**

As this introduction illustrates, there is a need for energy efficient and environmentally benign $CO_2$ capture strategies that can be implemented at the necessary scale. In the context of the reviewed technologies, we may establish several criteria that must be met for any potential postcombustion chemisorption $CO_2$ capture strategy to be viable. First, there must be a regenerative step that recycles the capture agent. Once-

through capture strategies are not realistic because the massive quantities of $CO_2$ that are emitted would quickly overwhelm the manufacturing capacity for any chemical sorbent. Second, any end-of-pipe capture technology must be immune to degradation and/or to passivation by other compounds that are present in flue gas. These include, but are not limited to, $SO_x$, $NO_x$, mercury, oxygen, and water vapor. Third, the sorbent must be environmentally benign due to the possibility of fugitive emissions. Escaped capture agent or degraded capture agent products must be either easily sequestered or not susceptible to unwanted side reactions that occur in the environment to produce potentially toxic substances. Finally, any capture strategy that is coupled to a chemical transformation of $CO_2$ must either produce a commodity chemical that is highly desirable, or the process must minimize the reaction products, especially if those products require special handling and/or storage. Ideally, captured $CO_2$ could be recycled into fuel to create a carbon-neutral energy supply.

In Chapter 2, this document provides an in-depth review of electrochemical strategies for $CO_2$ capture. As a brief prelude, DuBois et al. have proposed electrochemical pumping as an energy efficient carbon dioxide capture method[64] that employs a redox-active molecule that, in one if its oxidation states, strongly binds $CO_2$. Upon oxidation (or reduction) the binding constant for $CO_2$ of the redox-active species drastically decreases, thereby releasing the $CO_2$. To estimate the energy requirements for $CO_2$ capture from flue gas utilizing electrochemical pumping, we may employ Eq. 7

$$\Delta G = RT \ln\left(\frac{p_f}{p_i}\right) \tag{7}$$

where $\Delta G$ is the change in free energy, R is the ideal gas constant, T is the absolute temperature, $p_f$ is the final partial pressure of $CO_2$ recovered from the initial partial

pressure of $CO_2$, $p_i$. Isobaric recovery of pure $CO_2$ concentrated to 1 atm at 293 K from flue gas containing 8 (natural gas burning) to 14% (coal burning) carbon dioxide requires a theoretical minimum energy input of 6.2 kJ mol $CO_2^{-1}$ and 4.8 kJ mol $CO_2^{-1}$, respectively. Conversion of these free energy values to applied potential is accomplished the aid of Eq. 8

$$\Delta G = -nF(\Delta E) \quad (8)$$

where n is the number of electron moles and F is Faraday's constant. Assuming that the system requires one electron mole per mole of $CO_2$ captured, the theoretical minimum applied potential for electrochemical pumping is 64 mV for natural gas burning power plants and 50 mV for coal burning power plants. Overpotential and cell resistance losses may be reasonably estimated as necessitating an additional 0.3 V of applied potential, and mass-transfer effects within the cell may likewise be estimated as inducing a 20% loss in efficiency.[65] Accounting for these effects leads to an estimated energy cost for electrochemical pumping of 43.9 kJ mol $CO_2^{-1}$ for natural gas plants and 42.2 kJ mol $CO_2^{-1}$ for coal plants.

In the next chapter, proof of concept for an electrochemical $CO_2$ pump that employs electrogenerated sulfur nucleophiles is presented. We describe a model compound, benzyldisulfide, and demonstrate both electrochemical $CO_2$ capture and release. At glassy carbon cathodes in the ionic liquid 1-butyl-1-methylpyrrolidinium bis(trifluoromethylsulfonyl)-imide ([BMP] [TFSI]), this system is best formulated as a two-electron process with potential inversion. Briefly, the organic disulfide is electrochemically reduced by one electron, which populates an antibonding orbital. This results in rupture of the S–S bond and the formation of one thiolate anion and one thiyl

radical. The radical is reduced at a potential that is far more positive than that of the disulfide, so it quickly gains one electron to yield another thiolate. Electrogenerated thiolates are potent nucleophiles that can attack $CO_2$ at the electrophilic carbon to produce thiocarbonates. At the anode, thiocarbonates undergo a one-electron Kolbe oxidation to yield an unstable neutral radical, which rapidly decomposes to $CO_2$ and sulfur radicals. These sulfur radicals then couple to yield the original disulfide, thereby regenerating the masked $CO_2$ capture agent. It will be shown that the electrochemical pumping of $CO_2$ using the disulfide–thiolate–thiocarbonate system in ionic liquids is a strong candidate for an end-of-pipe CCS technology.

As a follow-up to the initial study of benzylthiolates as $CO_2$ chemisorbents, Chapter 4 details the possibility of utilizing waste heat from power generating facilities to drive the $CO_2$ capture–release process. Toward that end, a number benzylthiolates with various alkali metal cations were synthesized and a crystal structure of the 15-crown-5 sodium benzylthiolate was obtained. Benzylthiocarbonates were then produced by exposing the benzylthiolates to $CO_2$ in a methanol–THF solution. Results from thermal release experiments show that the temperature and kinetics for $CO_2$ release are strongly dependent upon the identity of the cation. In some instances, the benzylthiolate salt survived heating to 250 $^{o}$C, thus demonstrating the utility of this approach as a carbon capture strategy. It was further shown that tetrabutylphosphonium benzylthiolate is an ionic liquid at room temperature that solidifies upon exposure to $CO_2$. The $CO_2$ is liberated by placing the solid under vacuum at room temperature, which generates a pure $CO_2$ stream while concomitantly reclaiming the active $CO_2$ sorbent. This example is similar to the phase change ionic liquids discussed previously; however because exposure

to $CO_2$ results in solidification rather than liquefaction, this example will not have the same energetic benefits due to the enthalpy of fusion.

In the Appendix the functionalization of poly(2,6-dimethyl-1,4-phenylene oxide) (PPO) with pendant ferrocene moieties via the copper catalyzed azide–alkyne coupling (CuAAC) reaction and the electrochemical properties of the functionalized polymer is presented. The primary findings of the study are twofold: The first part details the synthesis the effect that copper(II) ions resulting from the CuAAC reaction have on the product if they are not removed during workup. Specifically, copper ions can coordinate to the nitrogen of the triazole ring to act as crosslinks making the product polymer an insoluble, blue mass. A model compound, 4-butyl-1-(phenylmethyl)-1*H*-1,2,3-triazolyl-copper(II)-acetate was prepared and fully characterized so that the spectroscopic data could be compared to the functionalized polymer. In the second part of the study, the electrochemical properties of the ferrocene-functionalized PPO was investigated by cyclic voltammetry. Findings from these experiments show that the electrochemical response of polymer films is sensitive to the nature of the electrolyte, specifically the size of the electrolyte anion. These results are discussed within the context of anion sensing and recognition applications.

# CHAPTER 2

**Abstract**

Understanding the chemistry of carbon dioxide is key to effecting changes in atmospheric concentrations. One area of intense interest is $CO_2$ capture in chemically reversible cycles relevant to carbon capture technologies. Most $CO_2$ capture methods involve thermal cycles in which a nucleophilic agent captures $CO_2$ from impure gas streams (e.g. flue gas), followed by a thermal process in which pure $CO_2$ is released. Several reviews have detailed progress in these approaches. A less explored strategy uses electrochemical cycles to capture $CO_2$ and release it in pure form. These cycles typically rely on electrochemical generation of nucleophiles that attack $CO_2$ at the electrophilic carbon atom, forming a $CO_2$ adduct. Then, $CO_2$ is released in pure form via a subsequent electrochemical step. In this chapter, electrochemical cycles for $CO_2$ capture and release, emphasizing electrogenerated nucleophiles are reviewed. Some advantages and disadvantages inherent in this general approach are discussed.

---

The relentless increase of atmospheric $CO_2$ concentrations driven by the cumulative effects of combustion of carbon-based fuels has driven a tremendous level of research activity in the chemistry of $CO_2$. With the goal of effecting change in the trajectory of atmospheric $CO_2$ concentrations, a primary area of recent focus has been the capture of $CO_2$ either from point sources like coal- or natural gas-fired power plants (point source emitters) or directly from the atmosphere (direct air capture). A number of different approaches have been explored. These have been extensively reviewed, with detailed analyses describing chemical principles, energy efficiencies, economics, and

technical readiness levels.[66] A variety of different types of chemical reactions with $CO_2$ have been explored in this context. Most of these chemistries rely on the use of a potent nucleophile to react with and capture $CO_2$ in the form of some type of adduct, which is later decomposed in some way to release $CO_2$, regenerating the capture agent. One of the more well-studied chemistries based on this tactic employs an amine reagent such as monoethanolamine (MEA) which acts as a nucleophile, attacking $CO_2$ at the electrophilic carbon center thereby forming a carbamate. Equation 9 summarizes this process.

$$2\,HO(CH_2)_2NH_2 + CO_2 \leftrightarrow HO(CH_2)_2NH_3^+ + HO(CH_2)_2NHCO_2^- + heat \quad (9)$$

As shown, two equivalents of the amine are required to capture one equivalent of $CO_2$ in the form of a carbamate ($RNHCO_2^-$). Equation 9 also shows that the reverse process, in which $CO_2$ is released (e.g. for permanent storage, use as a chemical feedstock, enhanced oil recovery, etc.), requires an increase in temperature to break the N–C bond. The amount of thermal energy required is exacerbated by the fact that the MEA process is typically operated under aqueous conditions, meaning that significant energy is also required to heat the aqueous solution in which the capture chemistry is contained. Under these conditions the energy required for recycling the MEA capture agent can consume between 14 and 30% of the output of a typical power plant, greatly impacting the economics of the capture process.[66c] As a result, though this process has been studied for many years and demonstrated at pilot scale, it is unlikely to ever be implemented on a broad scale. Similar to the MEA process, amines immobilized within a variety of matrices also have been shown capable of $CO_2$ capture. For these cases, the energy required for regeneration of the free capture agent scales with the heat capacity of the matrix, which can be substantially lower than that for the aqueous MEA solutions

described above.[67] Coupled with the design of new capture agents that release $CO_2$ at lower temperatures, these approaches may enable use of waste heat for the regeneration cycle, which could substantially change the energy and economics of the process compared to the MEA case. Nevertheless, the approaches described above all require substantial input of thermal energy for regeneration of the capture agent, which limits energy efficiency.

A fundamentally different approach employs electrochemical processes to drive the capture and release reactions. The use of electrochemistry for separation of carbon dioxide from complex gas streams has a long history, and has enjoyed a recent resurgence in activity. In this Perspective, we describe several different approaches that have been explored. Because electrochemical $CO_2$ capture–release systems employ a variety of conditions, and consequently have quite different energy efficiencies and economics, they are not equally applicable in all settings. Our focus here is not to identify the best situation for each approach, but rather to identify some common themes among them that can be used to inform future research efforts in the area. We focus especially on the use of electrogenerated nucleophiles to capture $CO_2$.

The prospective use of electrochemical systems for $CO_2$ capture and release leads to the identification of preferable characteristics for the reagents and the (electro)chemical processes in such schemes. These characteristics stem first and foremost from a desire to minimize the energy required for the "round trip" capture and release processes, but also include other considerations such as controlling (i.e. "tuning") the strength of $CO_2$ binding, and minimizing side reactions or other parasitic processes

that interfere with the capture and release chemistry. Given these and other constraints, one can formulate a list of the characteristics desired in such a scheme:

- A small potential difference between the electrochemical capture and release processes, to minimize energy consumption and cost of energy
- Relatively rapid electron transfer kinetics for the electrochemical steps
- Tunability of the binding constant for $CO_2$ with the capture agent, to maximize the efficiency of the process
- Relative insensitivity of the nucleophilic capture agent to dioxygen and water, since these are typically present in gas streams from which $CO_2$ would likely be captured
- Use of electrolyte media for the capture–release cycle that are low cost or are not lost during the cycle (e.g. use of volatile organic solvents is not likely to be attractive because of evaporative losses, thus favoring aqueous electrolytes or non-volatile media like ionic liquids)
- Design of capture and release mechanisms that avoid highly reactive intermediates that might become involved in unwanted side reactions that consume the capture agent

As we will see below, the electrochemical cycles described to date all suffer from one or more deficiencies with regard to these characteristics. However, one hopes that helping focus the broader community on these issues will bring forward better alternatives.

The original motivation of applying electrochemistry to $CO_2$ separation dates back to the need for removal of carbon dioxide from breathing gas mixtures on manned space flights.[68] These early efforts were based on molten carbonate fuel cell (MCFC)

systems that were reconfigured into molten carbonate $CO_2$ concentrators (MCCC). Carbon dioxide production by MCFC's is zero due to equal amounts of $CO_2$ being consumed (Equation 10) and generated (Equation 11) at the cathode and anode, respectively (net shown in Equation 12). Thus, fuel cell operation effectively serves to remove $CO_2$ from complex gas streams and concentrate it at a different location. This chemistry represents one of the more mature electrochemical approaches to $CO_2$ separation, and interest in these types of systems has recently been rekindled.[69] A typical MCCC uses two gas-breathing electrodes separated by a ceramic membrane impregnated with a molten carbonate salt. Use of this class of electrolyte necessitates operation at very high temperatures, typically near 650 $^{o}$C. Carbon dioxide is captured at the cathode where $O_2$ is reduced, driving $CO_3^{2-}$ formation from reaction between the resulting oxide species, $O^{2-}$, and $CO_2$. The anode gas feed is typically hydrogen, although methane may also be used as the fuel for the overall process.[69c] The latter is an attractive option for $CO_2$ separation from flue gas generated by natural gas-burning power plants. Hydrogen is oxidized at the anode to produce protons that react with $CO_3^{2-}$ yielding steam and $CO_2$, both of which exit the cell through the anode exhaust. The cell reactions are given by equations 10–12:

Cathode: $\frac{1}{2}\ O_2 + CO_2 + 2\ e^- \leftrightarrow CO_3^{2-}$ (10)

Anode: $H_2 + CO_3^{2-} \leftrightarrow H_2O + CO_2 + 2\ e^-$ (11)

Net: $H_2 + \frac{1}{2}\ O_2 + CO_{2,\ cathode} \leftrightarrow H_2O + CO_{2,anode}$ (12)

The overall energetics and practical utility of this approach are strongly impacted by the high temperatures required to achieve reasonable transport rates for $CO_3^{2-}$ across the membrane separator in the cell, which is typically an electrically insulating ceramic such

as lithium aluminate. Also, this approach does not produce a pure $CO_2$ stream, instead giving a mixture of $CO_2$ and $H_2O$.

Carbon dioxide separation can also be achieved using electrochemically controlled pH swings as the primary driver for $CO_2$ capture and release. These systems exploit the responsiveness of the thermodynamic equilibrium of $CO_2$ hydration to small pH changes. An increase in pH at a cathode drives capture of $CO_2$ as either $HCO_3^-$ or $CO_3^{2-}$, depending on the operating pH. Transport of the trapped $CO_2$ equivalents occurs either by physically pumping the process fluid or by electromigration of the carbonate or bicarbonate anions. Release occurs at an anode where acidic conditions are created, leading to regeneration of free $CO_2$. Several different approaches have been used to take advantage of pH swings for $CO_2$ separation. For example, bipolar membranes (BPM's) have been used as part of an electrodialysis scheme.[70] In another manifestation, electrodeionization has been employed, where both BPM's and cation exchange membranes were utilized to concentrate a ~15% $CO_2$ simulated flue gas stream to >98% $CO_2$ in the recovery stream.[71] Water electrolysis can also be used, though this process requires a minimum of 1.23 V to drive the pH changes.[72] A unifying feature of these approaches is the use of applied potentials to drive $CO_2$ capture via $OH^-$ generation and $CO_2$ release via $H^+$ generation.

An alternative method that also takes advantage of the pH sensitivity of the $CO_2$ hydration equilibrium uses the redox chemistry of quinones to generate pH changes. Here, the 2,6-dimethylbenzoquinone/2,6-dimethylhydroquinone redox couple has been used as part of an active liquid membrane system to pump $CO_2$.[73] In this approach, reduction of quinone to hydroquinone at a gas-breathing cathode leads to proton

Electromigration drives bicarbonate across the cell to the anode. Oxidation of hydroquinone at the anode releases protons producing a local pH decrease, which drives production of $CO_2$ from $HCO_3^-$, leading to $CO_2$ exit from the gas-breathing anode. The use of catalysts was explored to improve the kinetics of the quinone redox process, though complications from water electrolysis resulted due to the large applied potential across the cell.

A number of groups have explored $CO_2$ capture using potent electrochemically generated nucleophiles resulting from reduction of organic redox compounds. These electrogenerated nucleophiles bind to the electrophilic carbon center in $CO_2$, forming some type of stable adduct species. The key to this approach is the dramatic change in the $CO_2$ binding constant of the reduced species as compared to its oxidized redox

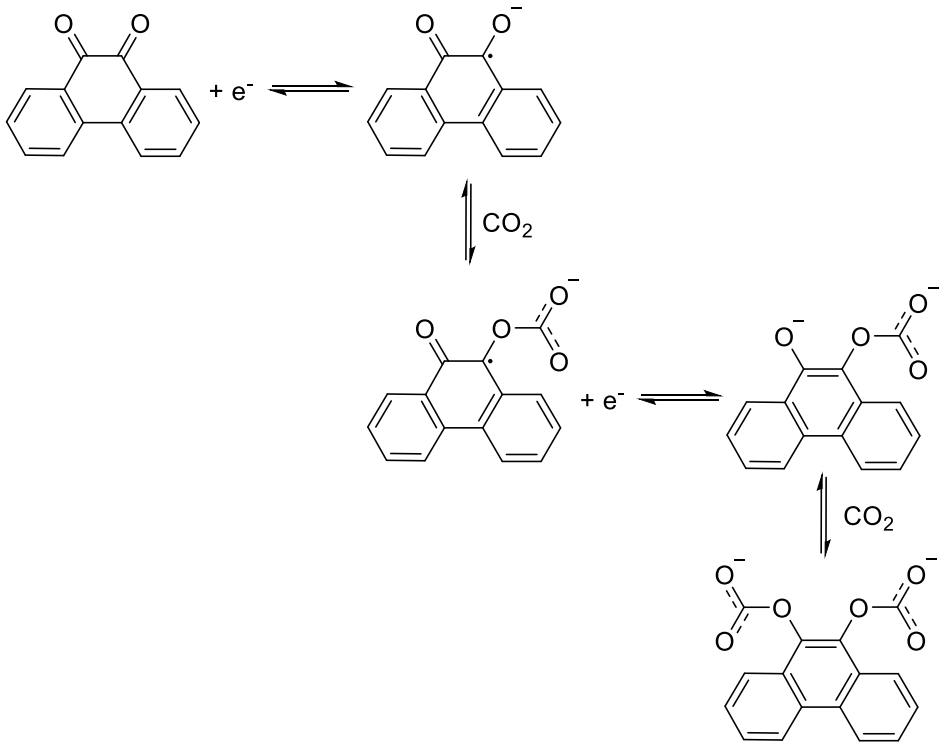


**Scheme 1.** Sequence of reactions showing the capture of $CO_2$ by electrochemically reduced 9,10-phenanthrenequinone (PAQ) proposed in Ref. 74.

partner. This requires that reduction produce substantial electron localization in the reduced product, thereby enhancing its nucleophilicity. Subsequently, $CO_2$ is released by oxidation of the $CO_2$ adduct at a different location, regenerating the organic reactant and producing a pure $CO_2$ stream. The first demonstration of this type of electrochemically driven adduct formation using electrogenerated nucleophiles was by Mizen and Wrighton.[74] Rather than using the redox chemistry of quinones to instigate a pH change, they showed that reduction of 9,10-phenanthrenequinone (PAQ) in aprotic media in the presence of dissolved $CO_2$ produced a bis(carbonate), $[PAQ{\cdot}2CO_2]^{2-}$. Scheme 1 shows the sequence of reactions they proposed for this system, which ultimately produces the bis(carbonate) shown at the lower right of the scheme. The trapping of $CO_2$ in this case relies on the electrochemical reduction of the parent quinone to produce a quinone anion radical with substantial electron density on the quinone oxygen. It is this nucleophilic species that attacks $CO_2$ at the electrophilic carbon. The initial adduct formed is reduced at a more positive potential than the PAQ parent, leading to further reduction and subsequent capture of a second equivalent of $CO_2$. This stepwise scheme ultimately produces the bis(carbonate) adduct shown in Scheme 1. This bis(carbonate) could be subsequently oxidized by two electrons, regenerating the parent quinone and releasing two equivalents of $CO_2$. Thus, electrochemical reduction of the parent quinone produces a potent nucleophile that reversibly captures $CO_2$ with a ratio of one electron required per equivalent of $CO_2$ captured.

Scovazzo *et al.* used a different quinone to show that this same type of reductive nucleophilic trapping and oxidative release could be used to separate $CO_2$ from gas

mixtures.[75] They used 2,6-di-*tert*-butyl-1,4-benzoquinone (DtBBQ) as the precursor to the quinone radical anion that served as the capture agent. Unlike the case studied by Mizen and Wrighton, this quinone required injection of two electrons to capture one equivalent of $CO_2$. This limits the Faradaic efficiency compared to the case for PAQ. Other workers also have explored the use of quinones as trapping agents for $CO_2$ capture. Apaydin and coworkers used thin insoluble films of the industrial pigment quinacridone immobilized on an indium-doped tin oxide electrode to demonstrate electrochemical $CO_2$ capture by the quinone radial anion, with release driven either electrochemically or thermally.[76] Hatton and coworkers used 1,4-naphthoquinone dissolved in the ionic liquid 1-ethyl-1-methylimidazolium tricyanomethanide to separate $CO_2$ from gaseous mixtures.[77] Interested readers should refer to Reference 77 for a schematic of the cell they employed for this purpose. As for the cases described above, $CO_2$ is captured by the radical anion of 1,4-naphthoquinone and released by oxidation of the stable adduct. Hatton also showed that this type of chemistry can be incorporated into a membrane format due to the very low vapor pressure of the ionic liquid. This demonstrates that this type of chemistry can be deployed in a separation format that may be technologically relevant.

In addition to quinone-based nucleophiles, other electrogenerated nucleophiles also can be used for $CO_2$ capture. Ishida *et al.* described an electrochemical cycle in which reduction of N-propyl-4,4'-bipyridinium ($PB^+$), a monoalkylated (quaternized) bipyridinium species, in the presence of $CO_2$ led to formation of a $CO_2$ adduct.[78] The mechanism is shown in Scheme 2. It involves a disproportionation of the one-electron reduced neutral radical, $PB^{\cdot}$, to give $PB^+$ and the two-electron reduced product $PB^-$. This

fully reduced compound then reacts with $CO_2$ to give a previously unreported type of nitrogen-bound $CO_2$ adduct. This adduct is somewhat similar to previously reported carbamates, though it is derived from reduction of a mono-quaternized bipyridinium compound. The adduct was characterized electrochemically and spectroscopically, and its stability was verified using molecular orbital theory calculations. Ishida also showed that electrochemical oxidation of PB-$CO_2^-$ by two electrons caused the release of $CO_2$,

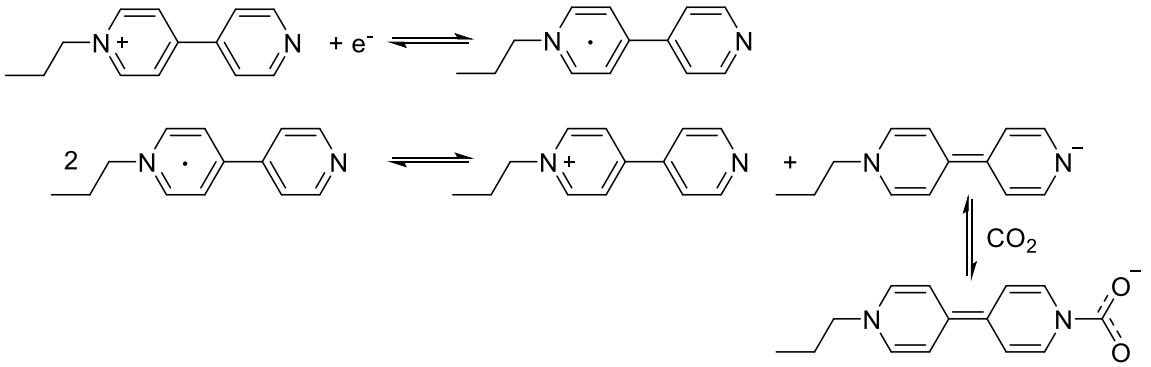

**Scheme 2.** Mechanism of reversible $CO_2$ capture by electrochemically reduced N-propyl-4,4'-bipyridinium ($PB^+$) proposed in Ref. 78.

regenerating the parent $PB^+$ species. Thus, the capture and release was shown to be chemically reversible. As for the DtBBQ case, capture of one equivalent of $CO_2$ requires injection of two equivalents of electrons. This is because one-electron reduction of $PB^+$ produces a PB· neutral radical in which the newly injected electron density is highly localized in the quaternized ring (as shown in Scheme 2). Thus, the PB· radical is not sufficiently nucleophilic to capture $CO_2$. However, because the subsequent reduction of PB· to $PB^-$ is only a few hundred mV more negative than the first reduction and because the binding of $CO_2$ to $PB^-$ is highly favorable, the disproportionation is driven by adduct formation.

Our laboratory recently described a related type of chemistry in which the one-electron reduction of 4,4'-bipyridine (Bipy) produces the $Bipy^{-}$ anion radical, which rapidly binds $CO_2$.[79] Electrochemical oxidation of the resulting Bipy-$CO_2^{-}$ adduct concomitantly regenerates the Bipy parent and releases $CO_2$. The cyclic voltammetric behavior for Bipy in absence and presence of $CO_2$ is shown in Reference 79. In the absence of $CO_2$, Bipy is reduced at –2.3 V in a reversible one- electron process, producing the $Bipy^{-}$ radical anion, which is oxidized on the subsequent positive-going scan near –2.2 V. When $CO_2$ is present, the reduction potential of Bipy is shifted to less negative potential due to the rapid reaction between the reduction product, $Bipy^{-}$, and $CO_2$ to form an adduct. On the subsequent, positive-going scan, a new oxidation peak is observed which corresponds to oxidation of Bipy-$CO_2^{-}$. The stoichiometry for the process reveals that one equivalent of electrons is required for each equivalent of $CO_2$ captured. The first reduction generates a highly nucleophilic radical anion that reacts with $CO_2$ in a nearly activationless process, with a very large second order rate constant ($>10^8$ $M^{-1}$ $s^{-1}$).[79] The resulting bipyridinyl radical-N-carboxylate adduct is likely oxidized at the radical center, which is expected to have facile kinetics due to a lack of a substantial reorganization barrier (i.e. no bond breaking and little solvent reorganization).[80] This produces a zwitterionic intermediate that decarboxylates with a first order rate constant in the range of $10^{10}$ to $10^{11}$ $s^{-1}$, according to high-level computational studies.[79] Thus, in this case, both the oxidative electron transfer step and the decarboxylation are extremely fast, which is an attractive feature for any $CO_2$ separation scheme.

The oxidation potential of Bipy-$CO_2^-$ is substantially positive of the oxidation potential of the $Bipy^-$ radical anion. In part, this shift can be thought of as a reflection of the stability of the N–C bond between $Bipy^-$ and $CO_2$ in the adduct. In other words, an energetic penalty for dissociating the adduct must be paid during oxidation. The difference in the peak oxidation potentials between $Bipy^-$ and Bipy-$CO_2^-$ is 0.85 V. This value is in reasonable agreement with the calculated binding energy of 73 kJ $mol^{-1}$ for the capture of $CO_2$ by $Bipy^-$ using quantum chemical calculations, reinforcing the notion that breaking the N–C bond between the ring system nitrogen and $CO_2$ requires additional energy input for the oxidation process of the adduct. The overall energy cost for the capture and release cycle is governed by the difference in reduction and oxidation potentials at which capture and release occur, –2.0 V and –1.3 V, respectively. Thus, the binding energy of $CO_2$ to $Bipy^-$ is seen to be a substantial factor in the total energy requirement of the capture–release cycle.

Both the quinone- and bipyridine-based approaches discussed above suffer from two undesirable characteristics of these nucleophilic capture agents, namely sensitivity to protonation and sensitivity to dioxygen. With regard to the former, the chemical cycles described above were all carried out under aprotic conditions. This is a strict requirement, because the reduced products are all susceptible to protonation, which would decrease their nucleophilicity, thwarting the desired reaction with $CO_2$. In other words, when protons are available, they out-compete $CO_2$ for the newly created nucleophile, preventing formation of a stable $CO_2$ adduct. The strong basicities of the reduced quinone and bipyridine species thus represent significant disadvantages of these species when considering their use in $CO_2$ capture and release cycles. The second issue

stems from sensitivity to dioxygen. Both the quinone radical anions and the reduced bipyridine species react rapidly with dioxygen.[79, 81] This consumes the newly created nucleophile, rendering it unavailable for reaction with $CO_2$. Furthermore, under aprotic conditions the initial product of these unwanted reactions reaction is superoxide, which participates in complex chemistry with $CO_2$.[82] Also of concern in any quinone-based $CO_2$ capture system is the possibility of the Kolbe-Schmidt ortho-carboxylation reaction, which would render $CO_2$ release impossible.[83] Thus, while interesting from an academic standpoint, neither the quinone-based nor the bipyridine-based capture-release cycles are likely to be technologically applicable.

Another strategy for using redox reactions to generate nucleophiles capable of capturing $CO_2$ was described by Hatton and coworkers.[84] In a process known as Electrochemically Mediated Amine Regeneration, Hatton employed the electrochemical reduction of Cu(II) ethylenediamine complexes to $Cu^0$ metal as a means to release the ligand, thereby generating free nucleophilic amines as the active $CO_2$ capture agents. The free amine binds to $CO_2$, producing a zwitterionic ammonium-carbamate adduct. The cycle operates as follows. A solution of diamine is exposed to $CO_2$ in a purge chamber. After the adduct is formed, the fluid is pumped to the anode chamber. Oxidation of a copper anode produces $Cu^{2+}$, which binds to the diamine, displacing $CO_2$. The cycle is completed by plating $Cu^{2+}$ in a cathode compartment, regenerating the free diamine for another cycle. The chemistry of this approach relies on the very strong binding of the diamine to the metal center, which facilitates release of $CO_2$ via cleavage of the N–C bond. The process was studied in some detail, with authors arguing that $CO_2$ separation could be achieved at an energy cost of less than 100 kJ $mol^{-1}$ using this type of

approach.[84b] This compares favorably with the 170 kJ $mol^{-1}$ reported from a thorough analysis of the MEA process.[66c]

DuBois *et al.* have also proposed the use of transition metal complexes for electrochemical $CO_2$ pumping.[85] In this paradigm, the transition metal complex has an exposed $CO_2$ binding site (a nitrogen or oxygen atom) on one of the ligands. Reduction or oxidation of the complex changes the electron density on the binding sites, thereby increasing or decreasing, respectively, the binding affinity for $CO_2$. Of the compounds studied, which contained Fe, Co, or Ru, binding sites were separated by one, two, or five atoms from the redox active metal center. Only the one-atom compound, a cyclopentadienyl indenyl $Co^{3+}$ complex with an oxygen atom binding site on the indenyl ligand, showed any $CO_2$ capture activity. In another use of metal complexes, DuBois and coworkers described a copper complex that reversibly binds carbonate in the Cu(II) redox state and releases it in the Cu(I) state.[86] This interesting chemistry relies on capture and release of $CO_2$ in the form of carbonate under aqueous conditions. They demonstrated a small scale separation experiment, showing that this chemistry could be used to pump $CO_2$ from a 10% concentration in a mixed gas input stream up to approximately 75% in the exit stream.

We recently described a new type of chemistry for $CO_2$ separation based on the potent nucleophilicity of thiolates.[87] We demonstrated this chemistry using benzylthiolate as a trapping agent for $CO_2$, generating a newly reported sulfur-bound benzylthiocarbonate species. In this approach, the two-electron reduction of benzyl-

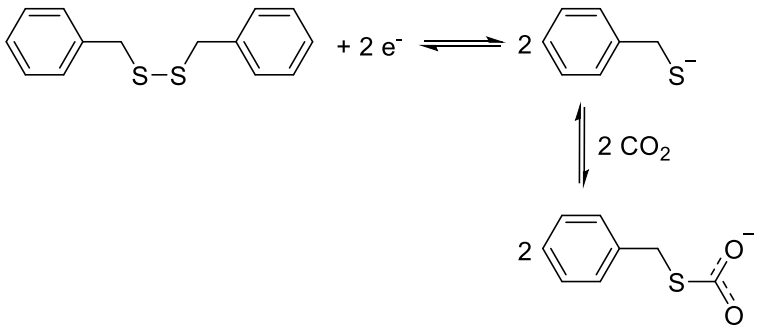


**Scheme 3.** Simplified scheme showing CO2 capture by electrogenerated sulfur nucleophiles from the parent disulfide.

disulfide (BDS) produces two equivalents of benzylthiolate. This species is a potent nucleophile that reacts with $CO_2$ to give *S*-benzylthiocarbonate. Scheme 3 shows a simplified reaction sequence for this process. The binding constant for this $CO_2$ capture process was calculated to be -66 kJ $mol^{-1}$.[87] Terminal thiocarbonates of this type have been reported previously only a few times,[88] and there are no previous descriptions of their electrochemical behavior. This stable $CO_2$ adduct can be electrochemically oxidized, releasing $CO_2$ and regenerating the parent disulfide, BDS. As shown in Scheme 3, each thiolate captures one $CO_2$, meaning that one electron is consumed for each $CO_2$ capture and release event. This is similar to the PAQ and Bipy cases described above, and contrasts with the DtBBQ case which required two electrons per $CO_2$ captured. Electrochemical of the capture-release cycle with BDS in the absence of $CO_2$ can be found in Reference 87. Briefly, in the absence of $CO_2$, after disulfide reduction at –2.2 V, thiolate oxidation occurs on the subsequent scan at –0.8 V. In the presence of $CO_2$ a new oxidation wave is observed at –0.3 V that corresponds to thiocarbonate oxidation. As in the case for Bipy–$CO_2^-$ discussed above, the difference in peak potential between thiolate and thiocarbonate oxidation, 0.5 V, is consistent with the $CO_2$ binding constant of 66 kJ $mol^{-1}$, and reflects the strength of the S–C bond.

The disulfide–thiocarbonate capture–release process is complicated by the detailed nature of the disulfide–thiolate redox mechanism.[89] Equations 13-15 describe the disulfide reduction, which consumes two electrons to produce two equivalents of thiolate. Equations 16 and 17 describe thiolate reoxidation to a thiyl radical intermediate, RS·, followed by radical-radical coupling to regenerate the disulfide. This same thiyl radical is likely produced when the thiocarbonate is oxidized, leading to $CO_2$ release and coupling to regenerate the disulfide. These equations show that the disulfide-thiolate

$$RSSR + e^- \leftrightarrow RSSR^- \quad (13)$$

$$RSSR^- \leftrightarrow RS^{\cdot} + RS^- \quad (14)$$

$$RS^{\cdot} + e^- \leftrightarrow RS^- \quad (15)$$

$$RS^- \leftrightarrow RS^{\cdot} + e^- \quad (16)$$

$$2\ RS^{\cdot} \leftrightarrow RSSR \quad (17)$$

redox couple is not microscopically reversible, i.e. the reaction paths in the reduction and oxidation processes are not the microscopic reverse of each other. The disulfide–thiocarbonate capture–release cycle is further complicated by the extremely slow heterogeneous electron transfer rate of disulfides.[90] Together, these issues lead to very large peak-to-peak separations between the potentials at which $CO_2$ is captured (–2.2 V) and released (–0.8 V). Thus, while the thiolate species is a potent nucleophile, capable of rapid capture of $CO_2$ with a high binding energy for $CO_2$ of –66 kJ $mol^{-1}$, this chemical system is not ideal for $CO_2$ capture because of the large potential difference between the capture and release processes. Further, unwanted side-reactions of the thiyl radical

represent an issue that should be further explored. Nevertheless, these types of thiolates are more attractive than the quinone- and bipyridine-based nucleophiles in part because they are much less basic, and therefore less susceptible to protonation if water is present.

We next briefly discuss the energetic requirements for $CO_2$ capture and release using electrochemical cycles such as those described here. As discussed by Scovazzo *et al.*,[75] the thermodynamic minimum for capture and release of $CO_2$ depends on the initial ($p_i$) and final ($p_f$) pressures for the process according to:

$$\Delta G = RT \ln(p_f/p_i) \quad (18)$$

$$|\Delta E| = RT [\ln(p_f/p_i)] / n F \quad (19)$$

where F is the Faraday constant, n is the number of electrons involved in the capture-release cycle and the other constants have their usual meaning. For a typical case of separation from flue gas (e.g. assuming 10% $CO_2$ at 1 atmosphere) and delivery to a pure gas stream at 1 atmosphere, Equation 18 gives a minimum energy cost of 5.7 kJ $mol^{-1}$ and an expected potential difference between the capture and release redox processes of 0.06 V. This difference in potential can be directly compared with the peak potential differences described above for $CO_2$ capture and release, for example, 0.7 V for the Bipy case (Scheme 2) and 1.4 V for the benzyldisulfide case (Scheme 3). Thus, the intrinsic energy requirements for a $CO_2$ separation cycle are small compared to the cases described above. This is because of the large $CO_2$ binding constants for the quinone, bipyridine and thiolate nucleophiles that have been studied. The implication is that

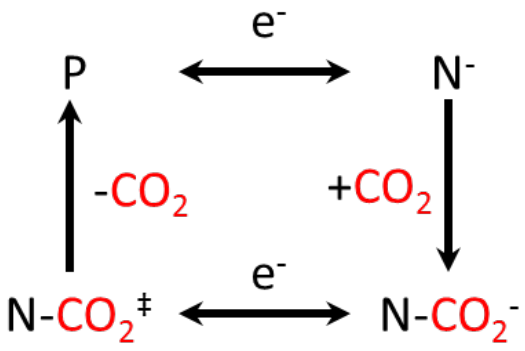


**Figure 3.** Square scheme for a generic $CO_2$ capture agent where P is a reducible precursor to the active $CO_2$ capture species, N. They convention that horizontal steps involve electron transfer and vertical steps involve chemical transformations has been adopted.

electrogenerated nucleophiles with much smaller binding constants will be needed to more closely match experimental results with the constraints imposed by thermodynamics. Further, real experimental systems will have other issues, notably including resistive (IR) losses due to limited electrolyte conductivity between the anode and cathode. These IR losses are also observed in redox flow batteries and comprise one of the primary design criteria for such systems.[91]

One can use a square scheme to consider the efficiencies of electrochemical $CO_2$ capture and release. Figure 3 shows such a scheme for a generic capture agent where we have adopted the convention that horizontal steps involve electron transfer and vertical steps involve capture or release of $CO_2$. Here P is a reducible precursor, $N^-$ is the nucleophilic capture agent, $N–CO_2^-$ is the $CO_2$ adduct, and $N–CO_2^‡$ represents a putative intermediate species generated by oxidation of the adduct. In this scheme, reduction of P produces $N^-$, which rapidly captures $CO_2$ to form the adduct, $N–CO_2^-$. Oxidation of this adduct results in $CO_2$ release and regeneration of the precursor. The oxidation of $N–CO_2^-$ which produces P and free $CO_2$ can occur in a stepwise or concerted manner.

Square schemes have been fruitfully employed in discussions of complex electrochemical mechanisms. A key reason for studying such processes is to differentiate between concerted and stepwise mechanisms. This is important because concerted pathways can bypass high energy intermediates that may be present in stepwise mechanisms. However, as pointed out by Savéant and coworkers, this may lead to sluggish kinetics due to the larger contribution of bond breaking to the electron transfer barrier.[92]

The square scheme in Figure 3 can be used as a framework to consider the Bipy case described above, where the $P/N^-$ redox process (i.e. Bipy/$Bipy^-$) is known to be extremely fast.[80] Further, $CO_2$ capture by $N^-$ is also very fast, as is the oxidative decarboxylation. Thus, the processes leading to $CO_2$ capture and release in this case are quite facile, and, based on the kinetics, the Bipy capture-release cycle appears quite attractive. However, this system also has a serious drawback, which results from the very high binding constant of $CO_2$ to $Bipy^-$. This high binding constant results in a significant positive shift in the oxidation potential for $N–CO_2^-$ (Bipy-$CO_2^-$) compared to $N^-$ ($Bipy^-$), leading to a large potential difference between the capture and release processes. Thus, even though the Bipy system has attractive kinetic features, the $N–CO_2^-$ adduct is simply too stable for this cycle to be practical. Further, the fast reaction between $Bipy^-$ and dioxygen is also a serious issue for this nucleophile, both due to consumption of the $Bipy^-$ nucleophile and production of the reactive superoxide species.

One can use similar thinking to consider the disulfide-thiocarbonate $CO_2$ separation cycle discussed above. There are two issues to consider. First, the potential difference between the capture step ($RS^-$ generation followed by $CO_2$ capture to form the adduct) and the release step (thiocarbonate oxidation) is roughly 2 V for this case. This

represents an energy input of roughly 200 kJ $mol^{-1}$ for the roundtrip capture-release cycle, larger than the value of 170 kJ $mol^{-1}$ for the benchmark MEA process. Second, based on the slow electron transfer kinetics for the disulfide reduction,[90] the thiocarbonate oxidation kinetics are also expected to be sluggish. Disulfide reduction by one electron results in substantial molecular reorganization, specifically the elongation, and eventual cleavage, of the S–S bond. In fact, in this case the inner reorganization energy contributes >60% of the total reorganization energy.[90] If the situation is similar for the Kolbe-like thiocarbonate oxidation (i.e. substantial S-C bond elongation, and ultimate cleavage), one might anticipate sluggish kinetics for the thiocarbonate oxidation. Thus, both the energy efficiency and the rate parameters for the disulfide-thiocarbonate cycle are likely to be poor compared to other systems.

The above considerations offer suggestions regarding the search for better nucleophilic capture agents that are suitable for electrochemical $CO_2$ separation cycles. Such capture agents must possess reversible redox reactions, lack of sensitivity to dioxygen and protonation and, most importantly, have a $CO_2$ binding constant that better matches the thermodynamic minimum energy required for the separation in the target application (see equations 18 and 19). Both the Bipy and disulfide–thiocarbonate systems discussed above suffer from overly large binding constants between the electrochemically generated nucleophiles and $CO_2$. Thus, one desires an ability to tune the interaction between $N^-$ and $CO_2$ to better match the intrinsic energy requirements for the separation process. It may be useful in this regard to make use of existing scales for nucleophilicity, such as that developed by Mayr, even though these are kinetic metrics.[93] It would be especially useful to add $CO_2$ to the list of electrophiles used to develop such a

scale, so that predictions could be made as to the expected reactivity of a wide range of nucleophiles toward $CO_2$. Ultimately, the potential utility of electrochemical approaches to $CO_2$ separation based on electrogenerated nucleophiles will depend on the ability to tune the $CO_2$ binding constants for redox couples with suitable properties. At present, the design space for new capture agents is relatively unexplored.

CHAPTER 3

**Abstract**

We describe a new electrochemical cycle that enables capture and release of carbon dioxide. The capture agent is benzylthiolate ($RS^-$), generated electrochemically by reduction of benzyldisulfide (RSSR). Reaction of $RS^-$ with $CO_2$ produces a terminal, sulfur-bound monothiocarbonate, $RSCO_2^-$, which acts as the $CO_2$ carrier species, much the same as a carbamate serves as the $CO_2$ carrier for amine-based capture strategies. Oxidation of the thiocarbonate releases $CO_2$ and regenerates RSSR. The newly reported *S*-benzylthiocarbonate (IUPAC name benzylsulfanylformate) is characterized by $^1H$ and $^{13}C$ NMR, FTIR and electrochemical analysis. The capture-release cycle is studied in the ionic liquid (IL) 1-butyl-1-methylpyrrolidinium bis(trifluoromethylsulfonyl)imide (BMP TFSI) and dimethylformamide (DMF). Quantum chemical calculations give a binding energy of $CO_2$ to benzyl thiolate of –66.3 kJ $mol^{-1}$, consistent with the experimental observation of formation of a stable $CO_2$ adduct. The data described here represent the first report of electrochemical behavior of a sulfur-bound terminal thiocarbonate

---

Climate impacts from high atmospheric $CO_2$ concentrations due to carbon-based fuel combustion continue to drive high levels of research activity in carbon capture and sequestration (CCS).[94] A number of approaches have been described for carbon capture, both at point sources such as power plants (postcombustion $CO_2$ capture) and directly from the atmosphere (direct air capture). Many of these approaches rely on chemical interaction between an electron rich nucleophile and $CO_2$ to form some type of adduct. One of the best known approaches in this vein involves reaction of amines with $CO_2$ to

give carbamates.[95] This chemistry can be carried out in basic aqueous solutions containing amines, with amines immobilized onto various types of solid supports, or with other solid or liquid media containing amine groups, such as ionic liquids.[95] In most such cases the release of $CO_2$ to recycle the capture agent requires heat. Few other chemistries have been described that enable reversible $CO_2$ capture. Thus, there is interest in exploring new methods for $CO_2$ capture. In addition, there is a broader need to more fully explore the chemistry of $CO_2$, and especially to explore the chemistry of compounds that form adducts with $CO_2$.

Several research efforts have explored approaches to capture $CO_2$ using electrochemically generated nucleophiles. Mizen and Wrighton demonstrated that electrochemical reduction of quinones under aprotic conditions produces radical anions capable of $CO_2$ capture at the quinone oxygen, producing aromatic carbonates.[74] They also showed that the resulting carbonates could be electrochemically oxidized, regenerating the quinone species and releasing $CO_2$. This stimulated a number of groups to explore $CO_2$ capture using quinones.[75-77] In a related approach, release of amine ligands from Cu(II) amine complexes by electrochemical reduction to Cu metal can be used to drive $CO_2$ capture via carbamate formation, connecting the traditional amine capture agent approach with the superior energetics inherent in electrochemical cycling.[84a] In a recent report, we examined the reaction between 4,4'-bipyridine radical anion (which can be produced either electrochemically or photochemically) and carbon dioxide, demonstrating formation of a unique N-bound $CO_2$ adduct species.[79] One electron oxidation of the adduct releases $CO_2$ and regenerates 4,4'-bipyridine. All of these systems demonstrate chemically reversible electrochemical capture and release of

$CO_2$. Their common theme is that electrochemical reduction of a precursor is employed to either directly generate or cause the release of a potent nucleophile that is capable of attacking the electrophilic carbon atom in $CO_2$, thereby forming an adduct. A subsequent oxidation process leads to $CO_2$ release and regeneration of the precursor to the capture agent. For the quinone and bipyridine cases, release is accomplished by oxidation of the adduct itself.

We describe here a new chemistry for electrochemical $CO_2$ capture and release that employs reduction of organic disulfide precursors to generate thiolate species that are potent nucleophiles toward $CO_2$. We show that benzylthiolate can bind $CO_2$ to form a sulfur-bound thiocarbonate and that subsequent oxidation of the thiocarbonate leads to release of $CO_2$ and regeneration of the disulfide. We are aware of only a few previous reports of S–bound terminal thiocarbonates,[88b, 88c, 96] and no previous reports of their electrochemical properties. In most of this study, the electrochemical capture and release of $CO_2$ is pursued in ionic liquid media. A substantial literature exists on capture of $CO_2$ using ionic liquids containing amines and other nucleophilic functional groups.[97] Their low volatility and suitability as electrochemical solvents makes ionic liquids especially useful as supporting electrolytes in the present study. In some experiments we also employ dimethylformamide (DMF) as solvent, demonstrating the broader applicability of this chemistry to more traditional solvents. The reasonable solubilities of benzyldisulfide in BMP TFSI and DMF (106 mM and 2 M, respectively) allow for facile electrochemical and synthetic experimentation.

Figure 4 shows a cyclic voltammogram (CV) of the reduction of benzyldisulfide (BDS) in BMP TFSI at a concentration of 20 mM. Reduction gives a well-formed

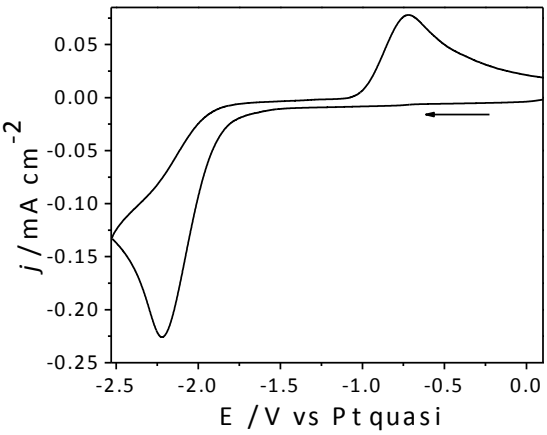


**Figure 4.** Cyclic voltammetry of 20 mM benzyldisulfide in BMP TFSI IL; working-glassy carbon electrode (GCE), reference and counter- Pt, scan rate-10 mV/s.

voltammetric wave with a peak potential near –2.2 V. This overall two-electron reduction process is as expected for reduction of organic disulfides, producing two equivalents of the corresponding thiolate.[98] Oxidation of the benzylthiolate that is produced is seen on the return scan as an oxidation wave with a peak potential of –0.7 V. The significant difference between the peak currents for disulfide reduction and thiolate oxidation is likely due to significant differences in diffusion coefficients for these two species. A similar phenomenon has been previously reported for the dioxygen/superoxide and ferrocene/ferrocenium redox couples in ionic liquids, and attributed to significantly lower diffusion coefficients for charged species compared to neutrals.[99] The large peak separation between disulfide reduction and thiolate oxidation results from the fact that this redox mechanism is not microscopically reversible. We explored the mechanism of this process in some detail previously for a related disulfide/thiolate redox couple.[89] Briefly, reduction initially produces the $RSSR^{-}$ radical anion. This species dissociates to produce one equivalent each of $RS^{-}$ and $RS\cdot$ (i.e. thiolate and thiyl radical).[100] The rapid electrochemical reduction of $RS\cdot$ produces a second equivalent of $RS^{-}$. On the

subsequent positive-going scan oxidation of the thiolate initially produces RS·, two of which rapidly couple to regenerate the parent disulfide. Subsequent work has confirmed the mechanistic aspects of this redox process, as well as providing more details about the nature of the dissociative electron transfer of the disulfides.[101] For the present purposes, a key feature of the disulfide reduction is that it produces thiolates, which are well known as potent nucleophiles, and have been previously reported to react with $CO_2$ to give S–bound thiocarbonates.[88b, 88c, 96]

Figure 5 shows the results of several experiments in 20 mM BDS in BMP TFSI in which the concentration of dissolved $CO_2$ was serially increased by increasing the $CO_2$ partial pressure in a purging gas stream comprising a mixture of $N_2$ and $CO_2$. As $[CO_2]$ is increased, the benzylthiolate oxidation peak at –0.7 V is decreased. At the same time, a new oxidation peak appears at –0.3 V. As will be shown further below, this new

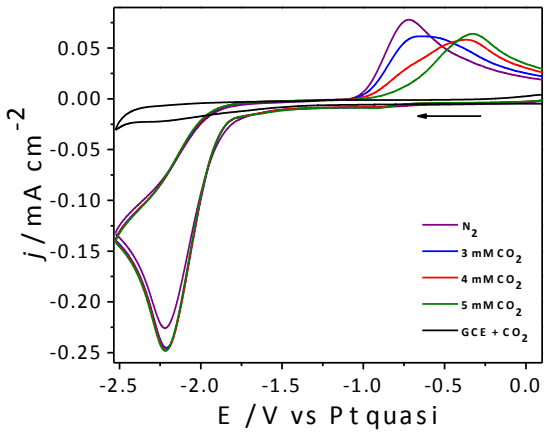


**Figure 5.** Cyclic voltammetry of 20 mM benzyldisulfide in BMP TFSI IL with different concentrations of $CO_2$; $N_2$ (purple), 3 mM $CO_2$ (blue), 4 mM $CO_2$ (red), 5 mM $CO_2$ (green), 100 mM $CO_2$ in absence of BDS in IL (black); working-GCE, reference and counter - Pt, scan rate -10 mV/s.

oxidation peak corresponds to oxidation of *S*-benzylthiocarbonate, $RSCO_2^-$. This is the first report of electrochemical behavior for a terminal S-bound thiocarbonate species. Figure 5 also shows a background CV at a glassy carbon electrode in pure BMP TFSI at 100 mM $CO_2$ but containing no BDS, demonstrating that $CO_2$ is electrochemically inactive at glassy carbon over the potential range shown in the CV. For comparison, Figure S7 shows the chemically irreversible reduction of $CO_2$ at Au over this same range of potentials, demonstrating a large reduction peak for $CO_2$ at –2.3 V. The lack of $CO_2$ electroactivity at glassy carbon over this potential range is likely due to the absence of strong adsorption at this surface. We take advantage of this lack of reactivity to explore the interactions between thiolates and $CO_2$ without interference by direct $CO_2$ reduction. The observation that 5 mM $CO_2$ is sufficient to completely eliminate the oxidation response from 40 mM benzylthiolate (produced by reduction of 20 mM BDS) is attributed to the much faster diffusion of $CO_2$ than benzylthiolate in the IL, similar to the discussion above regarding dissimilar diffusion coefficients.[99] In other words, the rapid diffusive transport of $CO_2$ to the region near the electrode allows a 5 mM $CO_2$ solution to provide sufficient $CO_2$ to completely consume the higher concentration of electrochemically generated thiolate through formation of the thiocarbonate.

The reversibility of the uptake of $CO_2$ by thiolate and release by thiocarbonate oxidation was also examined. Figures S8 and S9 show that the new thiocarbonate oxidation peak at -0.3 V can be caused to appear or disappear simply by purging a BDS solution in BMP TFSI with a $CO_2$-rich or $N_2$-rich gas stream, respectively, prior to a cyclic voltammetric scan over the disulfide reduction wave. This shows that the $CO_2$ capture and release cycle is chemically reversible under the conditions of these

experiments. Figure S10 shows the scan rate dependence of the capture and release cycle at a concentration of $CO_2$ sufficiently high to consume all of the thiolate produced during the reduction. The discussion of the Figure in the Supporting Information describes the mechanistic details of the adduct formation, revealing that it is not a simple EC type of mechanism due to the complexity of the RSSR reduction pathway.[102]

In order to show that the oxidation peak at –0.3 V is caused by a thiocarbonate species, the voltammetry of authentic samples of benzylthiolate and *S*-benzylthiocarbonate were directly compared. Figure 6 shows the results of cyclic voltammetric experiments in which authentic samples of the $P_{4444}^+$ salts of benzylthiolate and *S*-benzylthiocarbonate were sequentially added to DMF supporting electrolyte in equimolar amounts. Preparation and characterization of these samples are described in

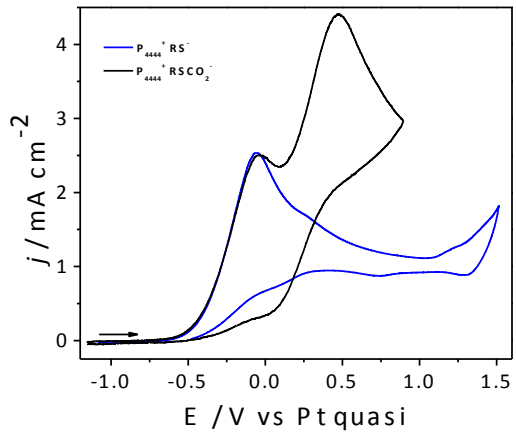


**Figure 6.** Cyclic voltammetry of 30 mM $P_{4444}^+$ $RS^-$ (blue) and 30 mM $P_{4444}^+$ $RSCO_2^-$ (black) in 0.1 M TBAP in DMF; working-GCE, reference and counter - Pt, scan rate- 50 mV/s

Supporting Information. As can be seen, the two species exhibit different oxidation potentials. The benzylthiolate oxidation peak is observed at –0.1 V. The *S*-benzylthiocarbonate oxidation peak is observed at +0.4 V, shifted in the positive direction

by 0.5 V compared to the thiolate oxidation peak. Figure S11 shows the CV for an equimolar solution of the $P_{4444}^{+}$ salts of benzylthiolate and *S*-benzylthiocarbonate in $P_{4444}$ TFSI. Again, one can see that the two species are oxidized at different potentials, though the broadness of the peaks in this much higher viscosity IL makes the individual responses less resolvable. The results in Figures 6 and S11 are consistent with the interpretation that the new oxidation observed in Figure 5 when $CO_2$ is dissolved into the IL solution is due to the appearance of a thiocarbonate species that is more difficult to oxidize than the thiolate.

To further demonstrate uptake and release of $CO_2$ for this system, we performed bulk electrolysis experiments in which purge gases were swept through the cell to monitor $CO_2$ uptake and release using a non-dispersive $CO_2$ gas sensor downstream from the cell. In Figure S12 we show the results of a reductive bulk electrolysis of benzyldisulfide in the presence of a flowing stream of 350 ppm $CO_2$ in $N_2$. The figure shows that $CO_2$ in the purge gas stream is completely consumed when reductive current is passed in the working electrode chamber, which produces benzylthiolate that subsequently reacts with $CO_2$. In Figure S13 we show the results of a quantitative oxidative bulk electrolysis of a sample of *S*-benzylthiocarbonate. In this experiment, we monitor the evolution of $CO_2$ during oxidation by sweeping it from the cell in a stream of pure $N_2$ and detecting it downstream. The right plot in the Figure shows that moles of e- (from the oxidative charge) and moles of $CO_2$ released (from integration of the sensor signal) are equal within experimental error. Except for a short lag time due to the transit time to the detector, the $CO_2$ release is seen to be coincident with the accumulation of oxidative charge. This plot shows clearly that $CO_2$ release in this experiment is due to

oxidation of the thiocarbonate, and that one equivalent of $CO_2$ is released for each equivalent of oxidative charge. Taken together, the results confirm that electrochemical generation of benzylthiolate in the presence of $CO_2$ produces *S*-benzylthiocarbonate. Oxidation of this thiocarbonate releases $CO_2$ and regenerates the disulfide, which can be observed on the following negative-going scan via its reduction as evidenced by the continuous scans in Figures S8 and S9. These observations show that oxidation of a terminal S-bound thiocarbonate is similar to the well-known Kolbe oxidation of organic carboxylates, where oxidation results in decarboxylation.[103] Thus, these results are consistent with the electrochemical capture and release of $CO_2$ as mediated by the disulfide/thiocarbonate redox couple.

Quantum chemical calculations at the B3LYP/aug-cc-pVQZ level were also used to understand the nature of the interaction between the thiolate and $CO_2$ and the stability of the thiocarbonate. Figure 7 shows the results of such a calculation done at the B3LYP/aug-cc-pVDZ level on *S*-benzylthiocarbonate. Calculations at this level of theory

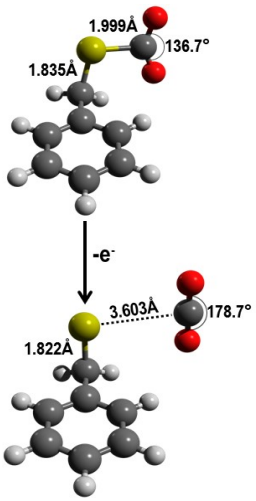


**Figure 7.** Quantum mechanical calculation of S-benzylthiocarbonate done at B3LYP/aug-cc-pVQZ level. S (yellow), O (red), H (light gray), C (dark gray).

were found to yield good agreement with experimental enthalpies of sulfur containing compounds.[104] The figure shows the minimized geometry of the thiocarbonate (upper structure). The C–S bond length is 1.999 Å, and the enthalpy calc-ulated for the binding of $CO_2$ to the thiolate is –66.3 kJ/mol. This enthalpy for binding shows formation of a stable S-bound terminal thiocarbonate for this case. These respective quantities are within the range expected for C-S single bonds and for other stable $CO_2$ adducts.[105] The OCO bond angle of 136.7° indicates considerable rehybridization around carbon resulting from strong interaction with the sulfur center. Thus, the quantum chemical calculations support the formation of a stable S-bound thiocarbonate from the reaction between benzylthiolate and carbon dioxide.

Figure 7 also shows the minimized geometry of the thiocarbonate after removal of one electron. The S–$CO_2$ bond length is dramatically elongated at 3.603 Å, and the OCO bond angle is increased to 178.7$^o$. These values confirm that there is essentially no bonding interaction of the $CO_2$ moiety with the S atom after oxidation, consistent with the release of $CO_2$ after oxidation. Figure S14 shows the HOMO and HOMO-1 electron density maps for the thiocarbonate. These orbitals are quasi-degenerate,[106] and show significant bonding electron density between the S atom and the carboxylate C atom. Thus, one electron oxidation should lead to destabilization of the S–C bond. This is similar to C–C bond cleavage leading to decarboxylation in Kolbe oxidation products, such as $H_3CCO_2\cdot$, the acetyloxyl radical.[107] In summary, these computational studies support the experimental results showing the formation of a stable terminal thiocarbonate from reaction of benzylthiolate and $CO_2$. They also show that thiocarbonate oxidation results in cleavage of the S–$CO_2$ bond, producing a benzyl thiyl radical (two of which

will then couple to form disulfide) and free $CO_2$. This is similar to the oxidative dissociation of $CO_2$ previously reported for the adduct between the 4,4'-bipyridine radical anion and $CO_2$, where oxidation from the HOMO leads directly to N–C bond scission and release of 4,4'-bipyridine and $CO_2$.[79] More extensive calculations on a range of benzyl and phenyl thiocarbonate derivatives, to be reported elsewhere, reveal that the energy for binding of $CO_2$ to the $RS^-$ species depends on the electron density on the sulfur atom in $RS^-$, implying that the enthalpy of $CO_2$ binding can be tuned through judicious choice of structural features on $RS^-$.

We have demonstrated a completely new type of chemically reversible, electrochemical process for capture and release of $CO_2$ based on an organic disulfide/thiocarbonate redox couple. These data also comprise the first report of the electrochemical behavior for terminal S-bound thiocarbonates. Quantum chemical calculations are consistent with the capture of $CO_2$ by $RS^-$, producing a stable thiocarbonate, and release of $CO_2$ after oxidation of the thiocarbonate. Additional experiments are underway to explore $CO_2$ separations based on this chemistry.

---

CHAPTER 3 SUPPLEMENTARY INFORMATION

## Experimental Details

### *General Considerations*

All manipulations were carried out using standard Schlenk or glovebox techniques under a nitrogen atmosphere. Solvents were purified and dried according to literature procedures,[108] degassed by four successive freeze-pump-thaw cycles, and stored in the glovebox. Deuterated solvents were purchased from Cambridge Isotope Laboratories, Inc., degassed by four successive freeze-pump-thaw cycles and stored in the glovebox. All other reagents and starting materials were purchased from commercial vendors and used without further purification unless otherwise noted. Compressed gas cylinders were furnished by Praxair, Inc.

### *Physical Methods*

$^{1}$H and $^{13}$C NMR spectra were collected on Varian 400 and 500 MHz NMR spectrometers. The $^{13}$C NMR spectrum of tetrabutylphosphonium *S*-benzylthiocarbonate was collected on a Brüker Ultra-Shield 600 MHz NMR spectrometer equipped with a cryoprobe. $^{1}$H and $^{13}$C NMR spectra are reported in parts per million relative to tetramethylsilane, using the residual solvent resonances as an internal standard.[109] FTIR measurements were performed on a Brüker Alpha spectrometer equipped with a diamond ATR. Residual water content of solvents and ionic liquids were measured with a Mettler Toledo C20 Coulometric KF Titrator. Electrochemical measurements were performed with a CH Instruments 618C Electrochemical Analyzer. Cyclic voltammograms were acquired using a glassy carbon working electrode, platinum counter electrode, and platinum quasi-reference electrode either in the glovebox or under a complex gas stream

consisting of dinitrogen, carbon dioxide, and/or dioxygen. All potentials are referenced to this Pt quasi-reference electrode, which was used in preference to conventional reference electrodes to prevent contamination of the supporting electrolyte by compounds that typically leach from other reference half cells. For comparison, the ferrocene/ferrocenium redox couple is observed at +0.20 V on this reference scale. Gas mixtures were generated from compressed gas cylinders whose output was controlled with Cole-Parmer PRM1-010547 gas flow regulators and measured using an Agilent Technologies ADM 2000 Universal Gas Flowmeter.

For bulk electrolysis experiments, a modified H-cell was used with airtight gas ports. The electrodes comprised a 1 cm x 2 cm x 0.3 cm glassy carbon working electrode, Pt mesh counter electrode and Ag/AgCl reference electrode. $CO_2$ measurements were made using a K-30 $CO_2$ sensor (www.co2meter.com). Specific details are given for the individual experiments described below.

**Computational Details**

Calculations using density functional theory (DFT) were carried out using the Becke gradient-corrected exchange functional and Lee−Yang−Parr correlation functional with three parameters (B3LYP) and the 6-31+G*, aug-cc-pVDZ, and aug-cc-pVQZ basis sets using the ORCA and Gaussian suites of programs.[110] Calculations at this level of theory have been found to yield energies and spectroscopic parameters comparable to those obtained with higher levels of theory.[104, 111]

**Syntheses**

Tetrabutylphosphonium benzylthiolate

For a typical experiment, 5.1906 g of tetrabutylphosphonium hydroxide solution (40 wt. % in $H_2O$, 7.5 mmol) was added to a Schlenk flask equipped with a stir bar and placed under vacuum overnight. The resulting white solid (tetrabutylphosphonium hydroxide) was then placed under a dinitrogen atmosphere and a 12.5 mL volume of methanol was added to the flask via syringe. After stirring for one hour, 1.1 mL of benzylthiol (9.4 mmol) that had undergone four successive freeze-pump-thaw cycles was added via syringe to the clear, stirring solution. The solution was allowed to stir under nitrogen for a minimum of four hours, then placed under vacuum at 50 $^{o}$C overnight. The product was isolated as a clear, viscous liquid in quantitative yield. $^{1}$H NMR (500 MHz, $CDCl_3$) in Figure S1: $\delta$ = 7.31–7.27 (m, 5 H), 3.73 (s, 2 H), 1.69–1.63 (m, 8 H), 1.56–1.52 (m, 8 H), 1.44–1.39 (m, 8 H), 0.94–0.91 (t, $J$ = 7.30 Hz, 12 H). $^{13}$C {$^{1}$H} NMR (125 MHz, $CDCl_3$) in Figure S2: $\delta$ = 141.29, 128.74, 128.09, 127.08, 29.06, 28.08–27.57 (d, $J^{13}_{C}$–$^{31}_{P}$ = 65.0 Hz), 24.47–24.35 (d, $J^{13}_{C}$–$^{31}_{P}$ = 14.2 Hz), 23.90, 13.73. FTIR (cm$^{-1}$) in Figure S5: 3054 (w), 3019 (w), 2959 (s), 2932 (s), 2871 (s), 1596 (w), 1489 (m), 1464 (m), 1412 (w), 1301 (w).

Tetrabutylphosphonium S-benzylthiocarbonate

Carbon dioxide that had passed through a drying column was bubbled into stirring tetrabutylphosphonium benzylthiolate at room temperature for 15 minutes. The flask was then sealed and the material was allowed to stir under a $CO_2$ atmosphere for four hours. A white solid was recovered in quantitative yield. $^{1}$H NMR (500 MHz, $CDCl_3$) in Figure S3: $\delta$ = 7.34–7.32 (m, 2 H), 7.19–7.15 (m, 2 H), 7.09–7.07 (m, 1 H), 3.95 (s, 2 H), 2.27–

2.21, (m, 8 H), 1.45–1.44 (m, 16 H), 0.92–0.90 (t, $J$ = 7.30 Hz, 12 H). $^{13}C$ {$^{1}H$} NMR (150 MHz, $CDCl_3$) in Figure S4: $\delta$ = 162.82, 142.72, 128.69, 128.04, 125.81, 24.05–23.84 (d, $J^{13}_{C}$–$^{31}_{P}$ = 31.5 Hz), 23.95–23.81 (d, $J^{13}_{C}$–$^{31}_{P}$ = 21.4 Hz), 18.93–18.62 (d, $J^{13}_{C}$–$^{31}_{P}$ = 46.5 Hz), 13.53. FTIR ($cm^{-1}$) in Figure S6: 3066 (w), 3027 (w), 2955 (s), 2929 (s), 2869 (s), 1670 (vs), 1600 (w), 1582 (w), 1494 (m), 1454 (m), 1414 (m), 1377 (w), 1317 (w), 1289 (m), 1246 (m), 1217 (m).

1-Butyl-1-methylpyrrolidinium bis(trifluoromethylsulfonyl)imide (BMP TFSI)

In a 500 mL round bottom flask equipped with a stir bar, 100.00 g of 1-butyl-methylpyrrolidinium chloride (0.563 mol) was added to 250 mL of deionized water and allowed to stir until the solid had completely dissolved. To the stirring solution, 161.55 g of lithium bis(trifluoromethane)-sulfonimide (0.563 mol) was added all at once and allowed to stir for two hours, during which time a viscous liquid collected at the bottom of the flask. The contents of the flask was poured into 500 mL of dichloromethane in a separatory funnel and washed with water (3 x 100 mL), the organic phase was isolated, and the dichloromethane was removed by rotary evaporation. Activated carbon was added to the clear, viscous liquid and the suspension was stirred under vacuum at 70 $^{o}$C for four days. BMP TFSI was isolated by passing the warm suspension through a plug of Celite in a fritted glass funnel to remove the activated carbon. Excess water was removed by heating the product at 100 $^{o}$C for 48 hours (< 3 ppm by Karl Fischer titration), and the ionic liquid was stored in the glovebox.

Tetrabutylphosphonium bis(trifluoromethylsulfonyl)imide ($P_{4444}$ TFSI)

In a 500 mL round bottom flask equipped with a stir bar, 150.00 g of tetrabutylphosphonium bromide (0.465 mol) was added to 250 mL of deionized water

and allowed to stir until the solid had completely dissolved. To the stirring solution, 133.59 g of lithium bis(trifluoromethane)-sulfonimide (0.465 mol) was added all at once and allowed to stir for two hours, during which time a viscous liquid collected at the bottom of the flask. The contents of the flask was poured into 500 mL of dichloromethane in a separatory funnel and washed with water (3 x 100 mL), the organic phase was isolated, and the dichloromethane was removed by rotary evaporation. Activated carbon was added to the clear, viscous liquid and the suspension was stirred under vacuum at 70 $^{o}$C for four days. $P_{4444}$ TFSI was isolated by passing the warm suspension through a plug of Celite in a fritted glass funnel to remove the activated carbon. Excess water was removed by heating the product at 100 $^{o}$C for 48 hours (< 3 ppm by Karl Fisher titration), and the ionic liquid was stored in the glovebox.

**Characterization of Thiolate and Thiocarbonate Compounds**

Figures S1 – S6 show $^{1}$H, $^{13}$C and FTIR spectra for the synthesized and purified salts of tetrabutylphosphonium thiolate and tetrabutylphosphonium *S*-benzylthiocarbonate. $^{1}$H NMR of the thiocarbonate (Figure S3) revealed the expected downfield shift of the benzyl proton signal as compared to that of the thiolate (from 3.73 to 3.95 ppm). $^{13}$C NMR of the thiocarbonate (Figure S4) shows a new signal at 162.82 ppm for the carboxylate carbon in the thiocarbonate. The FTIR spectrum of tetrabutylphosphonium *S*-benzyl thiocarbonate (Figure S6) is very similar to that of tetrabutylphosphonium benzylthiolate (Figure S5) except for the very strong peak at 1670 cm$^{-1}$, which is due to the OCO asymmetric stretch of the thiocarbonate. These data are all in good agreement with the solid state NMR and IR results obtained by Stueber et al. who examined $KO_2CSCH_3$ and $KO_2CSCH_2CH_3$.[88c] Both of the previously reported

compounds showed very strong IR features at 1617 and 1583 $cm^{-1}$, and solid state $^{13}C$ NMR signals between 170–171 ppm for the $O_2$***C***SR carbons. Although the previous authors' attempts to obtain solution phase NMR data of the potassium methyl- and ethyl-thiocarbonates were unsuccessful, the general trend they observed is an upfield shift of the relevant $^{13}C$ NMR signals as compared to the corresponding solution phase measurements of similar compounds.

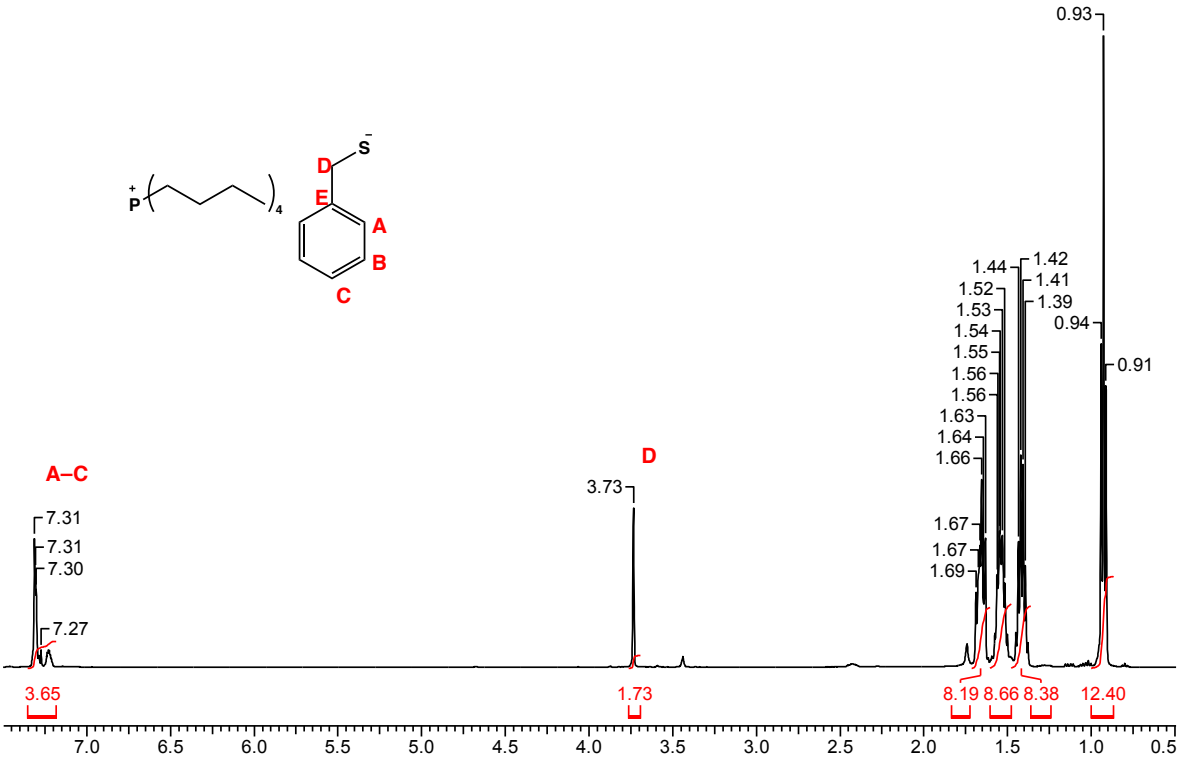


**Figure S1.** $^{1}H$ NMR of tetrabutylphosphonium benzylthiolate.

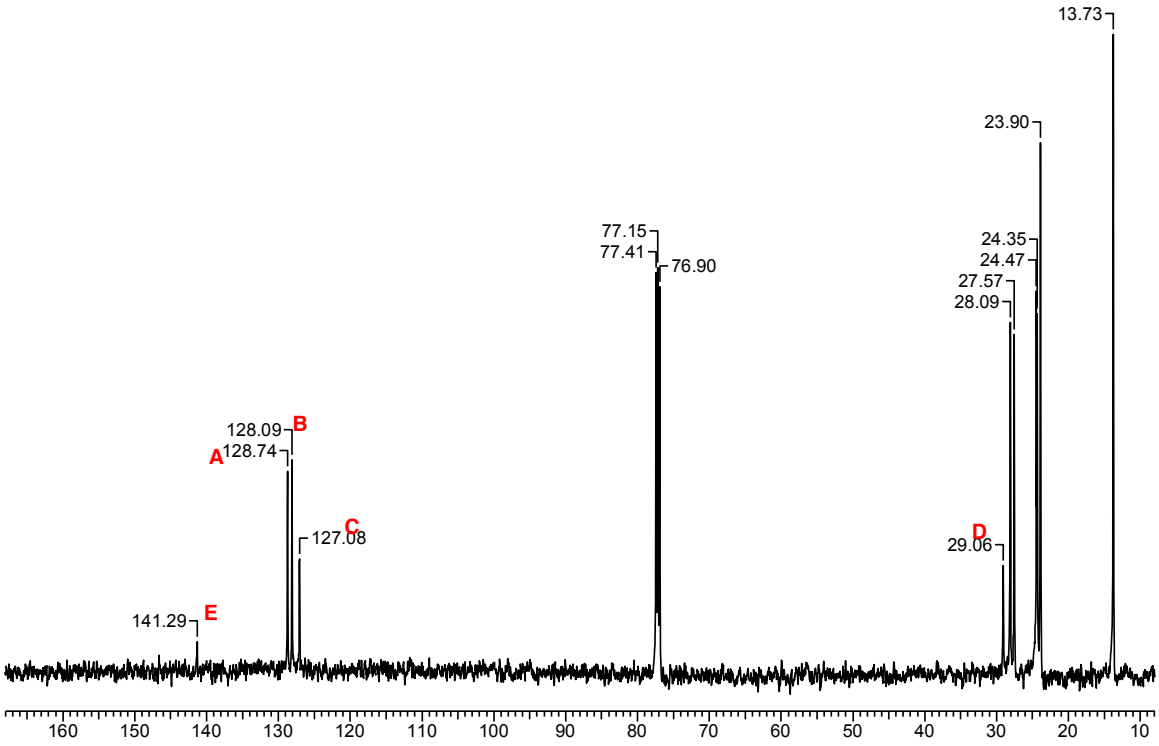


**Figure S2.** $^{13}$C NMR of tetrabutylphosphonium benzylthiolate.

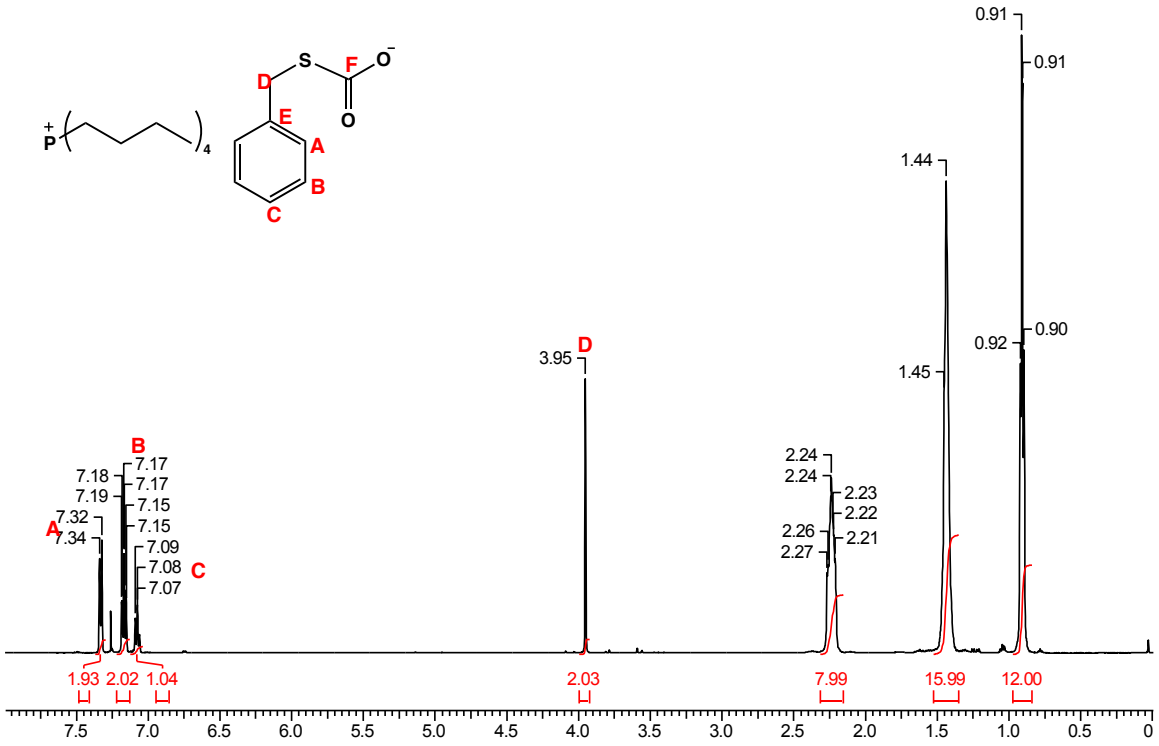


**Figure S3.** $^{1}$H NMR of *S*-benzylthiocarbonate.

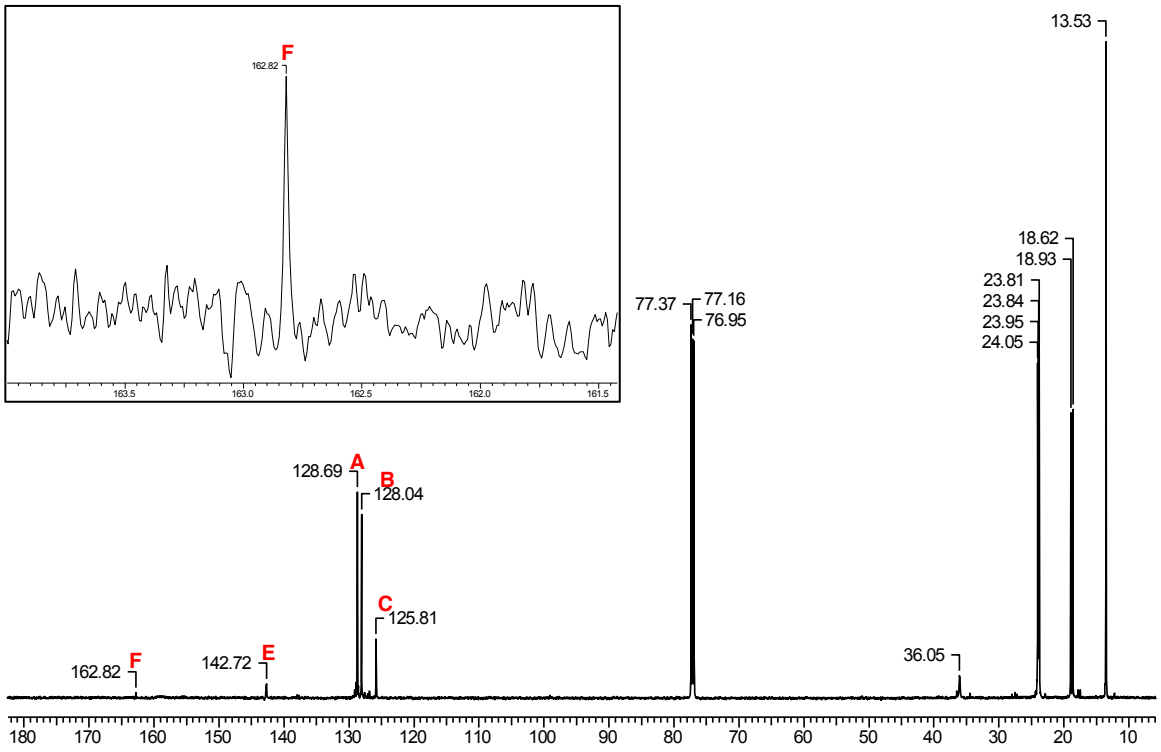


**Figure S4.** $^{13}$C NMR of *S*-benzylthiocarbonate.

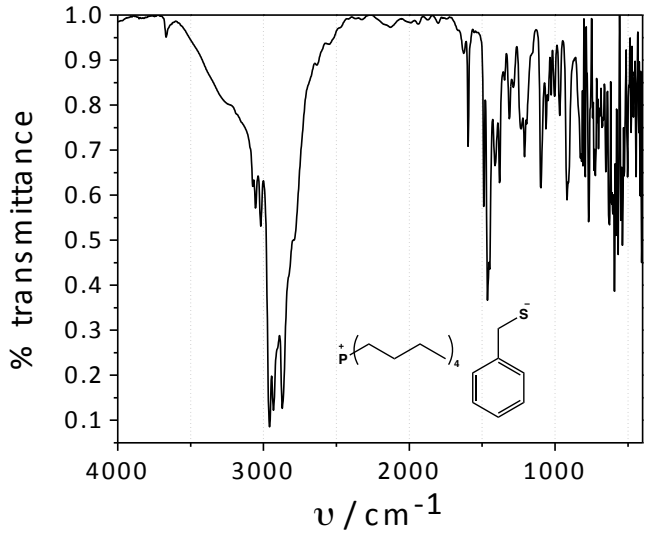


**Figure S5.** FTIR of tetrabutylphosphonium benzylthiolate.

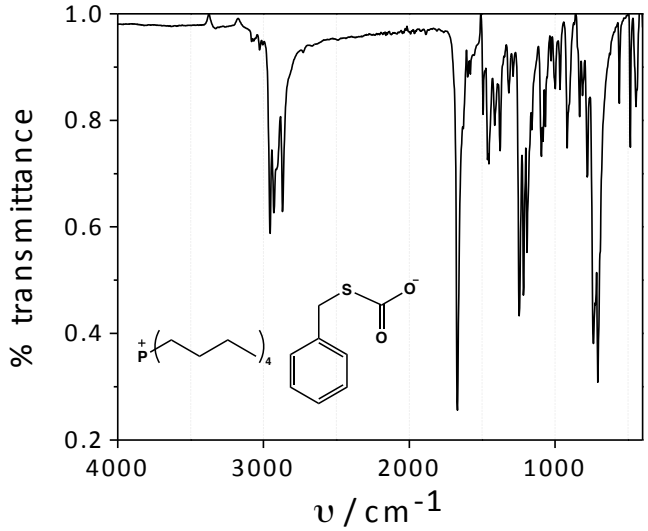


**Figure S6.** FTIR of tetrabutylphosphonium *S*-benzylthiocarbonate. Note the very strong feature at 1670 $cm^{-1}$ due to the $–CO_2^-$ asymmetric stretch.[88c]

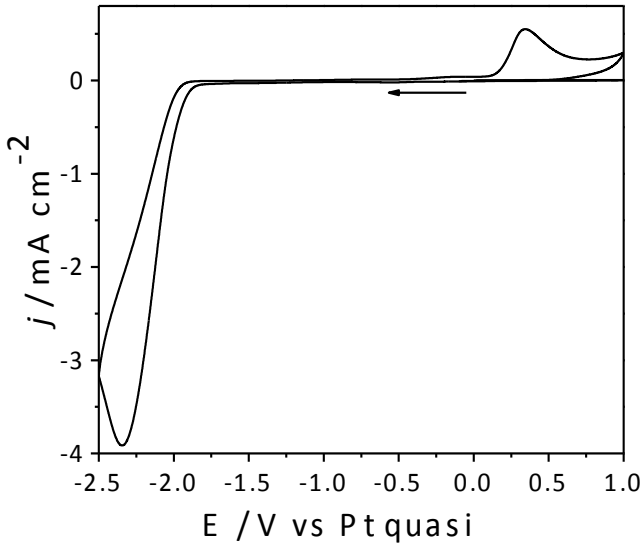


**Figure S7.** Cyclic voltammetry in $CO_2$ saturated (100 mM) BMP TFSI IL at Au electrode , reference and counter - Pt, scan rate -50 mV/s.

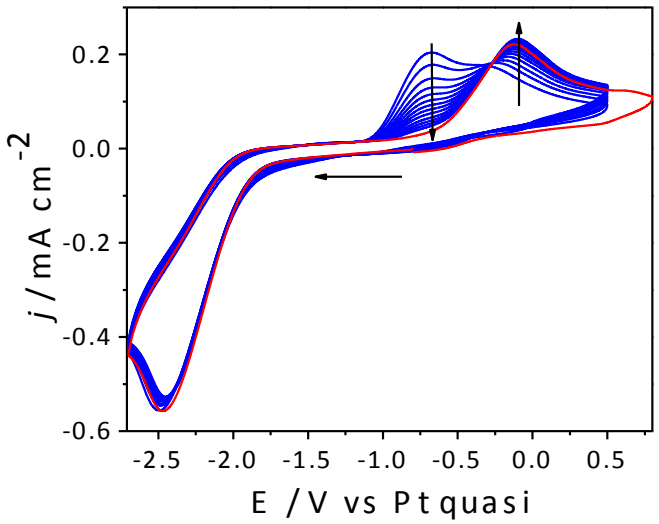


**Figure S8.** Cyclic voltammetry of 20 mM benzyldisulfide in BMP TFSI IL under $N_2$ (blue) to 8% $CO_2$ (red) with constant stirring and purging; working-GCE, reference and counter - Pt , scan rate – 100 mV/s.

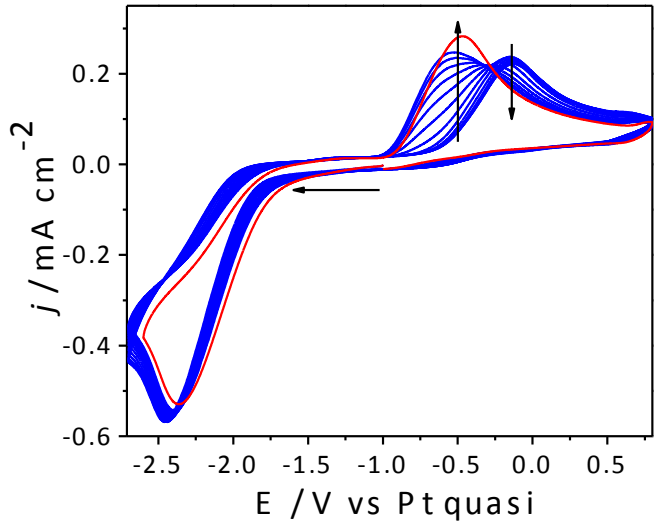


**Figure S9.** Cyclic voltammetry of 20 mM benzyldisulfide in BMP TFSI IL under 8% $CO_2$ (blue) to $N_2$ (red) with constant stirring and purging; working-GCE, reference and counter - Pt, scan rate – 100 mV/s.

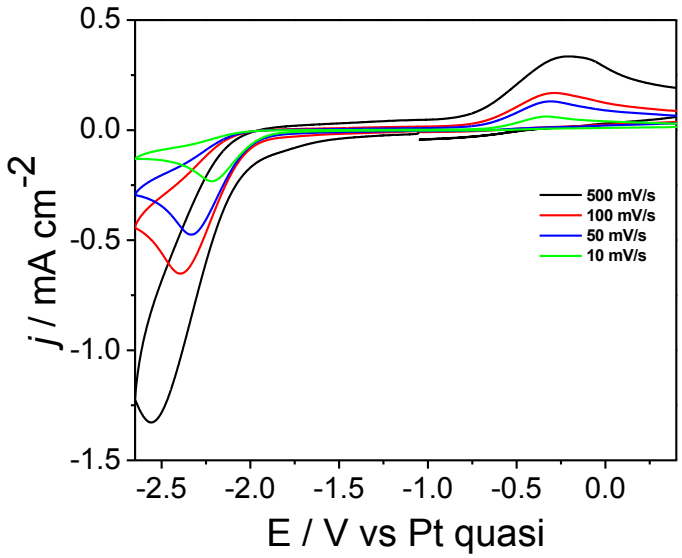


**Figure S10.** Cyclic voltammetry of 20 mM benzyldisulfide and 8 mM $CO_2$ in BMP TFSI at different scan rates; 500 mV/s (black), 100 mV/s (red), 50 mV/s (blue) and 10 mV/s (green); working-GCE, reference and counter - Pt, scan rate – 100 mV/s.

Figure S10 shows the scan rate dependence of the reversible capture and release of $CO_2$ by benzyldisulfide. Note that because of the much more rapid diffusion of $CO_2$ compared to BDS, 8 mM $CO_2$ is sufficient to consume all of the benzylthiolate produced during the negative scan. The scan rate dependence is not consistent with a typical EC (electrochemical step followed by chemical step) reaction mechanism. This is because the product of the initial reduction, $RSSR^-$, is not the species that reactions with $CO_2$. Instead, this species dissociates to form $RS^-$ and $RS\cdot$, which is further reduced to form a second equivalent of $RS^-$. Then, the two equivalents of $RS^-$ that were produced are both able to capture of two equivalents of $CO_2$. This complex reaction mechanism does not produce the typical EC response that might be expected for adduct formation following reduction. We also note that we see no evidence for film formation under the conditions used in this paper.

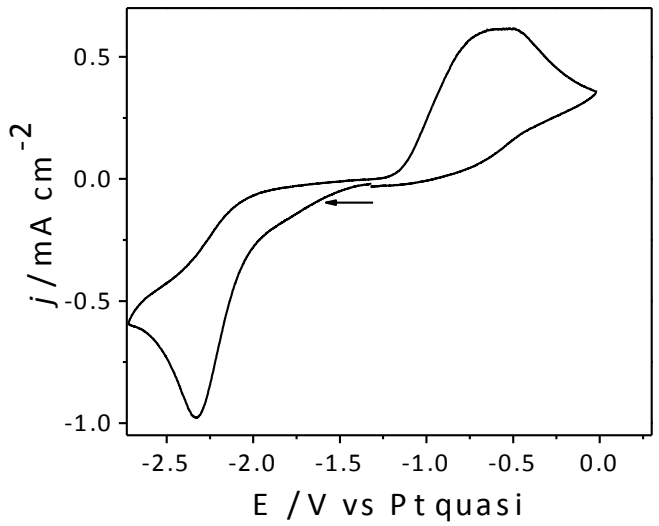


**Figure S11.** Cyclic voltammetry of 20 mM benzyldisulfide and 40 mM $P_{4444}^{+}$ $BnSCO_2^{-}$ in BMP TFSI IL; working-GCE, reference and counter - Pt, scan rate - 50 mV/s.

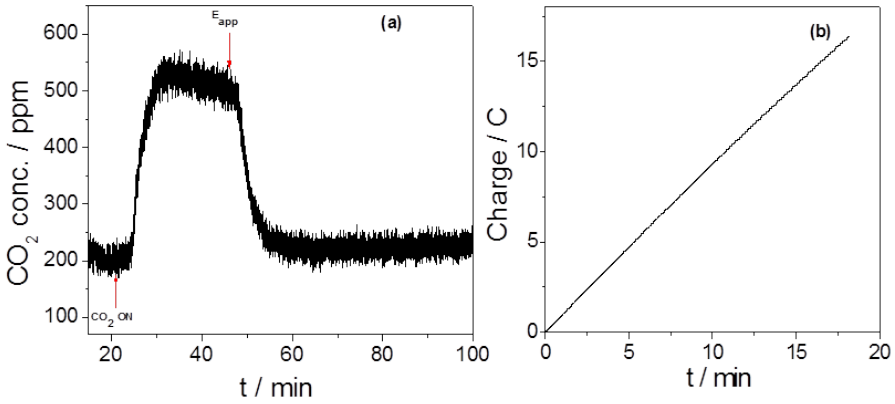


**Figure S12.** Right: Charge versus time during reduction of BDS under a flowing stream of 350 ppm $CO_2$. Left: Downstream $CO_2$ concentration versus time during the same reduction.

Figure S12 shows the results of a reductive bulk electrolysis performed in DMF solution to demonstrate $CO_2$ uptake by the thiolate. In this experiment a DMF solution containing 10 mM benzyldisulfide (BDS) was purged with $CO_2/N_2$ gas mixture with a concentration of 300 ppm $CO_2$ in $N_2$. In the left plot, the upward arrow shows the time at which $CO_2$ purging is initiated in the cell. One observes an increase in the $CO_2$ level in the downstream sensor caused by the delivery of $CO_2$ to the cell, its removal from the cell by the action of the purge stream and its ultimate detection by the downstream sensor. At a time indicated by the downward arrow, a reducing potential of -2.9 V was applied. At this potential reduction of BDS forms benzylthiolate, which reacts with the $CO_2$ being delivered to the cell. This consumption of $CO_2$ via reaction causes a decrease in the $CO_2$ level measured by the downstream sensor. Under these conditions (sub-stoichiometric delivery of $CO_2$ compared to the moles of thiolate generated by reduction), essentially all of the $CO_2$ delivered to the cell via the gas purge is being consumed, which causes the $CO_2$ signal to fall to background levels. Thus, the decrease in $CO_2$ signal under reducing conditions demonstrates $CO_2$ capture by the thiolate.

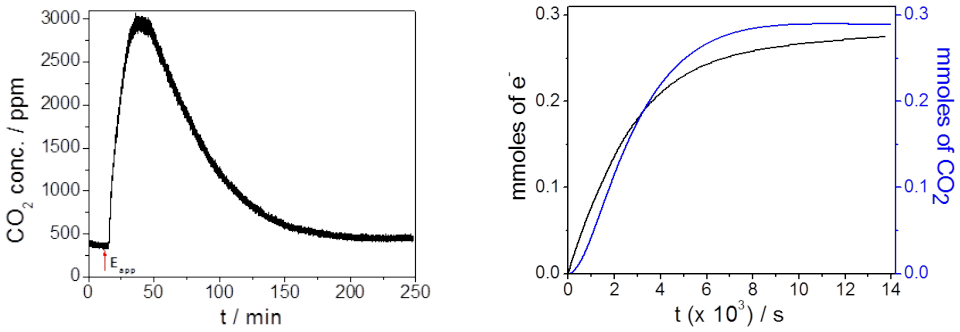


**Figure S13.** Left: Downstream $CO_2$ concentration versus time during the same oxidation. Right: Plot of moles $e^-$ (from charge) and moles $CO_2$ detected (integral of plot at left) versus time during oxidation of 10 mM *S*-benzylthiocarbonate under a flowing stream of pure $N_2$.

Figure S13 shows the results of a quantitative assay of $CO_2$ production during an oxidative bulk electrolysis of a synthetically prepared sample of *S*-benzylthiocarbonate performed in DMF solution. In this experiment, the oxidation potential was held at +0.9 V. The left plot shows the oxidative release of $CO_2$ detected downstream from the cell. The right plot shows moles of e- (from charge) and moles of $CO_2$ detected versus time. In the experimental configuration, the $CO_2$ that was produced via oxidation of the thiocarbonate was swept up into a stream of $N_2$ that was purged through the DMF solution and then exited the cell, flowing into the $CO_2$ sensor housing. The $N_2$ flow rate (43 mL $min^{-1}$) was chosen such that the $CO_2$ concentration would be within the sensitivity range of the $CO_2$ sensor. The $CO_2$ detection efficiency was calibrated by injecting aliquots of known concentrations of $CO_2$ in DMF into the cell, sweeping the $CO_2$ out with a $N_2$ purge stream and detecting it downstream with the $CO_2$ sensor. Detection efficiency is 100 ± 10 % (with most error due to flow rate instability). This allows direct comparison of moles of charge passed (26.5 C = 2.7 x $10^{-4}$ mol $e^-$) and moles of $CO_2$ released (2.9 x $10^{-4}$ mol) in the plots above, revealing release of one equivalent of $CO_2$ per equivalent of oxidative charge. This experiment unequivocally shows release of $CO_2$ during thiocarbonate oxidation with a stoichiometry of 1 to 1.

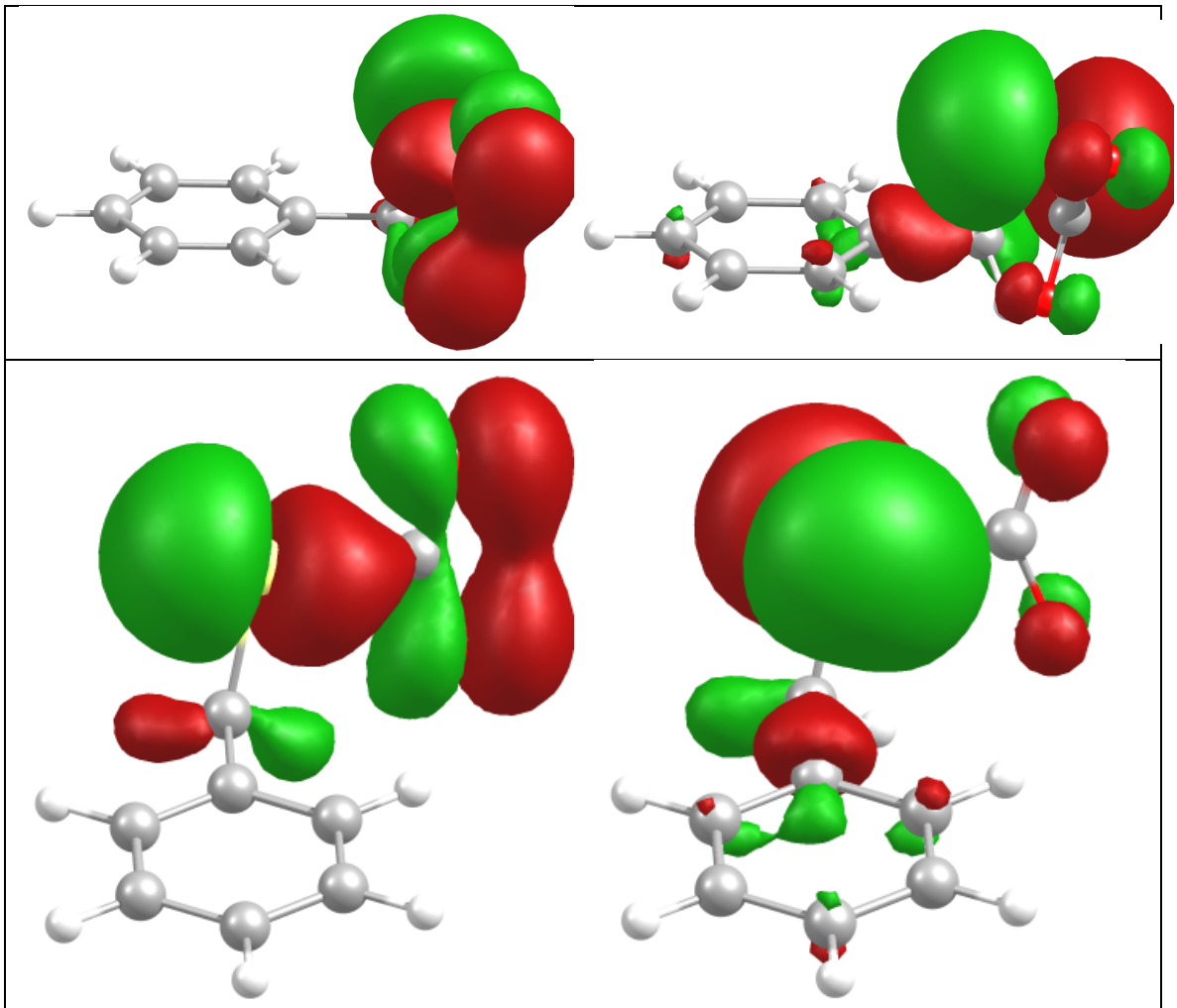

| HOMO-1 (-2.2 eV) | HOMO (-2.0 eV) |
|---|---|

**Figure S14.** Two different views of the electron densities of the HOMO and HOMO-1 orbitals of *S*-benzylthiocarbonate obtained at the B3LYP/aug-cc-pVQZ level of theory.

# CHAPTER 4

**Abstract**

Concern about the impacts of increased anthropogenic atmospheric carbon is motivating a great deal of research into carbon capture and sequestration strategies. Herein we report a novel thermal swing carbon capture and release scheme that employs benzylthiolates as the $CO_2$ chemisorbent. Alkali salts of benzylthiolate immediately precipitate from THF–$CH_3OH$ solution upon exposure to $CO_2$. Upon heating, $CO_2$ is liberated from the solid benzylthiocarbonate salts and the benzylthiolate can be recovered with little evidence of degradation. Release temperatures can be reduced by nearly 30 $^oC$ by a combination of modifying the aryl fragment of the benzylthiolate and using a crown ether to chelate the cation of the benzylthiolate. This strategy represents the first example of the effect that cation identity has on the $CO_2$ release properties of organosulfur compounds and could be employed to take advantage of the waste heat produced by power generating facilities to drive the $CO_2$ capture-release cycle.

---

There is broad consensus among climate scientists that anthropogenic $CO_2$ emissions are the primary contributor to global climate change.[11] In 2011 an estimated 34 billion tons of waste $CO_2$ were generated worldwide, with the top five emitters being China (29%), the United States (16%), the European Union (11%), India (6%), and the Russian Federation (5%).[12] The main sources of $CO_2$ pollution are from fossil fuel combustion, flaring of waste gas during oil production, and cement production, with coal-fired power plants being the largest stationary point-source $CO_2$ emitters.[14]

Ameliorating anthropogenic $CO_2$ emissions either by permanently sequestering $CO_2$ or by using the captured $CO_2$ as a chemical feedstock necessarily requires the controlled capture, storage, and/or release of $CO_2$. Presently, the most technologically ready and the most widely used methods for post-combustion carbon capture employ amines as the $CO_2$ sorbents.[20, 63] Despite this, there are serious drawbacks to amine capture that will likely prevent these systems from being widely implemented. Chief among these are both the energy required for $CO_2$ recovery and the likelihood for the unwanted emission of toxic and environmentally hazardous species during the capture and release process. With respect to the former, achieving 90% $CO_2$ capture by monoethanol amine (MEA) results in a 21% power loss (170 kJ mol $CO_2^{-1}$), which translates to a 44% increase in generating cost per MWh.[112] Though this may seem to be an insurmountable economic barrier to implementing amine scrubbing at scale, recent polling has shown that the average U.S. citizen will accept a 13% increase in electricity cost to support a national clean energy standard.[113] Another cost-based impediment to MEA scrubbing is the parasitic loss of the amine capture agent, which can amount to as much as 2 kg per ton $CO_2$.[13a, 114] Along this line, the environmental impacts of amine-based capture methods must also be addressed. Research in this area is incomplete; however, one can *a priori* identify a number of potential environmentally harmful outcomes to large-scale amine scrubbing. Since reclaiming the capture species requires heating, there is the potential for a large amount of waste generated during the reclamation step due to unwanted side reactions. Furthermore, it is likely that unwanted emissions will lead to highly toxic nitrosamines being formed in the atmosphere from either the emitted amine or degraded amine products.[63]

In an effort to develop new carbon capture and sequestration strategies that do not utilize amines as the $CO_2$ capture moiety, a number of groups have reported post-combustion $CO_2$ capture strategies that employ either carbon or oxygen nucleophiles as the $CO_2$ chemisorbent. Salient examples include several task specific ionic liquids (TSIL) where chemisorption of $CO_2$ is accomplished either by N-heterocyclic carbenes (NHC) or by alkoxides. With respect to the former, several groups have found that the imidazolium cation is the precursor to NHCs that have been shown to attack the electrophilic carbon of $CO_2$. In one of the first such examples, Gurau *et al.* detailed the chemisorption of carbon dioxide in 1,3-dialkylimidazolium acetate ionic liquids, where they provided substantial evidence of the imidazolium carboxylate in the ionic liquid.[115] Around the same time the Louie group detailed the synthesis and characterization of a wide array of imidazolium carboxylates on which they performed thermal gravimetric analysis (TGA) in order to fully understand how the imidazolium substituents affect the decarboxylation temperature.[116] Their findings show that the steric bulk of the *N*-substituent(s) is of primary importance, more so than electronic structure, with NHCs that have bulkier substituents on the nitrogen atoms exhibiting lower decarboxylation temperatures.

In their 2010 publication, Wang *et al.* report that a number of alcohols can be paired with a superbase,[42a, 117] and that the resulting acid–base reaction yields TSILs with alkoxides that act both as the TSIL anion and the $CO_2$ capture nucleophile.[118] The majority of these alkoxides show $CO_2$ capture at, or slightly above their theoretical limits. However, the phenoxide-based permutations show $CO_2$ capture slightly below 0.5 moles of $CO_2$ captured per mole of TSIL, or roughly half that expected by the reaction

stoichiometry. This result was confirmed in a 2011 study by the same authors in which the $CO_2$ capture medium was made by pairing phenoxide anions with trihexyl-(tetradecyl)phosphonium cations.[119] These data suggest that phenoxide is a lackluster $CO_2$ capture species as compared to some of the reported nitrogen anion TSILs. Manipulating the $CO_2$ absorption characteristics, particularly the absorption enthalpy, of phenoxide-based TSILs was shown to be quite facile. Wang *et al.* studied eighteen different trihexyl(tetradecyl)phosphonium phenoxide ionic liquids where they appended the phenoxide with various electron-donating (EDG) and electron-withdrawing (EWG) groups.[120] The authors found that the $CO_2$ absorption capacity increased with an increase in the pKa of the phenoxide conjugate acids. They also employed density functional theory (DFT) calculations and found that the more negative the Mulliken charge on the oxygen atom of the phenoxide anion, the more negative the absorption enthalpy i.e. the stronger the $CO_2$ binding.

In a previous publication from our laboratory the use of electrogenerated sulfur nucleophiles as part of a disulfide–thiolate–thiocarbonate electrochemical $CO_2$ pump was described.[121] That work showed that sufficiently nucleophilic thiolates can bind $CO_2$ at room temperature, forming a thiocarbonate species. The novelty of sulfur nucleophiles for post-combustion carbon capture and sequestration (CCS) prompted us to consider the possibility of utilizing similar compounds in a temperature swing carbon capture scheme. There is only one other report of sulfur-containing materials being employed for $CO_2$ capture.[122] In that case, S-doped microporous carbon materials showed large $CO_2$ absorption capacity of 4.5 mmol $g^{-1}$ at 1 atm $CO_2$, as well as a high degree of selectivity for $CO_2$ over $N_2$, $H_2$, and $CH_4$. In this report we establish proof-of-concept that $CO_2$ can

be liberated from thiocarbonates at modest temperatures, such as might be available from waste heat in power generating facilities. Additionally, similar to the studies of NHC and alkoxide $CO_2$ capture, we provide further insight into the factors that govern the physicochemical properties for $CO_2$ capture and release by organosulfur compounds.

**Results and Discussion**

Insight provided by density function theory (DFT) calculations into electrochemical $CO_2$ release by *S*-benzylthiocarbonate in our previous publication served as the impetus for adopting an *in silico* approach to estimate the decarboxylation temperature of benzylthiocarbonate. Toward that end, gas-phase optimization and frequency calculation of *S*-benzylthiocarbonate, benzyl-thiolate, and carbon dioxide were performed at the B3LYP/aug-ccPVTZ level of theory. The Gibbs free energy of *S*-benzylthiocarbonate at fifteen different temperatures ranging from 5 to 320 $^{o}$C was determined utilizing the Gaussian 09 freqchk utility. A plot of these data and the best-fit line ($R^2$ = 0.998) are shown in Figure 8a. An identical calculation was performed on benzylthiolate and carbon dioxide and the sum of the free energies over the same temperature range and the best-fit line ($R^2$ = 0.999) are also shown in Figure 8a. By finding the intersection of the regression lines, the estimated decarboxylation temperature for benzylthiocarbonate is 154.71 $^{o}$C, which is the temperature at which $\mathbf{\Delta}G_{BnSCO2^-} = \mathbf{\Delta}G_{BnS^-} + \mathbf{\Delta}G_{CO2}$. This value is consistent with the only previous study of the thermal decarboxylation of thiocarbonates having the general form RO2CSR', where $CO_2$ release occurred between 123–186 $^{o}$C depending upon the identities of R and R'.[123] Figure 8b is a plot of the predicted $CO_2$ release temperature vs. the relevant Hammett substituent constants for benzylthiocarbonate, 4-chlorobenzylthiocarbonate, 3,5-difluorobenzylthio-

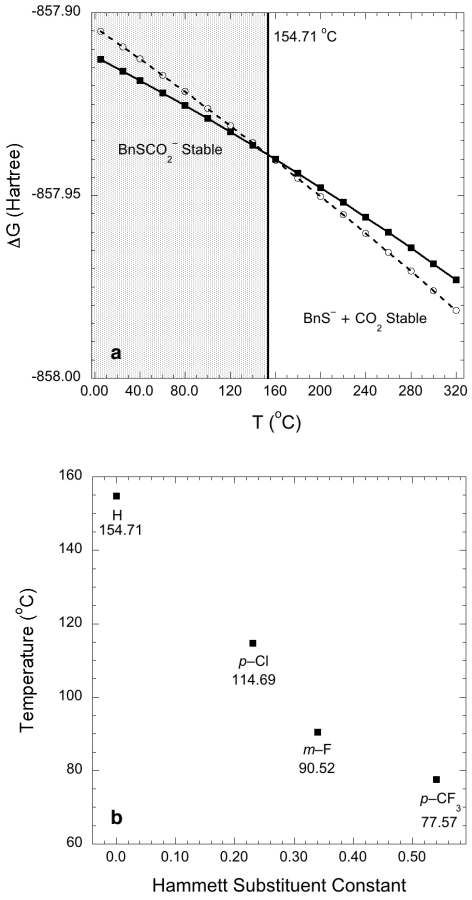


**Figure 8. a.** Gibbs free energy (Hartree) vs. temperature (°C) for *S*-benzylthiocarbonate (■) and the sum of the free energies of benzylthiolate and carbon dioxide (O). **b.** Predicted decarboxylation temperatures (°C) for *S*-benzylthiocarbonate (H), 4-chloro-*S*-benzylthiocarbonate (*p*-Cl), 3,5-difluoro-*S*-benzylthiocarbonate (*m*-F), and 4-trifluoromethyl-*S*-benzylthiocarbonate (*p*-$CF_3$) vs. Hammett substituent constant.[124]

carbonate, and 4-trifluoromethylbenzylthiocarbonate.[124] This plot indicates that it is possible to manipulate the decarboxylation temperature of benzylthiocarbonate by appending various electron-donating or electron-withdrawing groups to the aryl moiety, thus allowing for control of the temperature range for the capture and release cycle.

Encouraged by the computational results, residual gas analysis (RGA) was used to monitor the species released from sodium benzylthiocarbonate as a function of temperature. The results are shown in Figure 9. Between 30–200 °C, the five most

intense signals in order of decreasing intensity are m/z = 44 > 91 > 16 > 28 > 18. The signals at 44, 28, and 16 are all readily identifiable as $CO_2$, CO, and O, respectively, all of which are expected based upon the mass spectrum of $CO_2$.[125] The high probability that some of the thiocarbonate was swept into the carrier gas during the experiment supports the assignment of m/z = 91 as the tropylium ion, which is known to appear in the mass spectra of benzyl derivatives.[126] The signal at m/z = 18 is due to adventitious water that likely collected on the sample tube as it was being loaded into the instrument. What is clear from the RGA analysis is that the main decomposition product of sodium benzylthiocarbonate is $CO_2$, and that there is no further decomposition of the product thiolate into gaseous products at temperatures up to 200 °C.

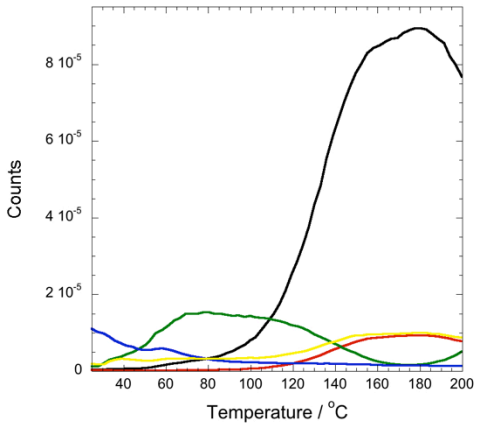


**Figure 9.** Counts vs. temperature (°C) for the five most intense signals from residual gas analysis of sodium benzylthiocarbonate; m/z = 44 (black), 91 (green), 16 (red), 28 (yellow), 18 (blue).

Further investigation of the temperature dependence of $CO_2$ release from thiocarbonates was accomplished utilizing the apparatus constructed in-house that is described in the Supporting Information. Figure 10 (black curve) shows the plot of $CO_2$ released as a function of sample temperature for the sodium benzylthiocarbonate salt. This curve shows that $CO_2$ release begins near 60 °C, maximizes near 125 °C and

continues on to the end of the experiment near 250 °C. Confirmation that sodium benzylthiolate is the product of the thermal decomposition of sodium benzylthiocarbonate was proved by analyzing the cooled sample by $^1$H NMR and comparing it to the $^1$H NMR of an authentic sample of sodium benzylthiolate (Figure 11).

Figure 10 (red curve) shows the plot for the corresponding potassium salt. This curve is substantially sharper and shows a higher temperature for the initial release of $CO_2$. For comparative purposes, we define an onset temperature for the release by

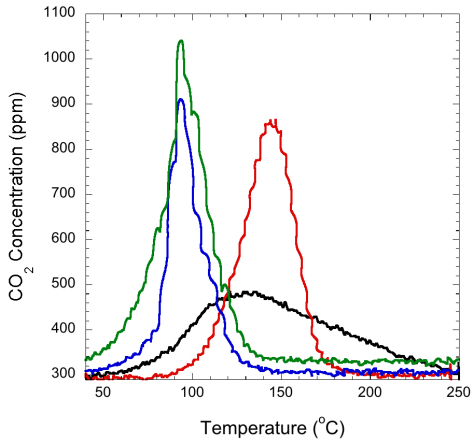


**Figure 10.** $CO_2$ concentration (ppm) vs. temperature (°C) for sodium *S*-benzylthiocarbonate (black), potassium *S*-benzylthiocarbonate (red), 15-crown-5 sodium *S*-benzylthiocarbonate (blue), 15-crown-5 sodium 4-chloro-*S*-benzylthiocarbonate (green).

**Table 1.**

| | Onset Temperature (°C) | Peak Temperature (°C) |
|---|---|---|
| sodium *S*-benzylthiocarbonate | 88 ± 3 | 121 ± 2 |
| potassium *S*-benzylthiocarbonate | 108 ± 4 | 141 ± 4 |
| 15-crown-5 sodium *S*-benzylthiocarbonate | 78 ± 2 | 92 ± 1 |
| 15-crown-5 sodium 4-chloro-*S*-benzylthiocarbonate | 61 ± 5 | 91 ± 3 |

extrapolating to the temperature axis from the midpoint (half-height) of the increasing, low T side of the release curve. This onset T allows comparison of the release behavior of different samples. There are a number of striking differences between the curves for the

potassium and sodium salts shown in Figure 10. First, both the onset temperature and the peak temperature for $CO_2$ release are higher for the potassium salt, as summarized in Table 1. This behavior may be related to the relative stability of the alkali metal thiocarbonates (reactants) or the alkali metal thiolates (products). Further study of the effects of ionic interactions in such experiments is certainly warranted. Second, the $CO_2$ release from sodium benzylthiocarbonate is sluggish in comparison to $CO_2$ release frompotassium benzylthiocarbonate, which is evidenced by the sharpness of the potassium benzylthiocarbonate curve. One possible explanation is that $CO_2$ release from salt powders of the type used here is influenced by the packing density in the sodium thiolate product. This has previously been observed for $CO_2$ release from dolomite ($MgCaCO_3$), where sluggish release was speculated to be due to formation of a high density MgO "skin" on the dolomite particles during the initial stages of $CO_2$ release.[127] In the present case, differences in packing density, either for the thiocarbonate or the thiolate salts, could be influencing the shape of the release curve. Thus, both ionic interactions and packing density in the solid could be influencing the release process in ways that are not yet understood.

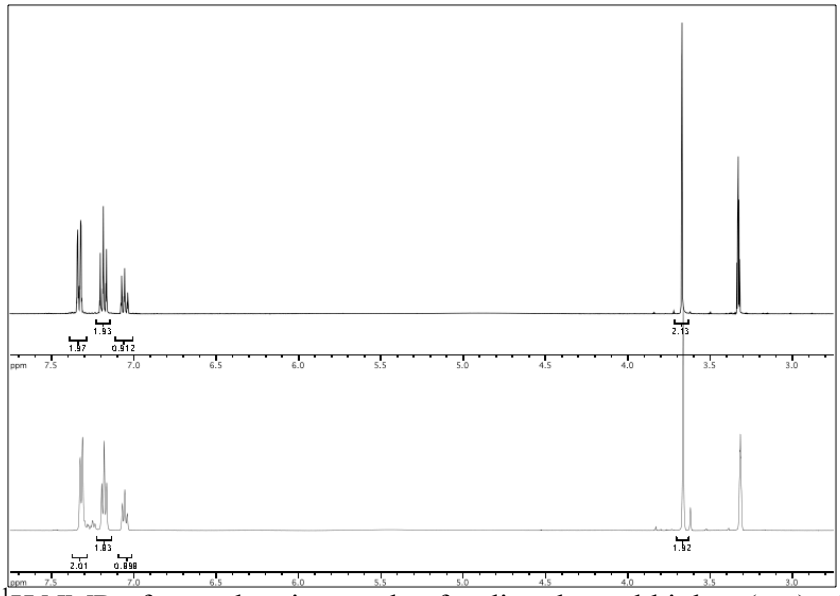

**Figure 11.** $^{1}$H NMR of an authentic sample of sodium benzylthiolate (top) ad the material recovered after thermal decarboxylation of sodium benzylthiocarbonate (bottom).

As will now be shown, increasing the free volume in the solid by associating the cation with a crown ether provides a means to facilitate the $CO_2$ release process. The blue curve in Figure 10 shows that the presence of the crown ether affects both the onset and release temperatures, as well as the release kinetics. Specifically, both the onset and peak $CO_2$ release temperatures for 15-crown-5 sodium benzylthiocarbonate are significantly lower than those of sodium benzylthiocarbonate (Table 1). Furthermore, the large crown ether makes $CO_2$ release from this material more facile as demonstrated by the sharpness of the release curve as compared to both sodium and potassium benzylthiocarbonate. The better behavior of the crown salt allowed for exploration of the effects summarized in Figure 8, namely the thermal stability of substituted benzylthiocarbonate derivatives. The green plot in Figure 10 shows the release curve for a sample of 15-crown-5 sodium 4-chloro-*S*-benzylthiocarbonate. Carbon dioxide release from this species is again facile, and there is a 17 $^{o}$C decrease in the onset temperature for the 4-chloro derivative compared to the parent benzyl compound (Table 1 and green

curve Figure 10). In contrast, DFT predicts a 40 $^{o}$C decrease (Fig. 8b). The lack of agreement suggests that the DFT calculations do not account for all of the physicochemical processes that contribute to the energetics of the $CO_2$ release process, but DFT does provide meaningful insight into how the $CO_2$ release temperature can be manipulated.

In one final example of how the cation identity affects the decarboxylation of benzylthiocarbonate, we describe the interesting case of the task specific ionic liquid (TSIL) tetrabutylphosphonium benzylthiolate ($P_{4444}^{+}$ $BnS^{-}$). Tetrabutylphosphonium benzylthiolate is a viscous, slightly yellow ionic liquid that when bubbled with $CO_2$ for 4 hours, yields tetrabutylphosphonium benzylthiocarbonate ($P_{4444}^{+}$ $BnSCO_2^{-}$) as a waxy, white solid in quantitative yield (Figure 12). Both $P_{4444}^{+}$ $BnS^{-}$ and $P_{4444}^{+}$ $BnSCO_2^{-}$ have been fully characterized in our previous report.[121] The white solid $P_{4444}^{+}$ $BnSCO_2^{-}$ was stable for weeks at 2 $^{o}$C; however, when $P_{4444}^{+}$ $BnSCO_2^{-}$ was placed under vacuum at room temperature, the solid returned to a viscous, slightly yellow liquid over a period of 12–16 hours. NMR verified that the liquid contained only thiolate and not thiocarbonate. Similarly, when left at atmospheric pressure and room temperature, the solid would fully return to the liquid phase after a period of 10 days, again showing loss of $CO_2$. In both cases, when the liquid was again exposed to $CO_2$ the white solid thiocarbonate reappeared. Thus, it is clear that the $P_{4444}^{+}$ $BnS^{-}$ liquid binds $CO_2$ to form a solid thiocarbonate salt, and that this binding is reversible and causes a phase change.

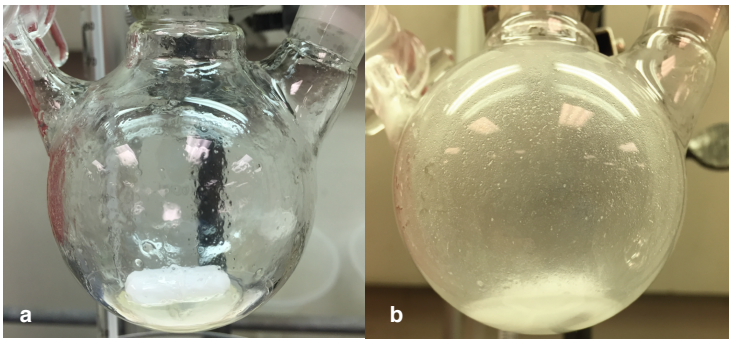


**Figure 12. a.** Tetrabutylphosphonium benzylthiolate (note the white stir bar in the flask). **b.** Tetrabutylphosphonium *S*-benzylthiocarbonate

The release of $CO_2$ from $P_{4444}^{+}$ $BnSCO_2^{-}$ under such mild conditions was unexpected in the context of the previous reports of the chemisorption of $CO_2$ by ionic liquids whose anion is a nitrogen base as detailed by Seo and coworkers.[40-41, 128] Seo *et al.* described a series of ionic liquids that changed phase from solid to liquid upon exposure to $CO_2$.[41] These so-called phase-change ionic liquids (PCIL) all had anionic nitrogen $CO_2$ capture sites in the form benzimidazolide, pyrrolide, or pyrazolide anions, and had either tetraethyl- or tetrabutylphosphonium cations. Carbon dioxide capture and release experiments with their model ionic liquid, tetraethylphosphonium benzimidazolide, were done at 70 $^{o}$C. Quantitative release of $CO_2$ was achieved at this elevated temperature under a reduced pressure of <0.01 bar over a period of 1 hour. The authors note that at there was some evidence of $CO_2$ release at room temperature over time, depending upon how carefully the samples were sealed. Seo *et al.* additionally found that when the cation of the benzimidazolide ionic liquid is changed to tetrabutylphosphonium $CO_2$ capture is still possible, but the melting point of the PCIL is nearly 100 $^{o}$C higher.

**Conclusions.**

A thermal swing capture and release process has been described that involves cycling between thiolate and thiocarbonate species. Specifically, salts of both *S*-benzylthiolate and 4-chloro-*S*-benzylthiolate are shown to be capable of this thermal swing process. A simple method for monitoring $CO_2$ release was described that gives a good estimate of $CO_2$ release temperature. Comparison of the release temperatures for benzylthiocarbonate and 4-chloro-*S*-benzylthiocarbonate shows reasonable agreement with predictions from DFT analysis of the relative stabilities predicted for these two thiocarbonate species. This represents the first report of a thermal swing capture and release cycle using thiolate nucleophiles.

CHAPTER 4 SUPPORTING INFORMATION

## Experimental Details

*General Considerations*

All manipulations were carried out using standard Schlenk or glovebox techniques under a nitrogen atmosphere. Solvents were purified and dried according to literature procedures, degassed by four successive freeze-pump-thaw cycles, and stored in the glovebox.[108] Deuterated solvents were purchased from Cambridge Isotope Laboratories, Inc., degassed by four successive freeze-pump-thaw cycles and stored in the glovebox. All other reagents and starting materials were purchased from commercial vendors and used without further purification unless otherwise noted. Compressed gas cylinders were furnished by Praxair, Inc.

*Physical Methods*

$^{1}$H NMR spectra were collected on a Varian 500 MHz NMR spectrometer. $^{13}$C NMR spectra were collected on a Brüker Ultra-Shield 600 MHz NMR spectrometer equipped with a cryoprobe. $^{1}$H and $^{13}$C NMR spectra are reported in parts per million relative to tetramethylsilane, using the residual solvent resonances as an internal standard.[129] FTIR measurements were performed on a Brüker Alpha spectrometer equipped with a diamond ATR. Gas output from compressed gas cylinders was controlled with Cole-Parmer PRM1-010547 gas flow regulator and measured using an Agilent Technologies ADM 2000 Universal Gas Flowmeter. Residual Gas Analyses (RGA) that measure the partial pressures of the individual gases in a mixture were performed using an in-house constructed stand-alone vacuum system that is differentially pumped to accept atmospheric pressure sample gas input. A small quantity of sample gas

is ionized, and the ions are accelerated into a mass separation filter, resulting in a mass spectrum showing partial pressure vs. gas species mass. Carbon dioxide release experiments were conducted utilizing the in-house constructed apparatus described below.

*Carbon Dioxide Release Apparatus*

An in-house apparatus was constructed as follows: Temperature control and charting was achieved utilizing an OMEGA CN8PT temperature controller outfitted with a type K thermocouple and the associated software. The temperature was initially held at 30 $^{o}$C for 15 minutes, followed by a temperature increase to 250 $^{o}$C at a rate of 3 $^{o}$C min$^{-1}$. This device was routed to an OMEGA 75 Amp solid-state relay that was used to switch the AC line voltage to an OptiChem Power Controller to which a Glas-Col heating tape was connected. The heating tape was wrapped around a 25 mL distilling bulb that served as the sample chamber. Ground glass adapters fitted on one side with gas-tight tubing were connected to the distilling bulb and sealed with Apiezon H grease. Medical grade $N_2$ was flowed through the sample chamber to a COZIR K-30 Ambient $CO_2$ sensor and finally through an Agilent ADM 2000 Universal Gas Flow Meter. Carbon dioxide concentration data was processed utilizing the method of least squares described by Savitzky and Golay.[130] The $N_2$ flow rate was set to 450 mL min$^{-1}$ at the output of the $CO_2$ sensor by utilizing a Cole-Parmer PRM1-010547 gas flow regulator. Injecting $CO_2$ directly into the sample chamber using a syringe showed virtually no delay between injection and detection. Evaluation of this apparatus with sodium bicarbonate showed peak $CO_2$ release at 145.8 +/- 2.5 $^{o}$C.

**Computational Details**

Calculations using density functional theory (DFT) were carried out using the Becke gradient-corrected exchange functional and Lee−Yang−Parr correlation functional with three parameters (B3LYP) and the aug-cc-pVTZ basis sets using the Gaussian suite of programs.[110] Calculations at this level of theory have been found to yield energies and spectroscopic parameters comparable to those obtained with higher levels of theory.[104, 111]

**Syntheses**

Sodium benzylthiolate

For a typical experiment, 245.0 mg (10.6 mmol) of sodium in mineral oil was weighed into a beaker containing 25 mL of hexane. The sodium metal was washed with 25 mL of hexane three additional times to remove the mineral oil, and then transferred to a round bottom flask equipped with a stirbar under a nitrogen atmosphere. The flask was placed under vacuum and then transferred to the glovebox. Tetrahydrofuran (15 mL) was added to the flask followed by the dropwise addition of 2.5 mL (21.3 mmol) of benzyl mercaptan, at which time a white solid immediately appeared. After reaching constant turbidity with concomitant dissolution of the sodium metal (4–6 hrs), the solution was allowed to stir for one hour then sodium benzylthiolate was isolated in quantitative yield on a sintered glass disk by vacuum filtration. $^{1}$H NMR (500 MHz, [D8] THF) in Figure S1: $\delta$ = 7.39–7.32 (m, 2 H), 7.09–7.06 (m, 2 H), 6.94–6.91 (m, 1 H), 3.69 (s, 2 H). $^{13}$C $\{^{1}$H$\}$ NMR (125 MHz, [D8] THF) in Figure S2: $\delta$ = 151.22, 128.75, 128.01, 124.60, 30.73. FTIR (cm$^{-1}$) in Figure S3: 3607 (s), 3079 (br), 3055 (s), 3024 (s), 2909 (m), 2839 (m), 1598 (s), 1491 (s), 1445 (w), 1310 (m), 1235 (s), 1067 (s).

Sodium *S*-benzylthiocarbonate

In a round bottom flask equipped with a stirbar, 73.10 mg (0.50 mmol) of sodium benzylthiolate was suspended in 50 mL of THF and $CH_3OH$ was added dropwise until the solid completely dissolved. Carbon dioxide that had passed through a drying column was bubbled into the solution and a white solid immediately appeared. After reaching constant turbidity roughly half the solvent was removed by vacuum. Sodium benzylthiocarbonate was isolated by vacuum filtration on a sintered glass disk in quantitative yield. $^1$H NMR (500 MHz, $CD_3OD$) in Figure S4: $\delta$ = 7.32–7.27 (m, 4 H), 7.21–7.18 (m, 1 H), 3.72 (s, 2 H). $^{13}$C {$^1$H} NMR (150 MHz, $CD_3OD$) in Figure S5: $\delta$ = 161.43, 142.98, 129.51, 129.07, 127.80, 29.17. FTIR ($cm^{-1}$) in Figure S6: 3062 (w), 3034 (w), 2954 (w), 2900 (w), 1670 (m), 1569 (vs), 1495 (s) , 1450 (s), 1435 (s), 1413 (s), 1322 (vs), 1292 (vs), 1234 (s), 1190 (m), 1100 (w), 1070 (m).

15-crown-5 sodium *S*-benzylthiocarbonate

Sodium *S*-benzylthiocarbaonate (50.0 mg, 0.26 mmol) was suspended in THF, and 52 µL (0.26 mmol) of 15-crown-5 was added by syringe all at once. The white solid dissolved over a period of five minutes and the solution was allowed to stir for an additional 15 minutes. The flask was placed under vacuum to remove all the solvent, and 15-crown-5 sodium benzylthiocarbonate was isolated as a white solid in quantitative yield. $^1$H NMR (500 MHz, $CD_3OD$) in Figure S7: $\delta$ = 7.33–7.31 (m, 2 H), 7.26–7.23 (m, 2 H), 7.16–7.14 (m, 1 H), 3.70 (s, 2 H), 3.68 (s, 20 H). $^{13}$C {$^1$H} NMR (150 MHz, $CD_3OD$) in Figure S8: $\delta$ = 161.44, 130.53, 129.28, 129.14, 127.09, 69.79, 29.69. FTIR ($cm^{-1}$) in Figure S9: 3062 (w), 3028 (w), 2909 (m), 2894 (m), 2874 (m), 1633 (s), 1601 (m), 1472 (s), 1452 (s), 1353 (s), 1288 (m), 1267 (s), 1249 (s), 1230 (s), 1096 (vs).

15-crown-5 sodium 4-chloro-*S*-benzylthiocarbonate

Sodium metal (46.2 mg, 2.0 mmol) in mineral oil was weighed into a beaker containing 10 mL of hexane, then washed with 25 mL of hexane three additional times to remove the mineral oil. The metal was transferred to a round bottom flask equipped with a stirbar that was under a nitrogen atmosphere, which was subsequently placed under vacuum and then transferred to the glovebox. Tetrahydrofuran (50 mL) was added to the flask followed by the dropwise addition of 0.33 mL (2.5 mmol) of 4-chlorobenzenemethanethiol, at which time a white solid immediately appeared. After reaching constant turbidity with concomitant dissolution of the sodium metal (4–6 hrs) the solution was allowed to stir for one hour, at which time 0.40 mL (2.05 mmol) of 15-crown-5 was added all at once. After the solid had completely dissolved, the solution was allowed to stir for an additional two hours, then placed under vacuum overnight. The following day 15-crown-5 sodium 4-cholorobenzylthiocarbonate was recovered as a white powder in quantitative yield. $^{1}$H NMR (500 MHz, $CD_3OD$) in Figure S10: $\delta$ = 7.33–7.28 (m, 4 H), 3.71 (s, 2 H), 2.68 (s, 20 H). $^{13}$C $\{^{1}H\}$ NMR (150 MHz, $CD_3OD$) in Figure S11: $\delta$ = 160.04, 143.02, 131.27, 129.36, 127.87, 68.43, 278.61. FTIR ($cm^{-1}$) in Figure S12: 2909 (m, br), 2872 (m, br), 2078 (w), 2055 (w), 1671 (m), 1621 (vs), 1487 (m), 1454 (m), 1355 (s, br), 1324 (s), 1249 (m), 1098 (vs), 1089 (vs).

Potassium *S*-benzylthiocarbonate

Following a procedure similar to the one detailed by Stueber et al.,[131] in the glovebox potassium metal (333.5 mg, 8.5 mmol) in mineral oil was added to 25 mL of hexane in a beaker. The potassium was washed three additional times to remove the mineral oil, then cut into small slivers. In a separate three neck round bottom flask equipped with a reflux condenser and a stirbar at 0 oC, 3.0 mL (25.6 mmol) of benzyl

mercaptan was added. The slivers of potassium metal were slowly added to the cooled mercaptan one at a time over a period of several hours. After complete dissolution of the potassium metal with the concomitant appearance of a suspended white solid, the suspension was stirred at 0 oC for one hour then slowly warmed to room temperature. The white solid, potassium benzylthiolate, was isolated on a sintered glass disk by vacuum filtration, then transferred to round bottom flask containing 50 mL of THF. Methanol was added dropwise until the solid had completely dissolved, then CO2 that had been passed through a drying column was bubbled into the solution, at which time a white solid appeared. After reaching constant turbidity, the CO2 was removed and potassium benzylthiocarbonate was isolated on a sintered glass disk by vacuum filtration. This compound is insoluble in all organic solvents that we tested, so NMR was not possible. FTIR ($cm^{-1}$) in Figure S13: 3153 (m, br), 2984 (m, br), 1672 (s), 1643 (m), 1436 (vs), 1358 (vs, br), 1261 (s), 1060 (m), 1034 (m), 1012 (m).

**Characterization of Thiolate and Thiocarbonate Compounds**

Figures S15 – S27 show $^{1}H$, $^{13}C$ and FTIR spectra for the synthesized and purified salts of the relevant *S*-benzylthiocarbonates. The $^{13}C$ NMR of the thiocarbonates show signals between 160.04–161.44 ppm for the carboxylate carbon in the thiocarbonate, which compares favorably to our previously reported result of 162.82 ppm for the same carbon in tetrabutylphosphonium *S*-benzylthiocarbonate.[121] The FTIR spectra of sodium *S*-benzylthiocarbonate, 15-crown-5 sodium *S*-benzylthiocarbonate, 15-crown-5 4-chloro-*S*-benzylthiocarbonate, and potassium *S*-benzylthiocarbonate exhibit very strong peaks at 1569, 1633, 1621, and 1672 $cm^{-1}$, respectively, which is due to the OCO asymmetric stretch of the thiocarbonate. These data are all in good agreement both with the solid state

NMR and IR results obtained by Stueber et al.,[131] and with our previous report. Due to the insolubility of potassium *S*-benzylthiocarbonate in all organic solvents that we tested (the insolubility of similar potassium thiocarbonates was also reported by Stueber et al.), only FTIR data is presented.

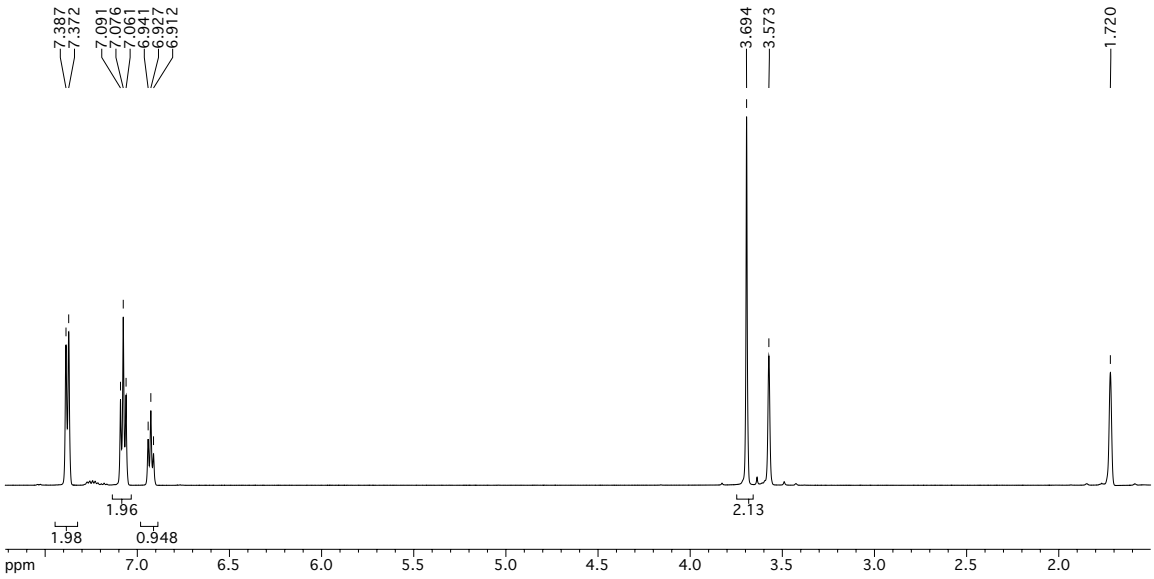


**Figure S15.** $^{1}$H NMR sodium benzylthiolate

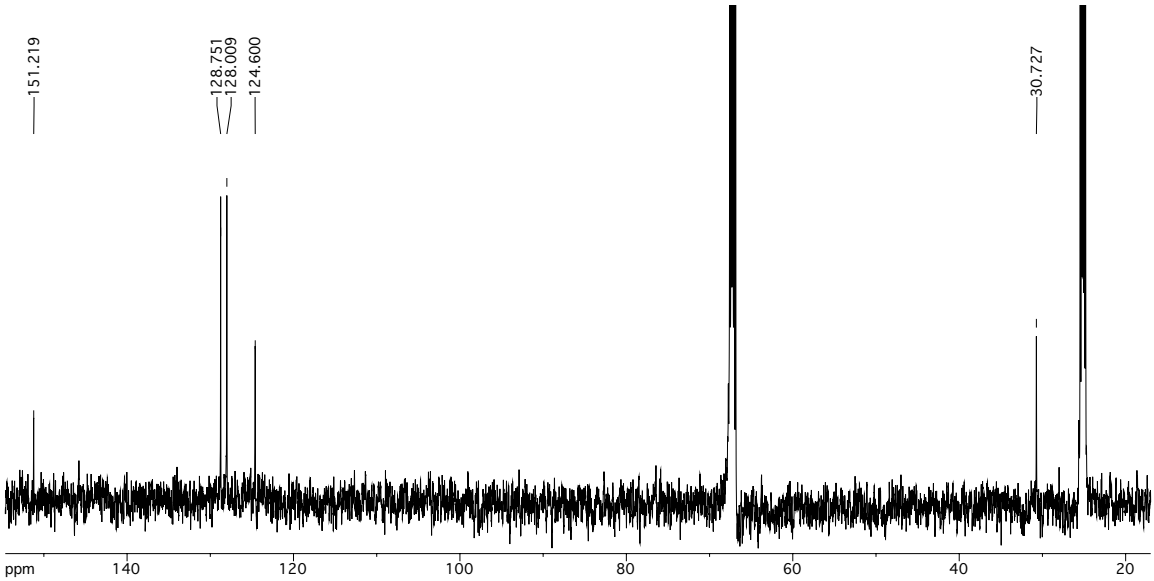


**Figure S16.** $^{13}$C NMR sodium benzylthiolate

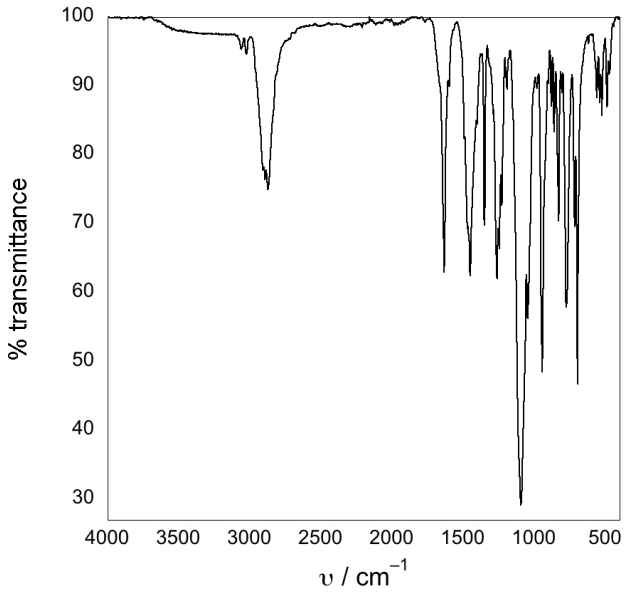


Figure **S17.** FTIR spectrum of sodium benzylthiolate

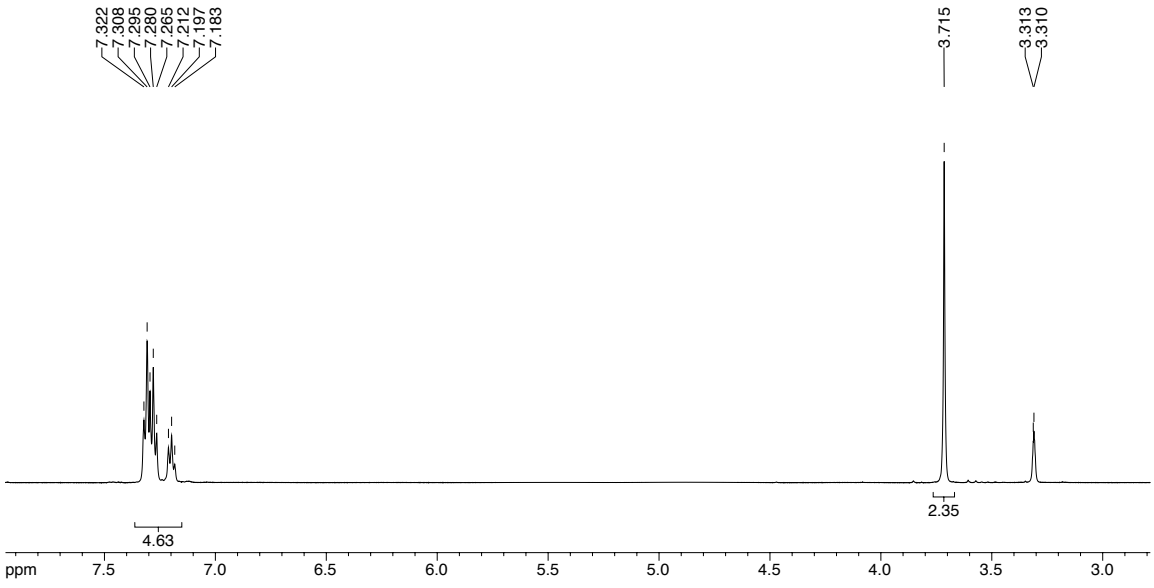


**Figure S18.** $^{1}$H NMR sodium *S*-benzylthiocarbonate

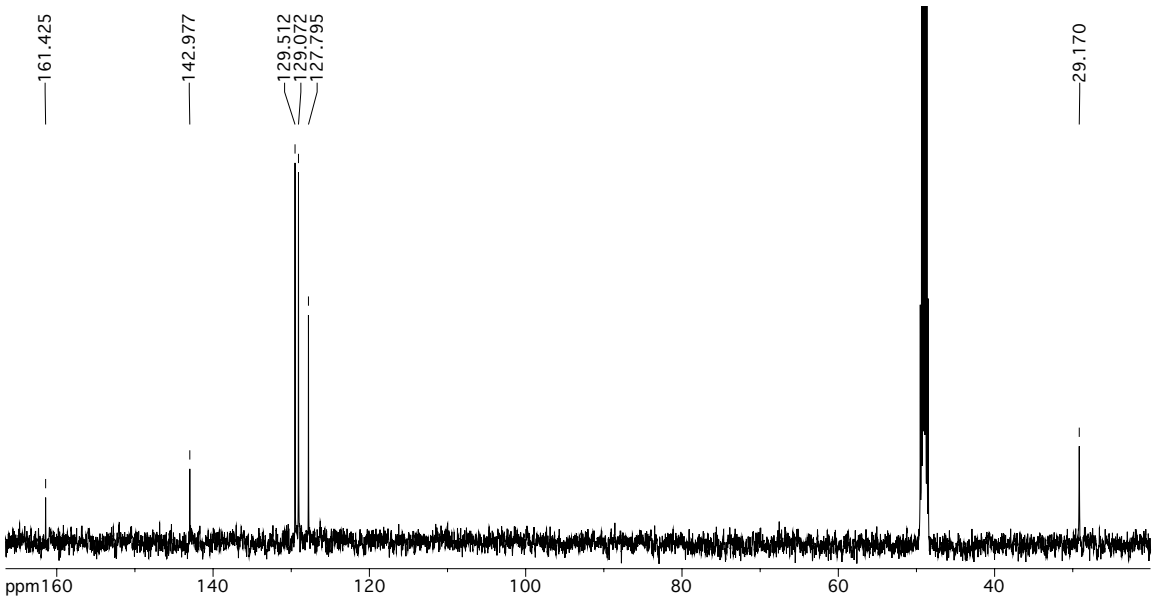


**Figure S19.** $^{13}C$ NMR sodium *S*-benzylthiocarbonate

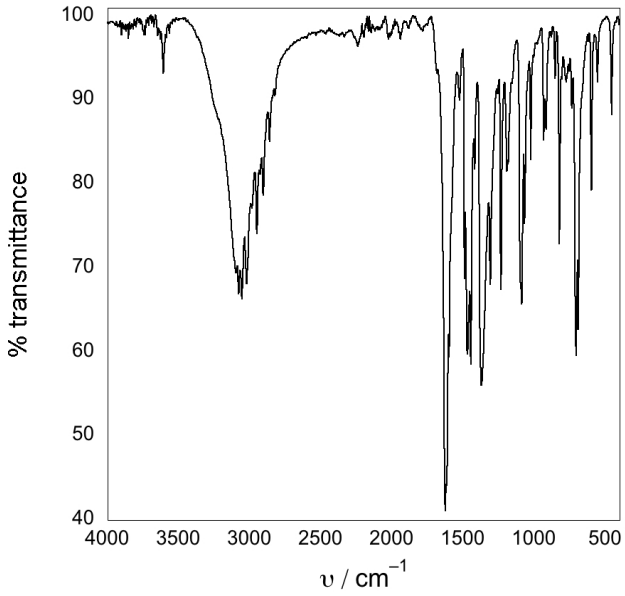


**Figure S20.** FTIR spectrum sodium *S*-benzylthiocarbonate

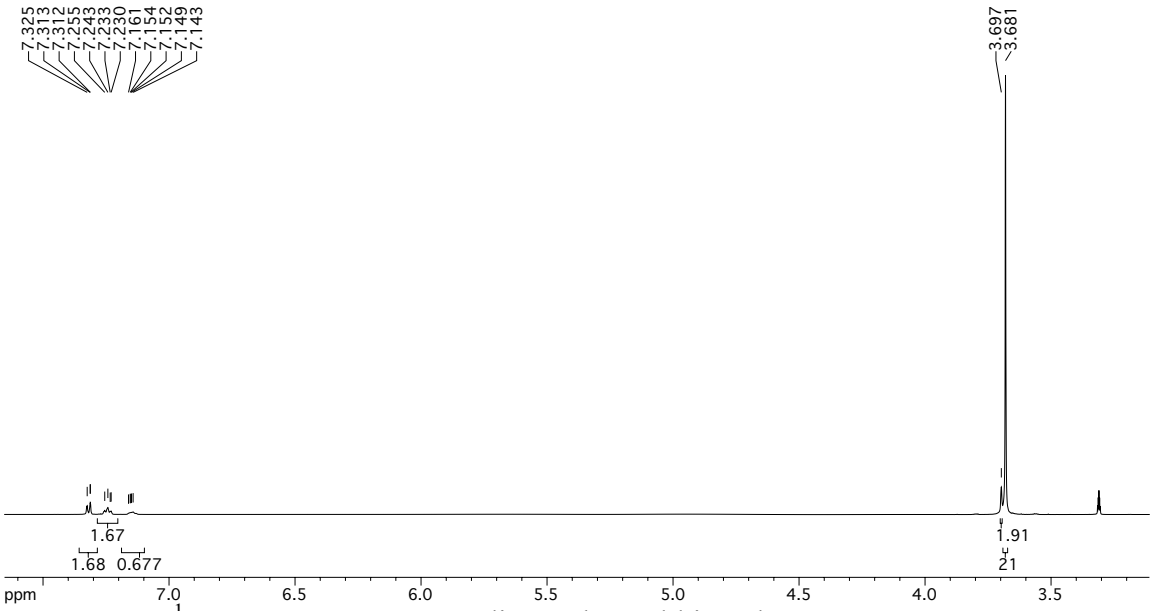


**Figure S21.** $^{1}$H NMR 15-crown-5 sodium *S*-benzylthiocarbonate

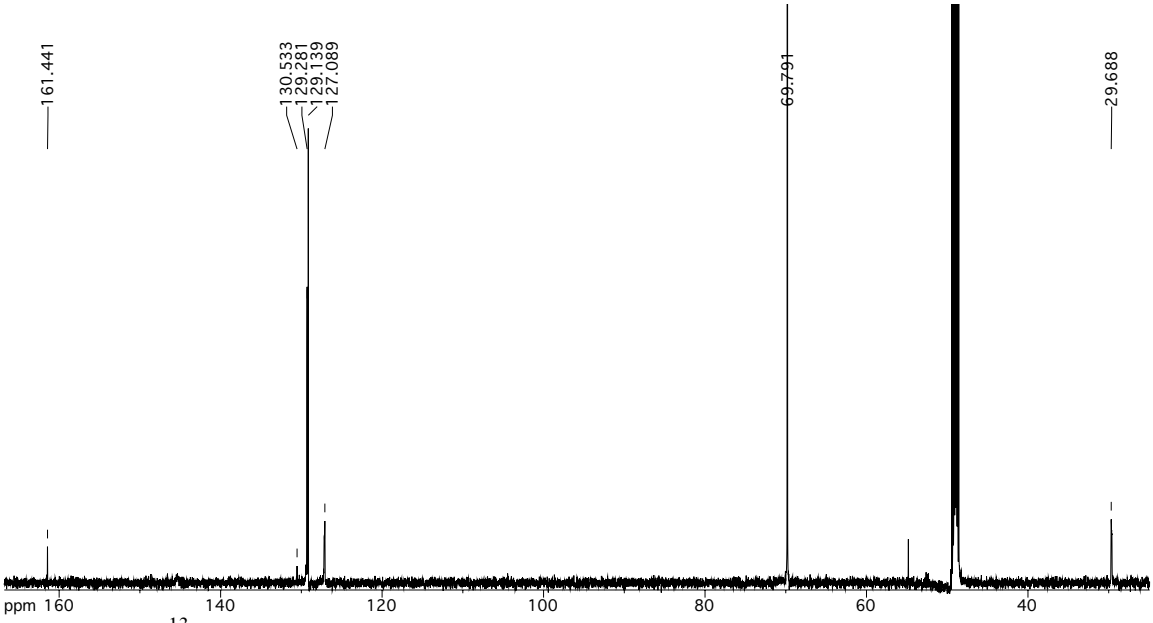


**Figure S22.** $^{13}$C NMR 15-crown-5 sodium *S*-benzylthiocarbonate

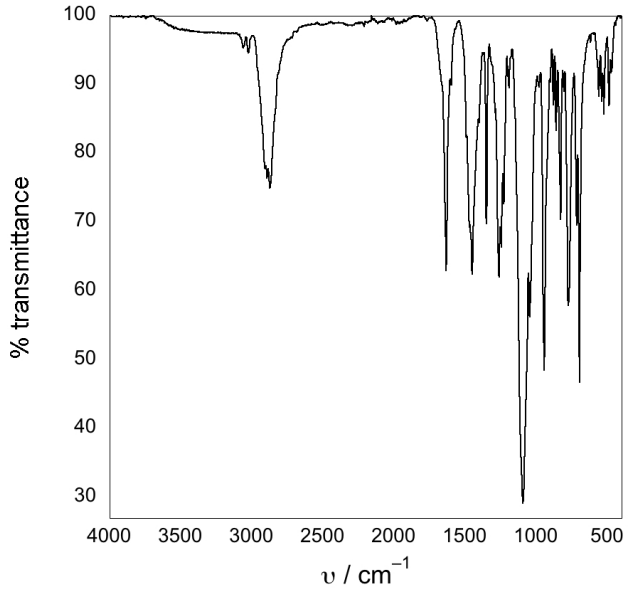


**Figure S23.** FTIR spectrum 15-crwon-5 sodium *S*-benzylthiocarbonate

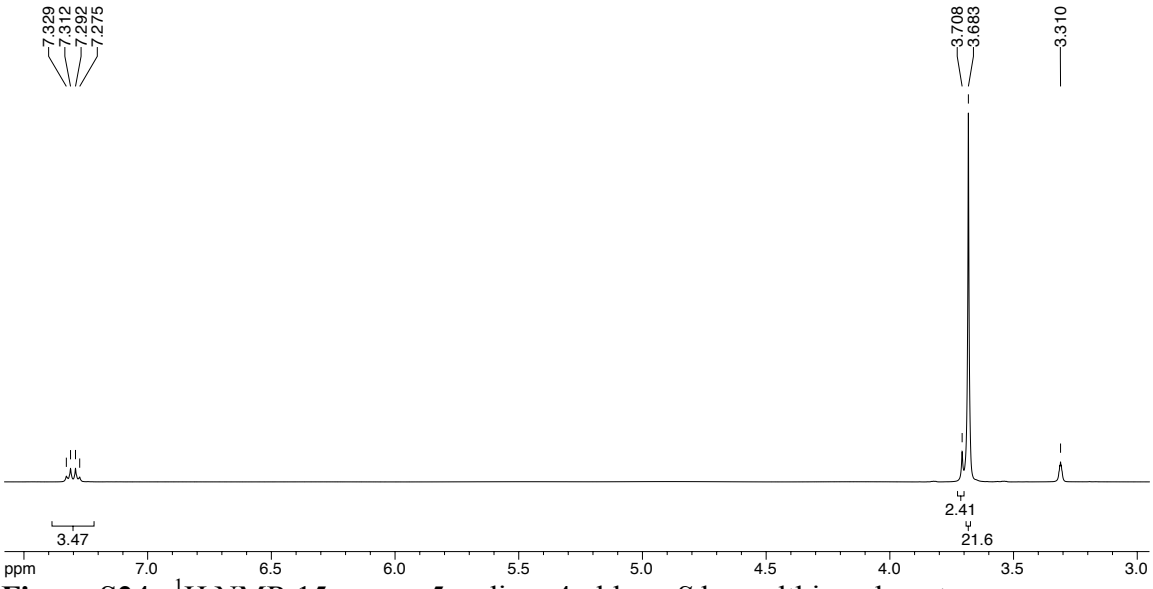


**Figure S24**. $^{1}$H NMR 15-crown-5 sodium 4-chloro-*S*-benzylthiocarbonate

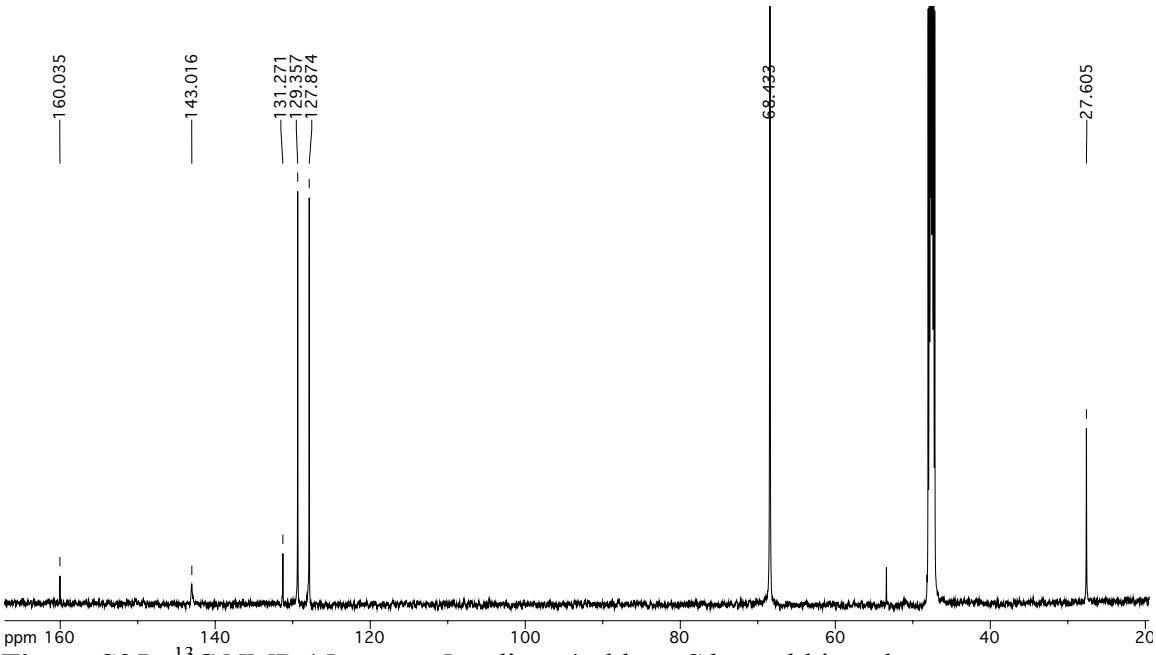


**Figure S25.** $^{13}$C NMR 15-crown-5 sodium 4-chloro-*S*-benzylthiocarbonate

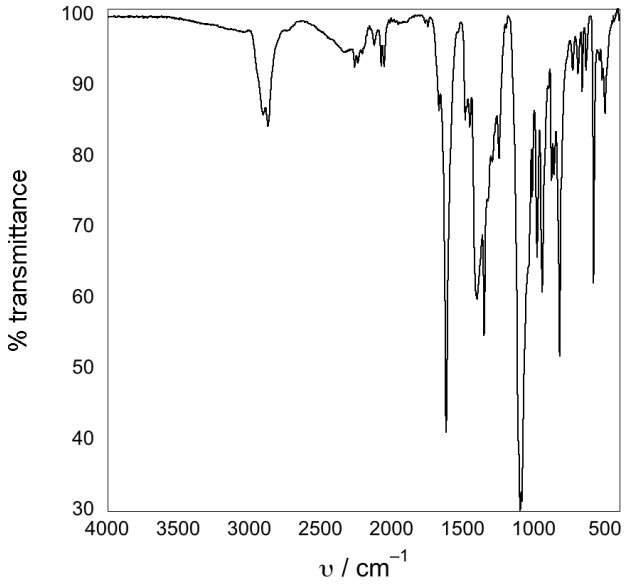


**Figure S26.** FTIR spectrum of 15-crown-5 sodium 4-chloro-*S*-benzylthiocarbonate

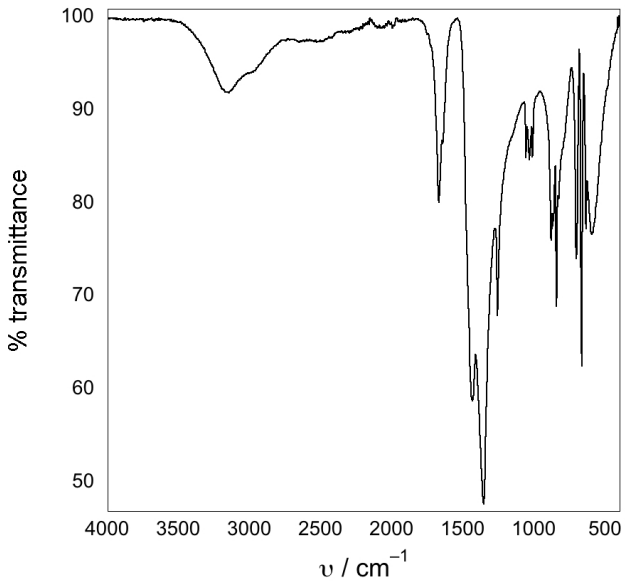


**Figure S27.** FTIR spectrum of potassium benzylthiocarbonate

REFERENCES

1. Cicerone, R. J.; Nurse, P. *Climate Change: Evidence & Causes*; Royal Society and National Academy of Sciences, The National Academies: Washington, DC, 2014.

2. Lunt, D. J.; Haywood, A. M.; Schmidt, G. A.; Salzmann, U.; Valdes, P. J.; Dowsett, H. J., *J. Nat. Geoscience* **2010,** *3*, 60-64.

3. Arrhenius, S. A., on the Influence of Carbonic Acid. *Phil. Mag. s.* **1896,** *41* (251), 237-276.

4. Högbom, A., Om Sannolikheten För Sekulära Förändringar I Atmosfärens Kolsyrehalt. *Svensk kemisk Tidskrift* **1894,** *6*, 169-177.

5. (a) Arrhenius, S. A., Über die Wärmeabsorption Durch Kohlensäure und Ihren Einfluss auf die Temperatur der Erdoberfläche. *Förhandlingar Svenska Vetenskapsakademiens* **1901,** *58*, 25-58; (b) Arrhenius, S. A., Über Die Wärmeabsorption Durch Kohlensäure. *Annalen der Physik* **1901,** *4*, 690-705; (c) Arrhenius, S. A., *World in the Making*. Harper & Brothers: New York, 1908.

6. Hansen, J.; Ruedy, R.; Sato, M.; Lo, K., Global Surface Temperature Change. *Reviews of Geophysics* **2010,** *48* (4).

7. NASA GISS Surface Temperature Analysis. https://data.giss.nasa.gov/gistemp/graphs_v3/ (accessed September 2017).

8. *Climate Change 2014 Synthesis Report*; Intergovernmental Panel on Climate Change; Pachauri, R. K.; Meyer, L. A., Geneva, Switzerland, 2014.

9. U.S. Department of Commerce, N. O. A. A. Trends in Atmospheric Carbon Dioxide. https://www.esrl.noaa.gov/gmd/ccgg/trends/global.html (accessed September 5, 2017).

10. Keeling, C. D.; Piper, S. C.; Whorf, T. P.; Keeling, R. F., Evolution of natural and anthropogenic fluxes of atmospheric CO2 from 1957 to 2003. *Tellus B: Chemical and Physical Meteorology* **2017,** *63* (1), 1-22.

11. Anderegg, W. R.; Prall, J. W.; Harold, J.; Schneider, S. H., Expert credibility in climate change. *Proceedings of the National Academy of Sciences of the United States of America* **2010,** *107* (27), 12107-9.

12. Olivier, J. G. J.; Janssens-Maenhout, G.; Muntean, M.; Peters, J. A. H. W., Trends in Global CO2 Emissions 2016 Report. *PBL Netherland Environmental Assessment Agency* **2016,** *2315*.

13. (a) Boot-Handford, M. E.; Abanades, J. C.; Anthony, E. J.; Blunt, M. J.; Brandani, S.; Mac Dowell, N.; Fernández, J. R.; Merrar, M. C.; Gross, R.; Hallett, J. P.; Haszeldine,

R. S.; Heptonstall, P.; Lyngfelt, A.; Makuch, Z.; Mangano, E.; Porter, R. T. J.; Pourkashanian, M.; Rochelle, G. T.; Shah, N.; Yao, J. G.; Fennell, P. S., Carbon Capture and Storage Update. *Energy Environ. Sci.* **2014,** *7*, 130-189; (b) Hasib-ur-Rahman, M.; Siaj, M.; Larachi, F., Ionic liquids for CO2 capture—Development and progress. *Chemical Engineering and Processing: Process Intensification* **2010,** *49* (4), 313-322; (c) MacDowell, N.; Florin, N.; Buchard, A.; Hallett, J.; Galindo, A.; Jackson, G.; Adjiman, C. S.; Williams, C. K.; Shah, N.; Fennell, P., An overview of CO2 capture technologies. *Energy & Environmental Science* **2010,** *3* (11), 1645.

14. Daily, S. Carbon Dioxide Emissions From Power Plants Rated Worldwide. (accessed September 3, 2017).

15. (a) (EIA), U. S. E. I. A. Inventory of U.S. Greenhouse Gas Emissions and Sinks: 1990-2008. (accessed September 2, 2017); (b) (EIA), U. S. E. I. A. Emissions of Greenhouse Gases in the United States. (accessed September 2, 2017).

16. Benson, S. M.; Orr, F. M., Carbon Dioxide Capture and Storage. *Environmental Policy Collection* **2010,** *33*, 303-305.

17. IPCC *Special Report on Carbon Dioxide Capture and Storage. Prepared by Working Group III of the Intergovernmental Panel on Climate Change*; Intergovernmental Panel on Climate Change: U.K., and New York, 2005.

18. (a) Heyong, T.; Wanfu, W.; Renfang, W., Study on Carbon Dioxide Capture Technology. *Energy Environmental Protection* **2012,** *26*, 39-41; (b) Hu, Y.; Yan, J., Oxyfuel Combustion for CO2 Capture. *International Journal of Greenhouse Gas Control* **2015,** *40*, 55-125; (c) Jordal, K.; Anheden, M.; Yan, J., Oxyfuel Combustion for Coal-Fired Power Generation with CO2 Capture-Opportunities and Challenges. *Greenhouse Gas Control Technologies* **2005**, 201-209.

19. Yuan, P.; Qiu, Z.; Liu, J., Recent enlightening strategies for co2 capture: a review. *IOP Conference Series: Earth and Environmental Science* **2017,** *64*, 012046.

20. Bhown, A. S.; Freeman, B. C., Analysis and Status of Post-Combustion Carbon Dioxide Capture Technologies. *Environ. Sci. Technol.* **2011,** *45*, 8624-8632.

21. (a) Council, A. C., *Guide to the Business of Chemistry*. Washington, DC, 2017; (b) Staff, C. E., Gains in Chemical Output Level Off. *Chem. Eng. News* 2008, pp 61-70.

22. Chemistry, I. U. o. P. a. A., Manual of Symbols and Terminology for Physicochemical Quantities and Units. In *Definitions, Terminoloy and Symbols in Colloid and Surface Chemistry*, International Union of Pure and Applied Chemistry: Washington, DC, 2002.

23. Tolman, W. B., Ed., *Activation of Small Molecules: Organometallic and Bioinorganic Perspectives;*. Wiley-VCH Verlag GmbH & Co.: Weinheim, Germany, 2006.

24. Scibioh, M. A.; Viswanathan, B., *Proc. Indian Natn. Sci. Acad.* **2004,** *70*, 1–65.

25. Lackner, K. S.; Ziock, H.; Grimes, P., Carbon Dioxide Extraction from Air: Is It an Option? In *In Proceedings of the 24th Annual Technical Conference on Coal Utilization & Fuel Systems*, Clearwater, FL, 1999; pp 885-896.

26. Goeppert, A.; Czaun, M.; Surya Prakash, G. K.; Olah, G. A., Air as the Renewable Carbon Source of the Future: An Overview of CO2 Capture from the Atmosphere. *Energy Environ. Sci.* **2012,** *5*, 7833-7853.

27. Sanz-Perez, E. S.; Murdock, C. R.; Didas, S. A.; Jones, C. W., Direct Capture of CO2 from Ambient Air. *Chemical reviews* **2016,** *116* (19), 11840-11876.

28. Society, A. P., Direct Air Capture of CO2 with Chemicals: A Technology Assesment for the APS Panel on Public Affairs. *APS* **2011**.

29. STOLAROFF, J. K.; KEITH, D. W.; LOWRY, G. V., Carbon Dioxide Capture from Atmospheric Air Using Sodium Hydroxide Spray. *Environ. Sci. Technol.* **2008,** *42*, 2728-2735.

30. (a) Baciocchi, R.; Storti, G.; Mazotti, M., Process design and energy requirements for the capture of carbon dioxide from air. *Chemical Engineering and Processing: Process Intensification* **2006,** *45*, 1047-1058; (b) Zeman, F., Energy and Material Balance of CO2

Capture from Ambient Air. *Environ. Sci. Technol.* **2007,** *41*, 7558-7563.

31. Shi, X.; Xiao, H.; Lackner, K. S.; Chen, X., Capture CO2 from Ambient Air Using Nanoconfined Ion Hydration. *Angewandte Chemie* **2016,** *55* (12), 4026-9.

32. (a) Abu Ghalia, M.; Dahman, Y., Development and Evaluation of Zeolites and Metal-Organic Frameworks for Carbon Dioxide Separation and Capture. *Energy Technology* **2017,** *5* (3), 356-372; (b) Bae, Y. S.; Snurr, R. Q., Development and evaluation of porous materials for carbon dioxide separation and capture. *Angewandte Chemie* **2011,** *50* (49), 11586-96; (c) Sabouni, R.; Kazemian, H.; Rohani, S., Carbon dioxide capturing technologies: a review focusing on metal organic framework materials (MOFs). *Environmental science and pollution research international* **2014,** *21* (8), 5427-49; (d) Yaumi, A. L.; Bakar, M. Z. A.; Hameed, B. H., Recent advances in functionalized composite solid materials for carbon dioxide capture. *Energy* **2017,** *124*, 461-480.

33. McDonald, T. M.; Lee, W. R.; Mason, J. A.; Wiers, B. M.; Hong, C. S.; Long, J. R., Capture of carbon dioxide from air and flue gas in the alkylamine-appended metal-organic framework mmen-Mg2(dobpdc). *Journal of the American Chemical Society* **2012,** *134* (16), 7056-65.

34. McDonald, T. M.; Mason, J. A.; Kong, X.; Bloch, E. D.; Gygi, D.; Dani, A.; Crocella, V.; Giordanino, F.; Odoh, S. O.; Drisdell, W. S.; Vlaisavljevich, B.; Dzubak, A. L.; Poloni, R.; Schnell, S. K.; Planas, N.; Lee, K.; Pascal, T.; Wan, L. F.; Prendergast, D.; Neaton, J. B.; Smit, B.; Kortright, J. B.; Gagliardi, L.; Bordiga, S.; Reimer, J. A.; Long, J. R., Cooperative insertion of CO2 in diamine-appended metal-organic frameworks. *Nature* **2015,** *519* (7543), 303-8.

35. (a) Kazakov, A. M., J.W.; Chirico, R.D.; Paulechka, E.; Diky, V.; Muzny, C.D.; Kroenlein, K.; Frenkel, M. NIST Standard Reference Database 147: NIST Ionic Liquids Database - (ILThermo)", Version 2.0. http://ilthermo.boulder.nist.gov (accessed September 15, 2017); (b) Dong, Q. M., C.D.; Kazakov, A.; Diky, V.; Magee, J.W.; Widegren, J.A.; Chirico, R.D.; Marsh, K.N.; Frenkel, M., ILThermo: A Free-Access Web Database for Thermodynamic Properties of Ionic Liquids. *J. Chem. Eng. Data* **2007,** *52* (4), 1151-1159.

36. (a) Firaha, D. S.; Holloczki, O.; Kirchner, B., Computer-Aided Design of Ionic Liquids as CO2 Absorbents. *Angewandte Chemie* **2015,** *54* (27), 7805-7809; (b) Firaha, D. S.; Kirchner, B., Tuning the Carbon Dioxide Adsorption in Aminio Acid Ionic Liquids. *Chem Sus Chem* **2016,** *9* (13), 1591-1599; (c) Garcia, G.; Atilhan, M.; Aparicio, S., Assessment of DFT methods for studying acid gas capture by ionic liquids. *Physical Chemistry Chemical Physics* **2015,** *17* (40), 26875-26891; (d) Izgorodina, E. I.; Seeger, Z. L.; Scarborough, D. L. A.; Tan, S. Y. S., Quantum Chemical Methods for the Prediction of Energetic, Physical, and Spectroscopic Properties of Ionic Liquids. *Chemical reviews* **2017,** *117* (10), 6696-6754; (e) Katsyuba, S. A.; Zvereva, E. E.; Vidis, A.; Dyson, P. J., Application of Density Functional Theory and Vibrational Spectroscopy Toward the

Rational Design of Ionic Liquids. *J Phys Chem A* **2007,** *111*, 352-370; (f) Wu, C.; Senftle, T. P.; Schneider, W. F., First-principles-guided design of ionic liquids for CO2 capture. *Physical chemistry chemical physics : PCCP* **2012,** *14* (38), 13163-70.

37. Lei, Z.; Dai, C.; Chen, B., Gas solubility in ionic liquids. *Chemical reviews* **2014,** *114* (2), 1289-326.

38. (a) Finotello, A.; Bara, J. E.; Narayan, S.; Camper, D.; Noble, R. D., *J. Phys. Chem. B* **2008,** *112*, 2335-2339; (b) Baltus, R. E.; Culbertson, B. H.; Dai, S.; Luo, H.; DePaoli|, D. W., *J. Phys. Chem. B* **2004,** *108*, 721-727; (c) Lei, Z.; Han, J.; Zhang, B.; Li, Q.; Zhu, J.; Chen, B., *Journal Chem. Eng. Data* **2012,** *57* (8), 2153-2159; (d) Shiflett, M. B.; Yokozeki, A., *J. Chem. Eng. Data* **2009,** *54*, 108-114; (e) Kühne, E.; Calvo, E. S.; Witkamp, G. J.; Peters, C. J., *J. Supercrit. Fluids* **2008,** *45* (3), 293-297; (f) Kühne, E.; Santarossa, S.; Perez, E.; Witkamp, G. J.; Peters, C. J., *J. Supercrit. Fluids* **2008,** *46* (2), 93-98; (g) Kühne, E.; Perez, E.; Witkamp, G. J.; Peters, C. J., *J. Supercrit. Fluids* **2008,** *45* (1), 27-31; (h) Zhang, Z.; Wu, W.; Wang, B.; Chen, J.; Shen, D.; Han, B., *J. Supercrit. Fluids* **2007,** *40* (1), 1-6; (i) Lei, Z.; Qi, X.; Zhu, J.; Li, Q.; Chen, B., *J. Chem. Eng. Data* **2012,** *57* (12), 3458-3466; (j) G. Hong, J. J., P. Husson, M. F. Costa Gomes, M. Deetlefs, M. Nieuwenhuyzen,; O. Sheppard, a. C. H., *Ind. Eng. Chem. Res.*

**2006,** *45*, 8180-8188; (k) Scurto, A. M.; Aki, S. N. V. K.; Brennecke, J. F., *Chem. Commun.* **2003,** (5), 572-573; (l) Scurto, A. M.; Aki, S. N. V. K.; Brennecke, J. F., *J. Am. Chem. Soc.* **2002,** *124*, 10277; (m) Aki, S. N. V. K.; Scurto, A. M.; Brennecke, J. F., *Ind. Eng. Chem. Res.* **2006,** *45*, 5574-5585; (n) Mellein, B. R.; Brennecke, J. F., *J. Phys. Chem. B* **2007,** *111*, 4837-4843; (o) Liu, Z.; Wu, W.; Han, B.; Dong, Z.; Zhao, G.; Wang, J.; Jiang, T.; Yang, G., *Chemistry* **2003,** *9* (16), 3897-903.

39. Eleanor D. Bates, R. D. M., Ioanna Ntai, and James H. Davis, J., CO2 Capture by a Task-Specific Ionic Liquid. *Journal of the American Chemical Society* **2002,** *124* (6), 926-927.

40. Seo, S.; Quiroz-Guzman, M.; DeSilva, M. A.; Lee, T. B.; Huang, Y.; Goodrich, B. F.; Schneider, W. F.; Brennecke, J. F., Chemically Tunable Ionic Liquids with Aprotic Heterocyclic Anion (AHA) for CO2 Capture. *J. Phys. Chem. B* **2014,** *118* (21), 5740-5751.

41. Seo, S.; Simoni, L. D.; Ma, M.; DeSilva, M. A.; Huang, Y.; Stadtherr, M. A.; Brennecke, J. F., Phase-Change Ionic Liquids for Postcombustion CO2 Capture. *Energy Fuels* **2014,** *28* (9), 5968-5977.

42. (a) Beer, P. D.; Gale, P. A., *Angew. Chem. Int. Ed.* **2001,** *40*, 486-516; (b) H. M. Luo, G. A. B., J. S. Lee, R. M. Pagni, S. Dai, *The journal of physical chemistry. B* **2009,** *113*, 4181; (c) I. Kaljurand, I. A. K., A. Kutt, E. I. Room, T. Rodima, I. Koppel, M. Mishima, I. Leito, *J Phys Chem A* **2007,** *111*, 1245.

43. Wang, C.; Luo, H.; Jiang, D. E.; Li, H.; Dai, S., Carbon dioxide capture by superbase-derived protic ionic liquids. *Angewandte Chemie* **2010,** *49* (34), 5978-81.

44. Wang, C.; Luo, X.; Luo, H.; Jiang, D. E.; Li, H.; Dai, S., Tuning the basicity of ionic liquids for equimolar CO2 capture. *Angewandte Chemie* **2011,** *50* (21), 4918-22.

45. Wang, C.; Luo, H.; Li, H.; Zhu, X.; Yu, B.; Dai, S., Tuning the physicochemical properties of diverse phenolic ionic liquids for equimolar CO2 capture by the substituent on the anion. *Chemistry* **2012,** *18* (7), 2153-60.

46. Boulas, P. L.; Gómez-Kaifer, M.; LEchegoyen, L., *Angew. Chem. Int. Ed.* **1998,** *37*, 216-247.

47. Gohndrone, T. R.; Bum Lee, T.; DeSilva, M. A.; Quiroz-Guzman, M.; Schneider, W. F.; Brennecke, J. F., Competing reactions of CO2 with cations and anions in azolide ionic liquids. *ChemSusChem* **2014,** *7* (7), 1970-5.

48. Lee, T. B.; Oh, S.; Gohndrone, T. R.; Morales-Collazo, O.; Seo, S.; Brennecke, J. F.; Schneider, W. F., CO2 Chemistry of Phenolate-Based Ionic Liquids. *The journal of physical chemistry. B* **2016,** *120* (8), 1509-17.

49. (a) Menard, G.; Stephan, D. W., Stoichiometric reduction of CO2 to CO by aluminum-based frustrated Lewis pairs. *Angewandte Chemie* **2011,** *50* (36), 8396-9; (b) Stephan, G. M. n. a. D. W., Room Temperature Reduction of CO2 to Methanol by Al-Based Frustrated Lewis Pairs and Ammonia Borane. *Journal of the American Chemical Society* **2010,** *132*, 1796-1797.

50. (a) Holbrey, J. D.; Reichert, W. M.; Tkatchenko, I.; Bouajila, E.; Walter, O.; Tommasi, I.; Rogers, R. D., 1,3-Dimethylimidazolium-2-carboxylate: the unexpected synthesis of an ionic liquid precursor and carbene-CO2 adductElectronic supplementary information (ESI) available: experimental data for 1,3-dimethylimidazolium-2-carboxylate. *Chemical Communications* **2003,** (1), 28-29; (b) Norbert Kuhn, M. S., Gerd Weyers, Synthese und Eigenschaften von l,3-Diisopropyl-4,5-dimethylimidazolium-2-carboxylat. Ein stabiles Carben-Addukt des Kohlendioxids [1]. *Z. Naturforsch. b* **1999,** *54*, 427-433.

51. Tudose, A.; Demonceau, A.; Delaude, L., Imidazol(in)ium-2-carboxylates as N-heterocyclic carbene precursors in ruthenium–arene catalysts for olefin metathesis and cyclopropanation. *Journal of Organometallic Chemistry* **2006,** *691* (24-25), 5356-5365.

52. Ishiguro Katsuya , H. K., Nojima Takayuki , Sawaki Yasuhiko, Nucleophilic O-Transfer, Cyclizaton, and Decarboxylation of Carbonyl Oxide Intermediate in the Reaction of Stable Imidazolylidene and Singlet Oxygen. *Chemistry Letters* **2002,** *31*, 796-797.

53. (a) Duong, H. A.; Tekavec, T. N.; Arif, A. M.; Louie, J., Reversible carboxylation of N-heterocyclic carbenes. *Chem Commun (Camb)* **2004,** (1), 112-3; (b) Van Ausdall, B. R.; Glass, J. L.; Wiggins, K. M.; Aarif, A. M.; Louie, J., A systematic investigation of factors influencing the decarboxylation of imidazolium carboxylates. *The Journal of organic chemistry* **2009,** *74* (20), 7935-42.

54. Manginn, E. J. *Design and evaluation of Ionic liquids as novel CO2 absorbents*; Department of Energy: 2005.

55. Gurau, G. R., H.; Kelley, S. P.; Janiczek, P.; Kalb, R. S.; Rogers, R. D., Demonstration of Chemisorption of Carbon Dioxide in 1,3-Dialkylimidazolium Acetate Ionic Liquids. *Angew Chem* **2011,** *123*, 12230-12232.

56. (a) Besnard, M.; Cabaco, M. I.; Chavez, F. V.; Pinaud, N.; Sebastiao, P. J.; Coutinho, J. A.; Danten, Y., On the spontaneous carboxylation of 1-butyl-3-methylimidazolium acetate by carbon dioxide. *Chem Commun (Camb)* **2012,** *48* (9), 1245-7; (b) Cabaco, M. I.; Besnard, M.; Chavez, F. V.; Pinaud, N.; Sebastiao, P. J.; Coutinho, J. A.; Mascetti, J.; Danten, Y., On the chemical reactions of carbon dioxide isoelectronic molecules CS2 and OCS with 1-butyl-3-methylimidazolium acetate. *Chem Commun (Camb)* **2013,** *49* (94), 11083-5; (c) Mao, J. X.; Steckel, J. A.; Yan, F.; Dhumal, N.; Kim, H.; Damodaran, K., Understanding the mechanism of CO2 capture by 1,3 di-substituted imidazolium acetate based ionic liquids. *Physical chemistry chemical physics*

: *PCCP* **2016,** *18*, 1911-1917; (d) Seo, S.; DeSilva, M. A.; Brennecke, J. F., Physical Properties and CO2 Reaction Pathway of 1-Ethyl-3-Methylimidazolium Ionic Liquids with Aprotic Heterocyclic Anions. *The journal of physical chemistry. B* **2014,** *118* (51), 14870-9.

57. Holloczki, O.; Firaha, D. S.; Friedrich, J.; Brehm, M.; Cybik, R.; Wild, M.; Stark, A.; Kirchner, B., Carbene formation in ionic liquids: spontaneous, induced, or prohibited? *The journal of physical chemistry. B* **2013,** *117* (19), 5898-907.

58. (a) Feroci, M.; Chiarotto, I.; Ciprioti, S. V.; Inesi, A., On the reactivity and stability of electrogenerated N-heterocyclic carbene in parent 1-butyl-3-methyl-1H-imidazolium tetrafluoroborate: Formation and use of N-heterocyclic carbene-CO2 adduct as latent catalyst. *Electrochimica Acta* **2013,** *109*, 95-101; (b) Feroci, M.; Chiarotto, I.; Forte, G.; Inesi, A., An electrochemical methodology for the cyclic CO2 "catch and release". The role of the electrogenerated N-heterocyclic carbene in BMIm-BF4. *Journal of CO2 Utilization* **2013,** *2*, 29-34; (c) Feroci, M.; Chiarotto, I.; Forte, G.; Vecchio Ciprioti, S.; Inesi, A., Stability and CO2Capture Ability of ElectrogeneratedN-Heterocyclic Carbene in Parent 1-Butyl-3-methylimidazoliun Ionic Liquid (BMIm-X): The Role of X−. *ChemElectroChem* **2014,** *1* (8), 1407-1414.

59. Mei, K.; He, X.; Chen, K.; Zhou, X.; Li, H.; Wang, C., Highly Efficient CO2 Capture by Imidazolium Ionic Liquids through a Reduction in the Formation of the Carbene–CO2 Complex. *Industrial & Engineering Chemistry Research* **2017,** *56* (28), 8066-8072.

60. Hammond, G. P.; Ondo Akwe, S. S., Thermodynamic and related analysis of natural gas combined cycle power plants with and without carbon sequestration. *International Journal of Energy Research* **2007,** *31* (12), 1180-1201.

61. Aldy, J. E.; Kotchen, M. J.; Leiserowitz, A. A., Willingness to pay and political support for a US national clean energy standard. *Nature Climate Change* **2012,** *2*, 596-599.

62. Thitakamol, B.; Veawab, A.; Aroonwilas, A., Environmental impacts of absorption-based CO2 capture unit for post-combustion treatment of flue gas from coal-fired power plant. *International Journal of Greenhouse Gas Control* **2007,** *1* (3), 318-342.

63. Kanniche, M.; Le Moullec, Y.; Authier, O.; Hagi, H.; Bontemps, D.; Neveux, T.; Louis-Louisy, M., Up-to-date CO 2 Capture in Thermal Power Plants. *Energy Procedia* **2017,** *114*, 95-103.

64. DuBois, D. L.; Miedaner, A.; Bell, W.; Smart, J. C., In *Electrochemical and Electrocatalytic reactions of Carbon Dioxide*, Sullivan, B. P. G., H. E., Ed. Elsevier Science Publishers B. V.: Amsterdam, 1993; pp 90-94.

65. Scovazzo, P.; Poshusta, J.; DuBois, D.; Koval, C.; Noble, R., Electrochemical Separation and Concentration of <1% Carbon Dioxide from Nitrogen. *Journal of The Electrochemical Society* **2003,** *150* (5), D91.

66. (a) Abanades, J. C.; Arias, B.; Lyngfelt, A.; Mattisson, T.; Wiley, D. E.; Li, H.; Ho, M. T.; Mangano, E.; Brandani, S., Emerging $CO_2$ capture systems. *International Journal of Greenhouse Gas Control* **2015,** *40*, 126-166; (b) Boot-Handford, M. E.; Abanades, J. C.; Anthony, E. J.; Blunt, M. J.; Brandani, S.; Mac Dowell, N.; Fernandez, J. R.; Ferrari, M. C.; Gross, R.; Hallett, J. P.; Haszeldine, R. S.; Heptonstall, P.; Lyngfelt, A.; Makuch, Z.; Mangano, E.; Porter, R. T. J.; Pourkashanian, M.; Rochelle, G. T.; Shah, N.; Yao, J. G.; Fennell, P. S., Carbon capture and storage update. *Energy & Environmental Science* **2014,** *7* (1), 130-189; (c) Hammond, G. P.; Akwe, S. S. O.; Williams, S., Techno-economic appraisal of fossil-fuelled power generation systems with carbon dioxide capture and storage. *Energy* **2011,** *36* (2), 975-984.

67. (a) Goeppert, A.; Zhang, H.; Czaun, M.; May, R. B.; Prakash, G. K. S.; Olah, G. A.; Narayanan, S. R., Easily Regenerable Solid Adsorbents Based on Polyamines for Carbon Dioxide Capture from the Air. *Chemsuschem* **2014,** *7* (5), 1386-1397; (b) Li, D.; Furukawa, H.; Deng, H. X.; Liu, C.; Yaghi, O. M.; Eisenberg, D. S., Designed amyloid fibers as materials for selective carbon dioxide capture. *Proceedings of the National Academy of Sciences of the United States of America* **2014,** *111* (1), 191-196.

68. (a) Huebsche, R. G.; Babinsky, A. D., *SAE Transactions* **1969,** *78*, 151; (b) Kang, M. P.; Winnick, J., C *Journal of Applied Electrochemistry* **1985,** *15* (3), 431-439; (c) Li, K.; Li, N., *Separation Science and Technology* **1993,** *28* (4), 1085-1090.

69. (a) Rexed, I.; della Pietra, M.; McPhail, S.; Lindbergh, G.; Lagergren, C., Molten carbonate fuel cells for $CO_2$ separation and segregation by retrofitting existing plants - An analysis of feasible operating windows and first experimental findings. *International Journal of Greenhouse Gas Control* **2015,** *35*, 120-130; (b) Campanari, S., Carbon dioxide separation from high temperature fuel cell power plants. *Journal of Power Sources* **2002,** *112* (1), 273-289; (c) Campanari, S.; Chiesa, P.; Manzolini, G., $CO_2$ capture from combined cycles integrated with Molten Carbonate Fuel Cells. *International Journal of Greenhouse Gas Control* **2010,** *4* (3), 441-451; (d) Chacartegui, R.; Monje, B.; Sanchez, D.; Becerra, J. A.; Campanari, S., Molten carbonate fuel cell: Towards negative emissions in wastewater treatment CHP plants. *International Journal of Greenhouse Gas Control* **2013,** *19*, 453-461.

70. (a) Eisaman, M. D.; Alvarado, L.; Larner, D.; Wang, P.; Garg, B.; Littau, K. A., $CO_2$ separation using bipolar membrane electrodialysis. *Energy & Environmental Science* **2011,** *4* (4), 1319-1328; (b) Eisaman, M. D.; Alvarado, L.; Larner, D.; Wang, P.; Littau, K. A., $CO_2$ desorption using high-pressure bipolar membrane electrodialysis. *Energy & Environmental Science* **2011,** *4* (10), 4031-4037; (c) Eisaman, M. D.; Parajuly, K.; Tuganov, A.; Eldershaw, C.; Chang, N. R.; Littau, K. A., $CO_2$ extraction from seawater using bipolar membrane electrodialysis. *Energy & Environmental Science* **2012,** *5* (6), 7346-7352.

71. Datta, S.; Henry, M. P.; Lin, Y. J.; Fracaro, A. T.; Millard, C. S.; Snyder, S. W.; Stiles, R. L.; Shah, J.; Yuan, J. W.; Wesoloski, L.; Dorner, R. W.; Carlson, W. M., Electrochemical CO2 Capture Using Resin-Wafer Electrodeionization. *Industrial & Engineering Chemistry Research* **2013,** *52* (43), 15177-15186.

72. Rau, G. H., Electrochemical Splitting of Calcium Carbonate to Increase Solution Alkalinity: Implications for Mitigation of Carbon Dioxide and Ocean Acidity. *Environmental Science & Technology* **2008,** *42* (23), 8935-8940.

73. Watkins, J. D.; Siefert, N. S.; Zhou, X.; Myers, C. R.; Kitchin, J. R.; Hopkinson, D. P.; Nulwala, H. B., Redox-Mediated Separation of Carbon Dioxide from Flue Gas. *Energy & Fuels* **2015,** *29* (11), 7508-7515.

74. Mizen, M. B.; Wrighton, M. S., REDUCTIVE ADDITION OF $CO_2$ TO 9,10-PHENANTHRENEQUINONE. *Journal of the Electrochemical Society* **1989,** *136* (4), 941-946.

75. Scovazzo, P.; Poshusta, J.; DuBois, D.; Koval, C.; Noble, R., Electrochemical separation and concentration of < 1% carbon dioxide from nitrogen. *Journal of the Electrochemical Society* **2003,** *150* (5), D91-D98.

76. Apaydin, D. H.; Glowacki, E. D.; Portenkirchner, E.; Sariciftci, N. S., Direct Electrochemical Capture and Release of Carbon Dioxide Using an Industrial Organic Pigment: Quinacridone. *Angewandte Chemie-International Edition* **2014,** *53* (26), 6819-6822.

77. Gurkan, B.; Simeon, F.; Hatton, T. A., Quinone Reduction in Ionic Liquids for Electrochemical $CO_2$ Separation. *ACS Sustainable Chemistry & Engineering* **2015,** *3* (7), 1394-1405.

78. Ishida, H.; Ohba, T.; Yamaguchi, T.; Ohkubo, K., INTERACTION BETWEEN $CO_2$ AND ELECTROCHEMICALLY REDUCED SPECIES OF N-PROPYL-4,4'-BIPYRIDINIUM CATION. *Chemistry Letters* **1994,** (5), 905-908.

79. Ranjan, R.; Olson, J.; Singh, P.; Lorance, E. D.; Buttry, D. A.; Gould, I. R., Reversible Electrochemical Trapping of Carbon Dioxide Using 4,4 '-Bipyridine That Does Not Require Thermal Activation. *Journal of Physical Chemistry Letters* **2015,** *6* (24), 4943-4946.

80. Saveant, J. M., *Elements of molecular and biomolecular electrochemistry: An electrochemical approach to electron transfer chemistry*. John Wiley & Sons: Hoboken, NJ, 2006.

81. Kullapere, M.; Seinberg, J. M.; Maeorg, U.; Maia, G.; Schiffrin, D. J.; Tammeveski, K., Electroreduction of oxygen on glassy carbon electrodes modified with in situ generated anthraquinone diazonium cations. *Electrochimica Acta* **2009,** *54* (7), 1961-1969.

82. Roberts, J. L.; Calderwood, T. S.; Sawyer, D. T., NUCLEOPHILIC OXYGENATION OF CARBON-DIOXIDE BY SUPEROXIDE ION IN APROTIC MEDIA TO FORM THE C2O6(2-) SPECIES. *Journal of the American Chemical Society* **1984,** *106* (17), 4667-4670.

83. Luo, J. F.; Preciado, S.; Xie, P.; Larrosa, I., Carboxylation of Phenols with CO2 at Atmospheric Pressure. *Chem.-Eur. J.* **2016,** *22* (20), 6798-6802.

84. (a) Stern, M. C.; Hatton, T. A., Bench-scale demonstration of $CO_2$ capture with electrochemically-mediated amine regeneration. *RSC Advances* **2014,** *4* (12), 5906-5914; (b) Stern, M. C.; Simeon, F.; Herzog, H.; Hatton, T. A., Post-combustion carbon dioxide capture using electrochemically mediated amine regeneration. *Energy & Environmental Science* **2013,** *6* (8), 2505-2517.

85. DuBois, D. L.; Miedaner, A.; Bell, W.; Smart, J. C., Chapter 4 - Electrochemical Concentration of Carbon Dioxide, Sullivan, B.P. In *Electrochemical and Electrocatalytic Reactions of Carbon Dioxide*, Elsevier: Amsterdam, 1993; pp 94-117.

86. Appel, A. M.; Newell, R.; DuBois, D. L.; DuBois, M. R., Concentration of carbon dioxide by electrochemically modulated complexation with a binuclear copper complex. *Inorganic Chemistry* **2005,** *44* (9), 3046-3056.

87. Singh, P.; Rheinhardt, J. H.; Olson, J. Z.; Tarakeshwar, P.; Mujica, V.; Buttry, D. A., Electrochemical Capture and Release of Carbon Dioxide Using a Disulfide-Thiocarbonate Redox Cycle. *Journal of the American Chemical Society* **2016,** *submitted*.

88. (a) Stueber, D.; Arif, A. M.; Grant, D. M.; Parry, R. W., Carbonates, thiocarbonates, and the corresponding monoalkyl derivatives. 2. X-ray crystal structure of potassium methyltrithiocarbonate (KS2CSCH3). *Inorganic Chemistry* **2001,** *40* (8), 1912-1914; (b) Stueber, D.; Orendt, A. M.; Facelli, J. C.; Parry, R. W.; Grant, D. M., Carbonates, thiocarbonates, and the corresponding monoalkyl derivatives: III. The C-13 chemical shift tensors in potassium carbonate, bicarbonate and related monomethyl derivatives. *Solid State Nuclear Magnetic Resonance* **2002,** *22* (1), 29-49; (c) Stueber, D.; Patterson, D.; Mayne, C. L.; Orendt, A. M.; Grant, D. M.; Parry, R. W., Carbonates, thiocarbonates, and the corresponding monoalkyl derivatives. 1. Their preparation and isotropic C-13 NMR chemical shifts. *Inorganic Chemistry* **2001,** *40* (8), 1902-1911.

89. Shouji, E.; Buttry, D. A., A mechanistic study of the influence of proton transfer processes on the behavior of thiol/disulfide redox couples. *Journal of Physical Chemistry B* **1999,** *103* (12), 2239-2247.

90. Daasbjerg, K.; Jensen, H.; Benassi, R.; Taddei, F.; Antonello, S.; Gennaro, A.; Maran, F., Evidence for large inner reorganization energies in the reduction of diaryl disulfides: Toward a mechanistic link between concerted and stepwise dissociative electron transfers? *Journal of the American Chemical Society* **1999,** *121* (8), 1750-1751.

91. Soloveichik, G. L., Flow Batteries: Current Status and Trends. *Chem. Rev.* **2015,** *115* (20), 11533-11558.

92. Costentin, C.; Robert, M.; Saveant, J. M.; Tard, C., Breaking Bonds with Electrons and Protons. Models and Examples. *Accounts Chem. Res.* **2014,** *47* (1), 271-280.

93. Mayr, H.; Ofial, A. R., Do general nucleophilicity scales exist? *Journal of Physical Organic Chemistry* **2008,** *21* (7-8), 584-595.

94. Kenarsari, S. D.; Yang, D. L.; Jiang, G. D.; Zhang, S. J.; Wang, J. J.; Russell, A. G.; Wei, Q.; Fan, M. H., Review of recent advances in carbon dioxide separation and capture. *Rsc Advances* **2013,** *3* (45), 22739-22773.

95. Dutcher, B.; Fan, M. H.; Russell, A. G., Amine-Based $CO_2$ Capture Technology Development from the Beginning of 2013-A Review. *Acs Applied Materials & Interfaces* **2015,** *7* (4), 2137-2148.

96. Stueber, D.; Grant, D. M., The C-13 chemical shift tensor principal values and orientations in dialkyl carbonates and trithiocarbonates. *Solid State Nuclear Magnetic Resonance* **2002,** *22* (4), 439-457.

97. Cui, G. K.; Wang, J. J.; Zhang, S. J., Active chemisorption sites in functionalized ionic liquids for carbon capture. *Chemical Society Reviews* **2016,** *45* (15), 4307-4339.

98. Liu, M. L.; Visco, S. J.; Dejonghe, L. C., Electrochemical Properties of Organic Disulfide Thiolate Redox Couples. *Journal of the Electrochemical Society* **1989,** *136* (9), 2570-2575.

99. (a) Buzzeo, M. C.; Klymenko, O. V.; Wadhawan, J. D.; Hardacre, C.; Seddon, K. R.; Compton, R. G., Voltammetry of oxygen in the room-temperature ionic liquids 1-ethyl-3-methylimidazolium bis((trifluoromethyl)sulfonyl)imide and hexyltriethylammonium bis((trifluoromethyl)sulfonyl)imide: One-electron reduction to form superoxide. Steady-state and transient behavior in the same cyclic voltammogram resulting from widely different diffusion coefficients of oxygen and superoxide. *Journal of Physical Chemistry A* **2003,** *107* (42), 8872-8878; (b) Barrosse-Antle, L. E.; Bond, A. M.; Compton, R. G.; O'Mahony, A. M.; Rogers, E. I.; Silvester, D. S., Voltammetry in Room Temperature Ionic Liquids: Comparisons and Contrasts with Conventional Electrochemical Solvents. *Chemistry-an Asian Journal* **2010,** *5* (2), 202-230.

100. Hoffman, M. Z.; Hayon, E., One-Electron Reduction of Disulfide Linkage in Aqueous-Solution - Formation, Protonation, and Decay Kinetics of Rssr- Radical. *Journal of the American Chemical Society* **1972,** *94* (23), 7950-&.

101. (a) Antonello, S.; Daasbjerg, K.; Jensen, H.; Taddei, F.; Maran, F., Formation and cleavage of aromatic disulfide radical anions. *Journal of the American Chemical Society* **2003,** *125* (48), 14905-14916; (b) Meneses, A. B.; Antonello, S.; Arevalo, M. C.;

Gonzalez, C. C.; Sharma, J.; Wallette, A. N.; Workentin, M. S.; Maran, F., Electron transfer to sulfides and disulfides: Intrinsic barriers and relationship between heterogeneous and homogeneous electron-transfer kinetics. *Chemistry-a European Journal* **2007,** *13* (28), 7983-7995.

102. Batchelor-McAuley, C.; Compton, R. G., Voltammetry of multi-electron electrode processes of organic species. *J. Electroanal. Chem.* **2012,** *669*, 73-81.

103. Utley, J., Trends in organic electrosynthesis. *Chemical Society Reviews* **1997,** *26* (3), 157-167.

104. Tian, Z. X.; Pawlow, A.; Poutsma, J. C.; Kass, S. R., Are carboxyl groups the most acidic sites in amino acids? Gas-phase acidity, H/D exchange experiments, and computations on cysteine and its conjugate base. *Journal of the American Chemical Society* **2007,** *129* (17), 5403-5407.

105. (a) D'Alessandro, D. M.; Smit, B.; Long, J. R., Carbon Dioxide Capture: Prospects for New Materials. *Angewandte Chemie-International Edition* **2010,** *49* (35), 6058-6082; (b) Heldebrant, D. J.; Yonker, C. R.; Jessop, P. G.; Phan, L., Organic liquid CO2 capture agents with high gravimetric CO2 capacity. *Energy & Environmental Science* **2008,** *1* (4), 487-493; (c) Koh, H. S.; Rana, M. K.; Hwang, J.; Siegel, D. J., Thermodynamic screening of metal-substituted MOFs for carbon capture. *Physical Chemistry Chemical Physics* **2013,** *15* (13), 4573-4581; (d) Lee, H. M.; Youn, I. S.; Saleh, M.; Lee, J. W.; Kim, K. S., Interactions of CO2 with various functional molecules. *Physical Chemistry Chemical Physics* **2015,** *17* (16), 10925-10933.

106. (a) Boixel, J.; Blart, E.; Pellegrin, Y.; Odobel, F.; Perin, N.; Chiorboli, C.; Fracasso, S.; Ravaglia, M.; Scandola, F., Hole-Transfer Dyads and Triads Based on Perylene Monoimide, Quaterthiophene, and Extended Tetrathiafulvalene. *Chemistry-a European Journal 16* (30), 9140-9153; (b) Pistner, A. J.; Pupillo, R. C.; Yap, G. P. A.; Lutterman, D. A.; Ma, Y. Z.; Rosenthal, J., Electrochemical, Spectroscopic, and O-1(2) Sensitization Characteristics of 10,10-Dimethylbiladiene Complexes of Zinc and Copper. *Journal of Physical Chemistry A 118* (45), 10639-10648.

107. Rauk, A.; Yu, D.; Armstrong, D. A., *Journal of the American Chemical Society* **1994,** *116* (18), 8222-8228.

108. Armarego, W. L. F.; Chai, C. L. L., *Purification of Laboratory Chemicals*. Fifth ed.; Butterworth-Heinemann: London, 2003.

109. Fulmer, G. R.; Miller, A. J. M.; Sherden, N. H.; Gottlieb, H. E.; Nudelman, A.; Stoltz, B. M.; Bercaw, J. E.; Goldberg, K. I., NMR Chemical Shifts of Trace Impurities: Common Laboratory Solvents, Organics, and Gases in Deuterated Solvents Relevant to the Organometallic Chemist. *Organometallics* **2010,** *29* (9), 2176-2179.

110. (a) Becke, A. D., *Journal of Chemical Physics* **1993,** *98* (7), 5648-5652; (b) Francl, M. M.; Pietro, W. J.; Hehre, W. J.; Binkley, J. S.; Gordon, M. S.; Defrees, D. J.;

Pople, J. A., *Journal of Chemical Physics* **1982,** *77* (7), 3654-3665; (c) Frisch, M. J., In *Gaussian 03, revision C.02*, Gaussian, Inc.: Wallingford, CT, 2004; (d) Harihara, P. C.; Pople, J. A., *Theoretica Chimica Acta* **1973,** *28* (3), 213-222; (e) Kendall, R. A.; Dunning, T. H.; Harrison, R. J., *Journal of Chemical Physics* **1992,** *96* (9), 6796-6806; (f) Lee, C. T.; Yang, W. T.; Parr, R. G.,. *Physical Review B* **1988,** *37* (2), 785-789; (g) Neese, F., The ORCA program system. *Wiley Interdisciplinary Reviews-Computational Molecular Science* **2012,** *2* (1), 73-78; (h) Rassolov, V. A.; Pople, J. A.; Ratner, M. A.; Windus, T. L., 6-31G* basis set for atoms K through Zn. *Journal of Chemical Physics* **1998,** *109* (4), 1223-1229; (i) Stephens, P. J.; Devlin, F. J.; Chabalowski, C. F.; Frisch, M. J., *Journal of Physical Chemistry* **1994,** *98* (45), 11623-11627; (j) Woon, D. E.; Dunning, T. H., *Journal of Chemical Physics* **1993,** *98* (2), 1358-1371.

111. Denis, P. A., Basis set requirements for sulfur compounds in density functional theory: a comparison between correlation-consistent, polarized-consistent, and pople-type basis sets. *Journal of Chemical Theory and Computation* **2005,** *1* (5), 900-907.

112. Hammond, G. P.; Ondo Akwe, S. S., Thermodynamic and related analysis of natural gas combined cycle power plants with and without carbon sequestration. *Int. J. Energy Res.* **2007,** *31* (12), 1180-1201.

113. Aldy, J. E.; Kotchen, M. J.; Leiserowitz, A. A., Willingness to pay and political support for a US national clean energy standard. *Nat. Clim. Change* **2012,** *2*, 596-599.

114. MacDowell, N.; Florin, N.; Buchard, A.; Hallett, J.; Galindo, A.; Jackson, G.; Adjiman, C. S.; Williams, C. K.; Shah, N.; Fennell, P., An overview of CO2 capture technologies. *Energy Environ. Sci.* **2010,** *3* (11), 1645.

115. Gurau, G. R., H.; Kelley, S. P.; Janiczek, P.; Kalb, R. S.; Rogers, R. D., Demonstration of Chemisorption of Carbon Dioxide in 1,3-Dialkylimidazolium Acetate Ionic Liquids. *Angew. Chem.* **2011,** *123*, 12230-12232.

116. (a) Duong, H. A.; Tekavec, T. N.; Arif, A. M.; Louie, J., Reversible carboxylation of N-heterocyclic carbenes. *Chem. Commun.* **2004,** (1), 112-3; (b) Van Ausdall, B. R.; Glass, J. L.; Wiggins, K. M.; Aarif, A. M.; Louie, J., A systematic investigation of factors influencing the decarboxylation of imidazolium carboxylates. *J. Org. Chem.* **2009,** *74* (20), 7935-42.

117. (a) H. M. Luo, G. A. B., J. S. Lee, R. M. Pagni, S. Dai, *J. Phys. Chem. B* **2009,** *113*, 4181; (b) I. Kaljurand, I. A. K., A. Kutt, E. I. Room, T. Rodima, I. Koppel, M. Mishima, I. Leito, *J. Phys. Chem. A* **2007,** *111*, 1245.

118. Wang, C.; Luo, H.; Jiang, D. E.; Li, H.; Dai, S., Carbon dioxide capture by superbase-derived protic ionic liquids. *Angew. Chem. Int. Ed.* **2010,** *49* (34), 5978-81.

119. Wang, C.; Luo, X.; Luo, H.; Jiang, D. E.; Li, H.; Dai, S., Tuning the basicity of ionic liquids for equimolar CO2 capture. *Angew. Chem. Int. Ed.* **2011,** *50* (21), 4918-22.

120. Wang, C.; Luo, H.; Li, H.; Zhu, X.; Yu, B.; Dai, S., Tuning the physicochemical properties of diverse phenolic ionic liquids for equimolar CO2 capture by the substituent on the anion. *Chem. Eur. J.* **2012,** *18* (7), 2153-60.

121. Singh, P.; Rheinhardt, J. H.; Olson, J. Z.; Tarakeshwar, P.; Mujica, V.; Buttry, D. A., Electrochemical Capture and Release of Carbon Dioxide Using a Disulfide–Thiocarbonate Redox Cycle. *J. Am. Chem. Soc.* **2017,** *139* (3), 1033-1036.

122. Seema, H.; Kemp, K. C.; Le, N. H.; Park, S.-W.; Chandra, V.; Lee, J. W.; Kim, K. S., Highly selective CO2 capture by S-doped microporous carbon materials. *Carbon* **2014,** *66*, 320-326.

123. Kice, J. L.; Bartsch, R. A.; Dankleff, M. A.; Schwartz, S. L., Mechanisms of SNi Reactions. The Decomposition of Aralkyl Thiocarbonates. *J. Am. Chem. Soc.* **1965,** *87*, 1734-1739.

124. Hansch, C.; Leo, A.; Taft, R. W., A Survey of Hammett Substituent Constants and Resonance and Field Parameters. *Chem. Rev.* **1991,** *91*, 165-195.

125. NIST Mass Spec Data Center, S. E. S., director NIST Chemistry WebBook, NIST Standard Reference Database Number 69. http://webbook.nist.gov/cgi/inchi?ID=C124389&Mask=200 - Mass-Spec (accessed October 18, 2017).

126. Tureček, F.; McLafferty, F. W., *Interpretation of Mass Spectra*. Fourth ed.; University Science Books: Sausalito, CA 94965, 1993.

127. (a) Powell, E. K.; Searcy, A. W., Kinetics and Thermodynamics of Decomposition of Dolomite to a Metastable Solid Product. *J. Am. Ceram. Soc.* **1978,** *61*, 216-221; (b) Powell, E. K.; Searcy, A. W., Surface Areas and Morphologies of CaO Produced by Decomposition of Large CaCO3 Crystals in Vacuum. *J. Am. Ceram. Soc.* **1982,** *65*, C42-C44.

128. Seo, S.; DeSilva, M. A.; Brennecke, J. F., Physical Properties and CO2 Reaction Pathway of 1-Ethyl-3-Methylimidazolium Ionic Liquids with Aprotic Heterocyclic Anions. *J. Phys. Chem. B* **2014,** *118* (51), 14870-9.

129. Fulmer, G. R.; Miller, A. J. M.; Sherden, N. H.; Gottlieb, H. E.; Nudelman, A.; Stoltz, B. M.; Bercaw, J. E.; Goldberg, K. I., *Organometallics* **2010,** *29*, 2176–2179.

130. Savitzky, A.; Golay, M. J. E., *Analytical Chemistry* **1964,** *36* (8), 1627-1639.

131. Stueber, D.; Patterson, D.; Mayne, C. L.; Orendt, A. M.; Grant, D. M.; Parry, R. W., *Inorganic Chemistry* **2001,** *40*, 1902-1911.

# APPENDIX A

# FUNCTIONALIZTION OF POLY(2,6-DIMETHYL-1,4-PHENYLENE OXIDE) WITH FERROCENE BY THE COPPER CATALYZED AZIDE–ALKYNE COUPLING REACTION

Metallopolymers are presently an active area in polymer research due to the interest in coupling the unique redox and catalytic properties of inorganic systems with the robustness and versatility of organic polymers. In particular, polymer materials with redox properties find uses in applications such as batteries,[1] chemical sensors,[2] photovoltaics,[3] electrochromic devices,[4] and responsive membranes.[5] A common strategy for achieving redox active polymers is to couple ferrocene moieties to the polymer structure. Ferrocene-containing polymers continue to attract a significant amount of interest due to the well-behaved, reversible redox properties. There are numerous reports and reviews detailing a great number of polymers to which ferrocene has been appended as well as a variety of strategies for achieving covalent attachment of ferrocene to polymers.[6]

In their pioneering work, Inzelt and Szabo described the effect that different electrolyte anions have on the redox potentials of poly(vinylferrocene) polymer film electrodes in aqueous media.[7] The authors observed that the anodic peak potential shifted positive by 76 mV and 71 mV in going from $ClO_4^- < NO_3^- < SO_4^{2-}$, respectively. Efforts to further understand this phenomenon were undertaken by Creager et al.[8], Uosaki et al.[9], and Kondo et al.[10] all of who investigated ferrocene-terminated alkanethiol self-assembled monolayers(SAM) on gold electrodes. By employing 6-ferrocenylhexanethiol monolayers, Uosaki et al. observed the same trend in oxidation potentials as Inzelt and Szabo. Without interference from the polymer matrix Uosaki et al. were able to establish a Nernstian relation between the formation constant of the $Fc^+ X^-$ ion pairs, with larger formation constants leading to more negative redox potentials. Similarly, Creager et al. probed the behavior of 6-ferrocenylhexanethiol as one

component of mixed monolayers with *n*-alkanethiols (1-$C_nH_{2n+1}SH$, $n$ = 4, 6, 8, 10, and 12) and observed that when the value of $n$ is increased, there is a concomitant shift of the ferrocene/ferrocenium redox potential to more positive values. The authors suggest that the longer alkyl chains serve to create a more alkane-like environment where ferrocenium is destabilized relative to ferrocene. Kondo et al. observed that the redox potentials for SAMs of 6-ferrocenylhexanethiol were sensitive both to the anion present in solution as well as the solvent in which the electrochemistry was performed. Specifically, when measured in aqueous electrolyte the redox potential shifted positive in the order $PF_6^- < ClO_4^- < HSO_4^-$, whereas in methylene chloride electrolyte the order was reversed. In a recent report, Neef et al. showed that copolymers from vinylferrocene and 3-phenyl[5]ferrocenophane with *N*-ethyl and *N*-phenylmaleimide exhibited different redox potentials when the supporting electrolyte was changed in aqueous solution. Specifically, there was a positive shift in the redox potentials in going from $ClO_4^- < NO_3^- \approx$ phosphate buffered saline (PBS).

In this paper, we report the synthesis and electrochemical behavior of poly(2,6-dimethyl-1,4-phenylene oxide) (PPO) functionalized with pendant ferrocene moieties. Poly(2,6-dimethyl-1,4-phenylene oxide) is a robust polymer that shows great potential for functional applications in high-temperature, chemically-reactive environments. PPO has excellent thermal and mechanical properties, possessing high dimensional stability and a glass transition temperature ($T_g$) of 220° C.[7, 8] Furthermore, the ferrocene moieties were easily coupled to the PPO backbone using the copper(I) catalyzed azide–alkyne cycloaddition (CuAAC) reaction. Despite the ease of synthesis, without proper workup copper coordination to the product triazole rings can result in a blue, insoluble material

where copper(II) ions act as crosslinkers in the functionalized materials. These materials show good electrochemical response in water–N-methylpyrrollidine (NMP) electrolyte demonstrating both electrochromic properties and sensitivity of the redox potentials to the nature of the electrolyte anion. The latter property of this material is investigated within the context of anion recognition and sensing applications.[11]

**Experimental**

**General Considerations.** All manipulations were carried out using standard Schlenk line techniques under a nitrogen atmosphere. Solvents were purchased from commercial vendors and purified according to literature methods.[12] Deuterated solvents were purchased from Cambridge Isotope Laboratories, Inc., degassed by four successive freeze-pump-thaw cycles and stored in the glovebox. Supporting electrolytes for electrochemical experiments were purified according to literature methods[12] and dried in a vacuum oven at 100 $^{o}$C. All other reagents and starting materials were purchased from commercial vendors and used without further purification unless otherwise noted.

**Physical Methods.** $^{1}$H and $^{13}$C NMR spectra were collected on Varian 400 and 500 MHz NMR spectrometers. $^{1}$H and $^{13}$C NMR spectra are reported in parts per million relative to tetramethylsilane, using the residual solvent resonances as an internal standard.[13] FTIR measurements were performed utilizing a Brüker Alpha spectrometer equipped with a diamond ATR. Photographs taken at 10x magnification were obtained utilizing a Nikon LABOPHOT microscope equipped with a Nikon E950 digital camera. Atomic force microscopy experiments were conducted with a Brüker MultiMode 8 equipped with a Brüker ScanAsyst tip in tapping mode at a scan rate of 0.883 Hz. Single crystals suitable for X-ray diffraction were suspended in Apiezon N grease and

then mounted on the goniometer head of a Bruker APEX diffractometer equipped with Mo Kα radiation. A hemisphere routine was used for data collection and determination of the lattice constants. The space group was identified, and the data were processed using the Bruker SAINT+ program and corrected for absorption using SADABS. The structures were solved using direct methods (SHELXS), completed by subsequent Fourier synthesis, and refined by full-matrix, least-squares procedures on $|F|^2$ (SHELXL). Electrochemical measurements were performed with a CH Instruments 618C Electrochemical Analyzer or a Gamry Reference 3000 Potentiostat/Galvanostat. Cyclic voltammograms were acquired using a polymer-coated glassy carbon working electrode, platinum counter electrode, and Ag/AgCl reference electrode that was –0.417 V against the ferrocene/ferrocenium redox couple. Polymer films were deposited on the glassy carbon electrode from a 2 wt% solution in $CH_2Cl_2$ by pipetting 5 μL of the solution onto the electrode surface and allowing the solvent to evaporate under a stream of $N_2$ over 30 minutes. Prior to each electrochemical experiment, the electrolyte was purged with medical grade $N_2$ for 30 minutes.

**Computational Methods.** Density functional theory (DFT) calculations were carried out using Becke's three-parameter hybrid functional[14] with the Lee−Yang−Parr correlation functional[15] (B3LYP) and the 6-311++G** basis set using the Gaussian suite of programs.[16] This level of theory was selected because it has produced theoretical vibrational spectra that are in good agreement with experiment for a variety of triazoles and benzotriazoles.[17]

**Bromomethylated Poly(2,6-dimethyl-1,4-phenylene oxide) (PPO–Br).** This compound was synthesized according to literature procedures.[18] In a typical experiment,

a 1000 mL round bottom flask equipped with a reflux condenser and a stir bar was charged with 420 mL of chlorobenzene. Subsequently, the apparatus was placed under a nitrogen atmosphere, 10.0 g of poly(2,6-dimethyl-1,4-phenylene oxide) (PPO) was added all at once, and the solution was stirred at room temperature until the PPO had completely dissolved (typically 1 hour). To the stirring solution, 9.9 g of *N*-bromosuccinimide, which had been previously recrystallized from $H_2O$ and dried under vacuum overnight, and 410.5 mg of azobisisobutyronitrile were added all at once. After allowing the solution to stir for ten minutes at room temperature, the apparatus was placed in an oil bath and the reaction mixture was refluxed for four hours. The solution was then cooled to room temperature and roughly half the solvent was removed by rotary evaporation. Upon pouring the resulting viscous, brown fluid into 1000 mL of stirring MeOH, a fibrous brown solid appeared, which was recovered in on filter paper utilizing a Büchner funnel. Purification of the bromomethylated polymer was achieved by Soxhlet extraction with MeOH overnight, then the polymer was transferred to a round bottom flask and placed under vacuum at 70 $^{o}$C overnight. The product was recovered in 95% yield and the degree of bromination was determined to be 50% by NMR. $^{1}$H NMR (500 MHz, $CDCl_3$): $\delta$ = 6.73–6.48 (m, 4 H), 4.35 (s, 2 H), 2.10 (s, 9 H). FTIR ($cm^{-1}$): 3034 (w), 2955 (s), 2922 (s), 2660 (w), 1721 (m), 1605 (s), 1477 (vs), 1460 (vs), 1360 (m), 1306 (s), 1221 (s), 1207 (s).

**Azidified Poly(2,6-dimethyl-1,4-phenylene oxide) (PPO–$N_3$).** Following a similar procedure to that found in the literature,[19] 160 mL of a 3:1 THF:MeOH solution was added to a 500 mL round bottom flask equipped with a stir bar and a reflux condenser. The apparatus was placed under a nitrogen atmosphere, and 5.0 g of PPO–Br was added

all at once. Once all of the PPO–Br had dissolved (typically 30 minutes), 2.5 g of sodium azide was added in three equal portions, allowing 15 minutes between each addition. After the final addition, the flask was sealed and the apparatus was placed in an oil bath. The reaction mixture was refluxed for 16 hours, then cooled to room temperature. Roughly half of the solvent was removed via rotary evaporation, and the contents of the flask was poured into a 3:1 MeOH:$H_2O$ solution at which time a tan-colored precipitate appeared. This material (PPO–$N_3$) was recovered on a filter paper using a Büchner funnel, washed three times with cold methanol, and then repeatedly washed with water until the silver–halide test indicated that no bromide was present. $^1$H NMR (500 MHz, $CDCl_3$): $\delta$ = 6.68–6.48 (m, 4 H), 4.21 (s, 2 H), 2.09 (s, 9 H). FTIR ($cm^{-1}$): 2954 (s), 2923 (s), 2960 (m), 2737 (w), 2101 (vs, $N_3$), 1717 (w), 1604 (s), 1478 (vs), 1458 (vs), 1380 (w), 1344 (s), 1305 (s), 1209 (vs).

**5-Ferrocenyl-1,2,3-Triazole Poly(2,6-dimethyl-1,4-phenylene oxide) (1).** In a 100 mL Schlenk flask equipped with a stir bar, 0.200 g of PPO–$N_3$ was added to 5 mL of chlorobenzene and the solution was placed under a nitrogen atmosphere. Ethynylferrocene (0.147 g, 0.7 mmol) was added to the flask all at once and the solution was allowed to stir for 30 minutes. In a separate 50 mL Schlenk flask equipped with a stir bar, 2 mL of chlorobenzene was added and the solvent was degassed and placed under a nitrogen atmosphere. To the stirring chlorobenzene, 0.232 g of CuBr (1.6 mmol) and 3.2 mL of *N*,*N*,*N*′,*N*″,*N*″-pentamethyldiethylenetriamine (PMDETA, 15.3 mmol) were added and the solution was allowed to stir at room temperature for one hour. Subsequently, 2.3 mL of the CuBr–PMDETA solution was removed from the Schlenk flask by syringe and added dropwise to the ethynylferrocene–PPO–$N_3$ solution

over a period of 15 minutes. The reaction mixture was stirred at room temperature for four hours, at which time it was poured into 100 mL of chloroform in a separatory funnel. Deionized water was added to the funnel and the organic phase was washed repeatedly until the blue color, indicating the presence of copper ions, was no longer observed in the aqueous phase (typically 5 washes). The organic phase was dried over $MgSO_4$, and the solvent was removed by means of rotary evaporation leaving **1** as an orange–brown solid in 91% yield. $^1$H NMR (500 MHz, $CDCl_3$): $\delta$ = 7.27 (bs, 1 H), 6.62–6.47 (m, 4 H), 5.36 (bs, 2 H), 4.74–4.11 (bm, 9 H), 2.09–2.05 (m, 9 H). FTIR ($cm^{-1}$): 3092 (b), 2959 (s), 2921 (s), 2853 (s), 1711 (vw), 1599 (s), 1466 (vs), 1379 (w), 1345 (w), 1302 (m), 1261 (m).

**5-Butyl-1,2,3-Triazole Poly(2,6-dimethyl-1,4-phenylene oxide) (2).** This material was synthesized in a procedure identical to that described above for the synthesis of **1**, except for the use of 1-hexyne (0.1 mL, 0.7 mmol) that was added via syringe all at once. The product was isolated as a light brown solid in 87% yield. $^1$H NMR (500 MHz, $CDCl_3$): $\delta$ = 7.21 (bs, 1 H), 6.62–6.45 (m, 4 H), 5.33–5.29 (m, 2 H), 2.64 (bs, 2 H), 2.10–2.04 (m, 9 H), 1.58 (bs, 2 H), 1.33 (bs, 2 H), 0.90 (bs, 3H). FTIR ($cm^{-1}$): 2961 (m), 2925 (m), 2857 (w), 1720 (w), 1602 (m), 1466 (s), 1379 (w), 1351 (w), 1302 (m), 1259 (s).

**4-Butyl-1-(phenylmethyl)-1*H*-1,2,3-triazole (3).** In a 250 mL Schlenk flask equipped with a stir bar under $N_2$, 50 mL of chlorobenzene was added, along with 3.00 g (22.5 mmol) of benzyl azide and 2.6 mL of (22.5 mmol) of 1-hexyne. In a separate Schlenk flask equipped with a stir bar, 30 mL of chlorobenzene, 3.23 g (22.5 mmol) of CuBr, and 5.6 mL (27.0 mmol) of PMDETA were added and allowed to stir for 30 minutes. Cannula transfer was employed to add the CuBr solution to the benzyl azide–1-hexyne

solution over a period of 30 minutes. After stirring at room temperature for 3 hours, the contents of the flask was emptied into 100 mL of chloroform in a separatory funnel. The organic phase was washed with water (4 x 50 mL), dried over $MgSO_4$, and then the solvent was removed by rotary evaporation. The product was recovered as a white solid in 94 % yield. $^1$H NMR (500 MHz, $CD_3OD$): $\delta$ = 7.69 (s, 1 H), 7.36–7.29 (m, 5 H), 5.40 (s, 2 H), 2.69–2.66 (t, $J$ = 7.5 Hz, 2 H), 1.66–1.60 (m, 2 H), 1.40–1.32 (m, 2 H), 0.94–0.92 (t, $J$ = 7.0 Hz, 3 H). $^{13}$C {$^1$H} NMR (125 MHz, $CD_3OD$): $\delta$ = 149.66, 136.96, 129.97, 129.49, 128.98, 123.11, 54.80, 32.69, 25.97, 23.22, 14.08. FTIR ($cm^{-1}$): 3113 (m), 3063 (s), 2959 (s), 2923 (s), 2875 (m), 2855 (s), 1706 (w), 1556 (s), 1495 (s), 1448 (vs), 1366 (w), 1352 (w), 1332 (m), 1310 (m), 1294 (s), 1228 (s), 1215 (s), 1206 (s).

**4-Butyl-1-(phenylmethyl)-1*H*-1,2,3-triazolyl-Copper(II)-Acetate (4).** Copper(II) acetate monohydrate (58.0 mg, 0.29 mmol) was suspended in 25 mL of $CH_2Cl_2$ in a Schlenk flask equipped with a stir bar and a reflux condenser. The apparatus was placed under a nitrogen atmosphere, and 250.0 mg (1.16 mmol) of **6** was added all at once. After stirring the resulting solution at room temperature for 5 minutes, the apparatus was placed in an oil bath and the solution was refluxed for two hours. Upon cooling the reaction to room temperature, the solvent was removed by rotary evaporation, and the resulting blue solid was washed with cold $Et_2O$ and **7** was isolated in 65 % yield. Crystals suitable for x-ray diffraction were grown by diffusing $Et_2O$ into a $CH_2Cl_2$ solution of **7**. $^1$H NMR (500 MHz, $CD_3OD$): $\delta$ = 12.22 (br, 6 H), 8.18 (s, 1 H), 7.34–7.27 (m, 5 H), 5.56 (s, 2 H), 2.67 (br, 2 H), 1.66 (br, 2 H), 1.37 (br, 2 H), 0.93–0.91 (t, $J$

= 6.5 Hz, 3 H). FTIR ($cm^{-1}$): 2964 (w), 2931 (w), 2858 (vw), 1615 (vs), 1552 (m), 1496 (w), 1423 (vs), 1341 (m), 1264 (m), 1220 (m), 1136 (m).

**Results and Discussion**

*3.1. Polymer synthesis*

5-Ferrocenyl-1,2,3-Triazole Poly(2,6-dimethyl-1,4-phenylene oxide) (**1**) was prepared via the synthetic route shown in Scheme A1. The first step is radical bromination of the methyl groups on the PPO backbone by NBS to yield bromomethylated poly(2,6-dimethyl-1,4-phenylene oxide) (PPO–Br). Subsequently, PPO–Br was combined with sodium azide in a 3:1 THF:$CH_3OH$ solution and refluxed for 16 hours. After cooling to room temperature, roughly half the solvent was removed

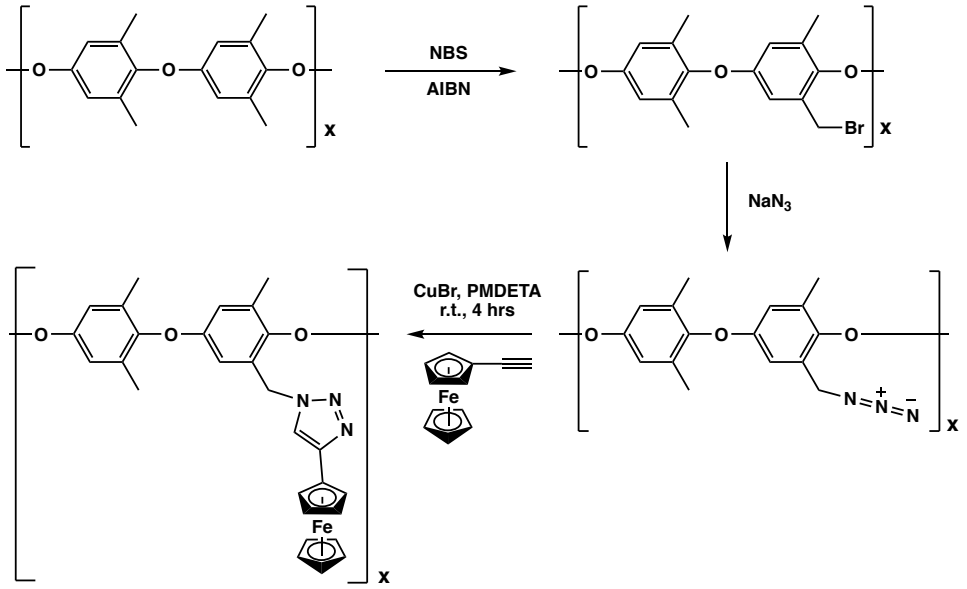


**Scheme A1.** Synthesis of **1** by the copper catalyzed azide–alkyne 1,3-dipolar cycloaddition reaction.

by rotary evaporation and the solution was poured into a beaker containing a 3:1 $CH_3OH$:$H_2O$ solution, at which time a tan solid, azidified poly(2,6-dimethyl-1,4-phenylene oxide) (PPO–$N_3$), appeared. This material was recovered on a filter paper

using a Büchner funnel, washed three times with cold methanol, and then repeatedly washed with water until the silver–halide test indicated that no bromide was present. PPO–$N_3$ was dried, then added to a round bottom flask containing chlorobenzene under a nitrogen atmosphere. Upon complete dissolution of the polymer, ethynylferrocene was added to the solution all at once, followed by the dropwise addition of a chlorobenzene solution of a stoichiometric amount of CuBr–PMDETA. After stirring the solution for 4 hours at room temperature the copper catalyzed azide–alkyne coupling (CuAAC) reaction was judged complete by NMR, and in our initial experiments the contents of the round bottom flask was poured into a beaker of stirring methanol. A soft, blue material immediately precipitated that was found to be insoluble in THF, DMSO, toluene, chloroform, methylene chloride, NMP, methanol, MEK and water.

*3.2. Influence of copper ions*

There were two plausible possibilities as to the identity of the soft, insoluble, blue material: Either the ferrocene moieties were oxidized to ferrocenium, or copper(II) ions that formed during the CuAAC reaction were coordinated to the product triazole rings and were acting as crosslinks. Deeming the latter to be more likely based upon earlier work of Doran et al.,[20] 5-butyl-1,2,3-triazole poly(2,6-dimethyl-1,4-phenylene oxide) (**2**) was synthesized according to the same initial procedure for **1**, and again, a soft, blue, insoluble material was recovered. After modifying the workup protocol as described in the Experimental section, copper-free **2** was isolated. Copper(I) bromide was then added to an NMP solution of **2** and was allowed to stir overnight under air during which time a blue–green gel formed. The gel was transferred to a glass slide, spread with a spatula, then dried on a hot plate at 70 $^{o}$C to yield the familiar soft, blue

insoluble material. Similarly, an NMP solution of **2** with no added copper salt was pipetted onto a glass slide, dried on a hot plate, and then both were examined by FTIR, optical microscopy, and AFM. Shown in Figure A1 is the FTIR of **2** in the absence (black curve) and presence (red curve) of CuBr. Note that the feature at 1720 $cm^{-1}$ for **2** is no longer observed and that there is a decrease in the intensity of the peak at1259 $cm^{-1}$

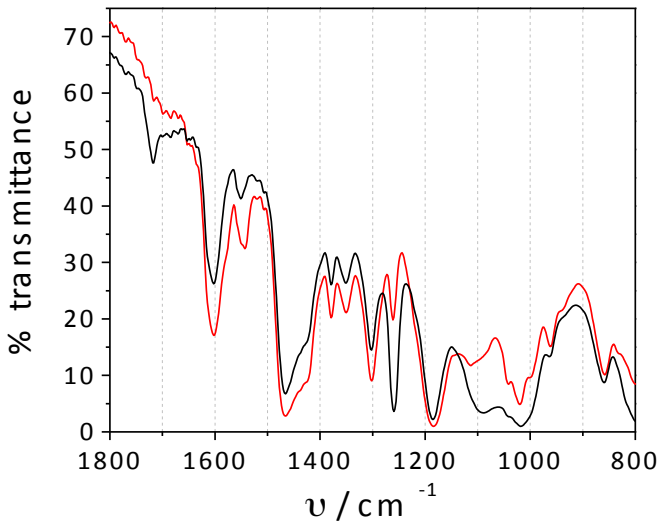


**Figure A1.** FTIR spectrum of polymer **2** in the absence (black curve) and presence (red curve) of CuBr from 800–1800 $cm^{-1}$.

when copper ions are present. Further, as seen by the optical microscope images in Figure A2, there are striking differences in morphology of **2** when Cu ions are present. While there is evidence of trapped CuBr in Figure A2 panel (b), the images indicate that these are, in fact, two different materials. Further evidence of this can be observed in the AFM images in Figure A3. These experiments support the conclusions drawn from the optical microscope images, namely that copper salts are trapped in the polymer matrix, but the difference in polymer morphology indicates that these are two different materials.

Triazoles are known to bind both Cu(I) and Cu(II) ions,[21] and a common feature of the proposed mono- and bi-metallic catalytic cycles for the CuAAC reaction is the

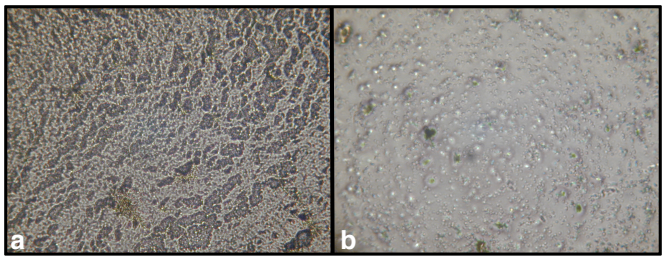


**Figure A2.** Optical microscope images of **2** in the (a) absence and (b) presence of CuBr.

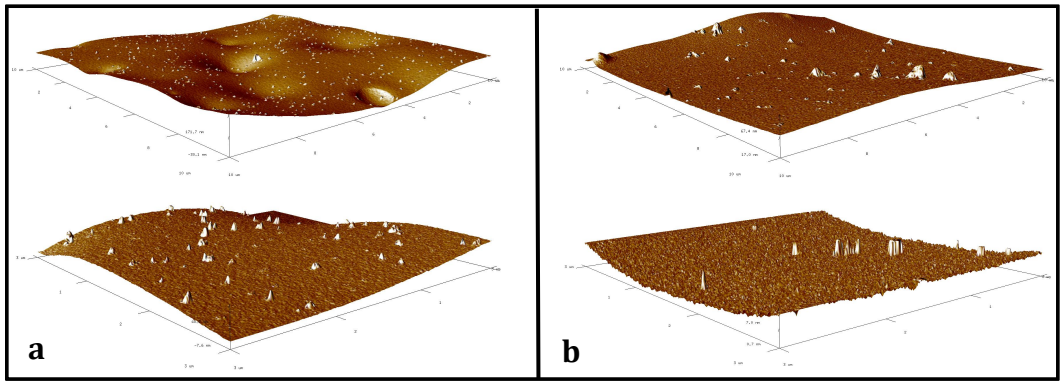


**Figure A3.** Atomic force microscope images of **2** in the (a) absence and (b) presence of CuBr. Top images are 10 μm × 10 μm, bottom images are 3 μm × 3 μm.

existence of a Cu–$C_{triazole}$ bond that is cleaved by protonation in the final step to regenerate the copper catalyst and free the triazole.[22] Though the presence of Cu(I) species cannot be ruled out, the blue color of the recovered material indicates the presence of Cu(II). With this in mind, 4-butyl-1-(phenylmethyl)-1*H*-1,2,3-triazole (**3**) was synthesized as a surrogate for a monomer unit of **1**. Subsequently, 4-butyl-1-(phenylmethyl)-1*H*-1,2,3-triazolyl-copper(II)-acetate (**4**) was synthesized and the crystal structure is shown Figure A4. Although the paddle-wheel structure shown in Figure A4 is unlikely in the functionalized PPO due to the absence of acetate ions, the structure shows that the triazole nitrogen of **3** is coordinated to a Cu(II) ion. Additional evidence

of Cu(II) coordination is seen in the $^{1}$H NMR of **3** in the absence and presence of copper(II) bromide (Figure A5). In the presence of Cu(II) ions the $^{1}$H NMR peaks of **3**

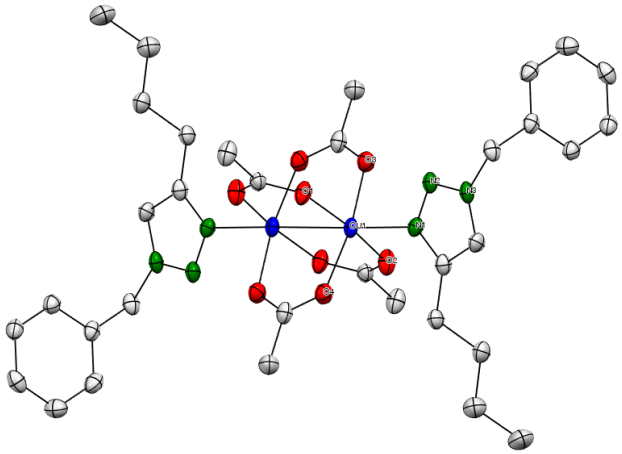

**Figure A4.** Solid-state structure of **4** with hydrogen atoms removed for clarity.

are broadened, and there is a substantial downfield shift in the triazole hydrogen signal. Similar to the FTIR spectra of **2** in the absence and presence of Cu ions, comparison of the FTIR spectra of **3** and **4** (Figure A6) shows that the feature at 1706 cm$^{-1}$ of **3** (black curve) is absent when the triazole is bound to copper in **4** (red curve).

To assign the modes responsible for the features at 1706/1720 and 1259 cm$^{-1}$, density functional theory calculations at the B3LYP/6-311++G** level of theory were performed. Using the work of Aziz et al. as a guide,[17] the computed spectra were

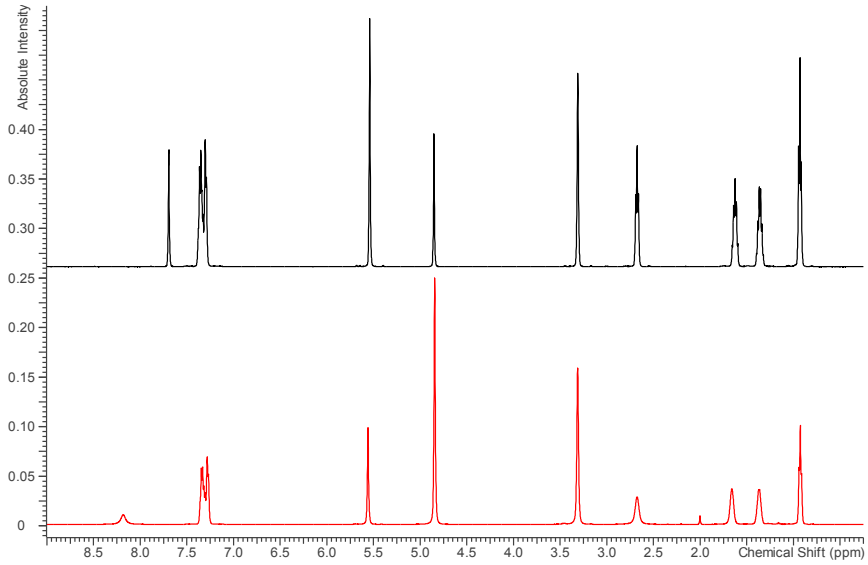


**Figure a5**. $^{1}$H NMR of **3** in the absence (top, black curve) and presence (bottom, red curve) of copper(II) bromide.

multiplied by a scaling factor of 0.975 for a more accurate comparison to their experimental counterparts. Acetate ions were replaced with chloride ions because their presence in the calculations would be an impediment to observing the effect of copper on the triazole fragment in the polymer. Based upon the current work as well as the previously reported spectrum of 1H-1,2,3-triazole,[23] the mode 1259 $cm^{-1}$ is likely a ring-based N–N stretching mode, which would undoubtedly be impacted by the presence of a copper ion bound to a ring nitrogen. Our calculations also indicate that there is a significant contribution from C–H wagging on the alkyl and benzyl fragments. The mode at 1706/1720 $cm^{-1}$ is more difficult to assign, and although similar peaks are observed in the experimental spectra of a variety of triazoles,[24] there is no discussion as to the source of this spectral feature. Since there are no peaks between 1653 and 3012 $cm^{-1}$ in the computed spectra, it is possible that the peak at 1720 $cm^{-1}$ is either a combination band or an overtone. Despite not being able to rigorously make this

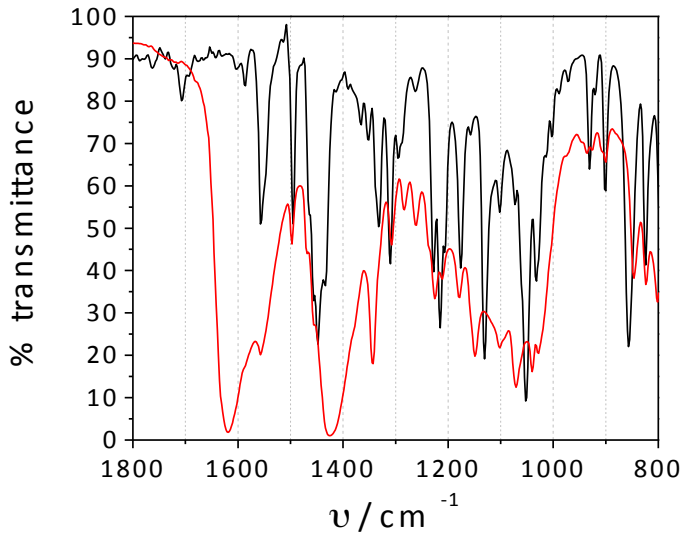


**Figure A6.** FTIR spectra of **3** (black curve) and **4** (red curve)

assignment, we are confident that this peak is due to a triazole mode or combination of modes, and that it is sensitive to the presence of a Cu–N bond.

*3.3. Electrolyte Effects*

Cyclic voltammograms (CVs) of glassy carbon electrodes coated with films of **1** in 4:1 NMP:H2O–0.1 M $NaNO_3$ electrolyte are shown in Figure A7. As the scan rate ($v$) was increased from 5 to 100 mV $s^{-1}$ a concomitant increase in peak current was observed that scaled with the square root of the scan rate ($v^{1/2}$). Figure A8a is a plot of

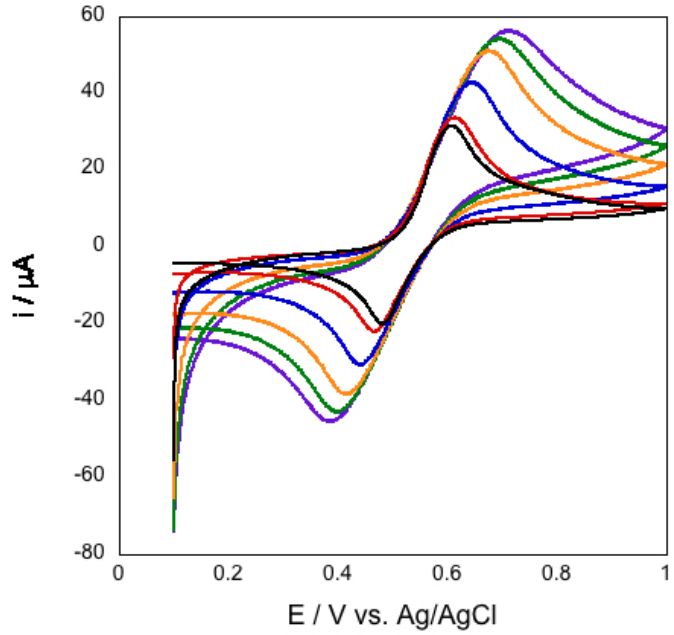


**Figure A7.** Cyclic voltammograms recorded with a glassy carbon disk electrode with films of **1** at 5 mV $s^{-1}$ (black), 10 mV $s^{-1}$ (red), 25 mV $s^{-1}$ (blue), 50 mV $s^{-1}$ (orange), 75 mV $s^{-1}$ (green), and 100 mV $s^{-1}$ (violet) in oxygen-free 4:1 NMP:$H_2O$–0.1 M $NaNO_3$.

$i_{pa}$, vs. $v$ and of $i_{pa}$ vs. $v^{1/2}$, with the values and the best fit line for the latter shown in blue. The $R^2$ value for this line was 0.97, while the $R^2$ value for $i_{pa}$ vs. ν was 0.89 (not shown), indicating that the oxidation of **1** is a diffusion controlled process in accordance with the Randles–Sevcik equation.[25] Similar results were obtained for 4:1 NMP:$H_2O$ containing 0.1 M $N(C_4H_9)_4ClO_4$, 0.1 M $NH_4PF_6$, and 0.1 M $LiN(SO_2CF_3)_2$ (Figures A8b–d), respectively. Figure A9 shows CVs of films of **1** on glassy carbon electrodes at

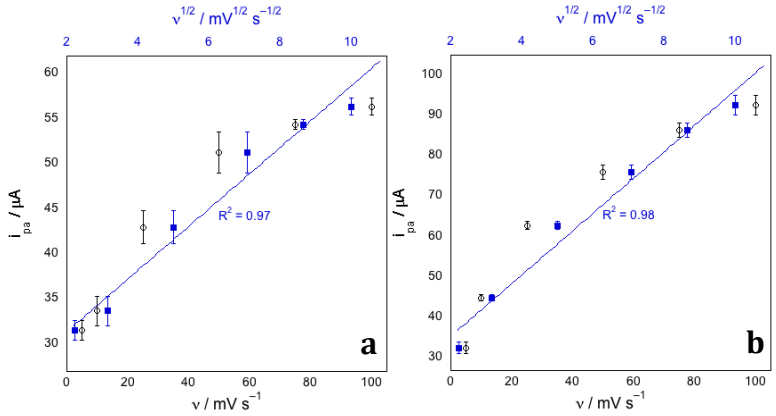

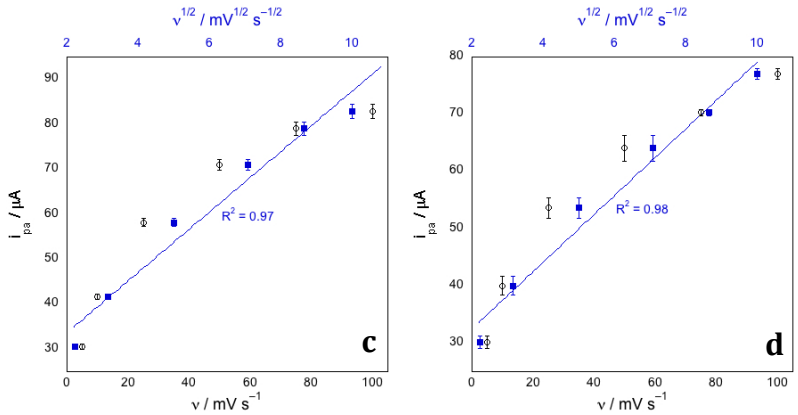


**Figure A8.** Dependence of $i_{pa}$ on the scan rate (O) and the square root of the scan rate (■) in cyclic voltammetry experiments of glassy carbon disk electrodes with films of **1** from 5 mV $s^{-1}$ to 100 mV $s^{-1}$ in oxygen-free 4:1 NMP:$H_2O$ with (a) 0.1 M $NaNO_3$ (b) 0.1 M $N(C_4H_9)_4ClO_4$ (c) 0.1 M $NH_4PF_6$ and (d) 0.1 M $LiN(SO_2CF_3)_2$ as the electrolyte (Pt counter electrode; Ag/AgCl reference electrode).

25 mV $s^{-1}$ in these same electrolytes, and the relevant data are summarized in Table A1. In each of these electrolytes there are distinct oxidation and reduction peaks with mean potentials ($\bar{E}_p$) between 0.541–0.579 V vs. Ag/AgCl, which falls in the range of reported redox potentials for ferrocene-containing polymers.[26] Furthermore, the peaks are quite broad, indicating that the ferrocene moieties are in a variety of microenvironments, each of which gives rise to slightly different oxidation and reduction potentials.[26d, 27]

Of particular applicability to anion sensing applications is the observation that the peak anodic potential ($E_{pa}$) of **1** is sensitive to the identity of the electrolyte. Figure

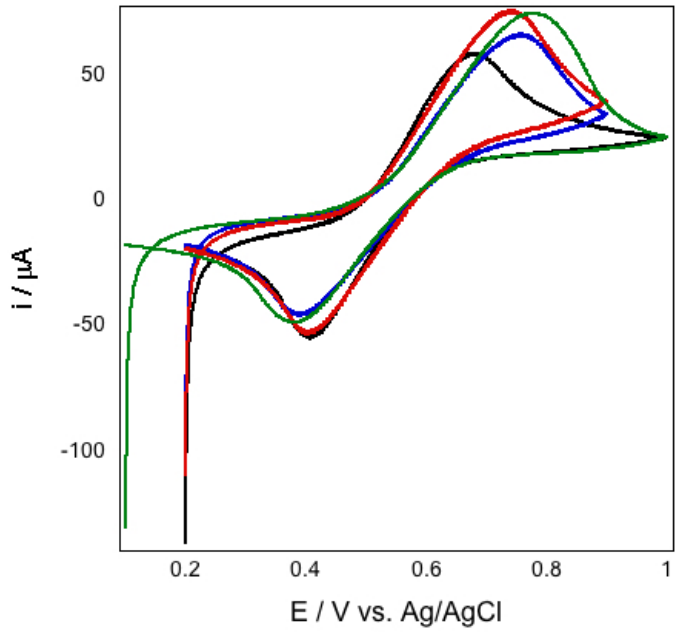


**Figure 9.** Cyclic voltammograms recorded with a glassy carbon disk electrode with films of **1** at 25 mV $s^{-1}$ in oxygen-free 4:1 NMP:$H_2O$ 0.1 M $NaNO_3$ (black), 0.1 M $N(C_4H_9)_4ClO_4$ (red), 0.1 M $NH_4PF_6$ (blue), and 0.1 M $LiN(SO_2CF_3)_2$ (green).

**Table A1.**

| Electrolyte | $E_{pa}$ [a] | $i_{pa}$ [b] | $E_{pc}$ [c] | $i_{pc}$ [d] | $\Delta E_p$ [e] | $\bar{E}_p$ [f] |
|---|---|---|---|---|---|---|
| $NaNO_3$ | 0.676 ± 0.001 | 59 ± 3 | 0.406 ± 0.001 | –54 ± 4 | 0.270 | 0.541 |
| $N(C_4H_9)_4ClO_4$ | 0.742 ± 0.002 | 76 ± 9 | 0.405 ± 0.010 | –53 ± 9 | 0.337 | 0.573 |
| $NH_4PF_6$ | 0.755 ± 0.014 | 67 ± 9 | 0.392 ± 0.010 | –45 ± 6 | 0.363 | 0.574 |
| $LiN(SO_2CF_3)_2$ | 0.776 ± 0.006 | 75 ± 2 | 0.382 ± 0.009 | –48 ± 1 | 0.394 | 0.579 |

[a] Anodic peak potential in V vs. Ag/AgCl
[b] Anodic peak current in µA
[c] Cathodic peak potential in V vs. Ag/AgCl
[d] Cathodic peak current in µA
[e] Peak-to-peak separation in V
[f] Mean peak-to-peak potential vs. Ag/AgCl

A9 shows that the $E_{pa}$ shifts to more positive values when the electrolyte is changed from $NaNO_3$ < $N(C_4H_9)_4ClO_4$ ≈ $NH_4PF_6$ < $LiN(SO_2CF_3)_2$. Because this ordering follows neither the Hofmeister series,[28] which orders anions by their hydrophobicity, nor the previously reported trends where the ferrocenium$^+$anion$^-$ formation constant is thought to be responsible for the shift in $E_{pa}$,[7-10, 29] we hypothesize that the size of the

electrolyte anion is the factor that is most responsible for the observed shift in $E_{pa}$. Table A2 summarizes both the $E_{pa}$ values and the reported anionic radii and volumes for the supporting electrolytes used in this study,[30] and Figure A10 is a plot of $E_{pa}$ vs. the anion radii and volumes. It has been previously shown that PPO films cast from organic

**Table A2.**

| Electrolyte | $E_{pa}$ | r (pm)[a] | V ($10^7$ pm$^3$)[a] | $\Delta G_{hyd,calc}$[b] | $\Delta G_{hyd,exp}$[c] |
|---|---|---|---|---|---|
| $NaNO_3$ | 0.676 ± 0.001 | 179 ± 19 | 64 ± 11 | -300 | -300 |
| $N(C_4H_9)_4ClO_4$ | 0.742 ± 0.002 | 225 ± 19 | 82 ± 13 | -252 | -205 |
| $NH_4PF_6$ | 0.755 ± 0.014 | 242 ± 19 | 109 ± 8 | -237 | – |
| $LiN(SO_2CF_3)_2$ | 0.776 ± 0.006 | 325 | 146 | -184 | – |

[a] Anionic radii and volumes from Ref. 23
[b] $\Delta G_{hyd,calc}$ was found using the method detailed by Marcus in Ref. 31
[c] $\Delta G_{hyd,exp}$ from Ref. 31

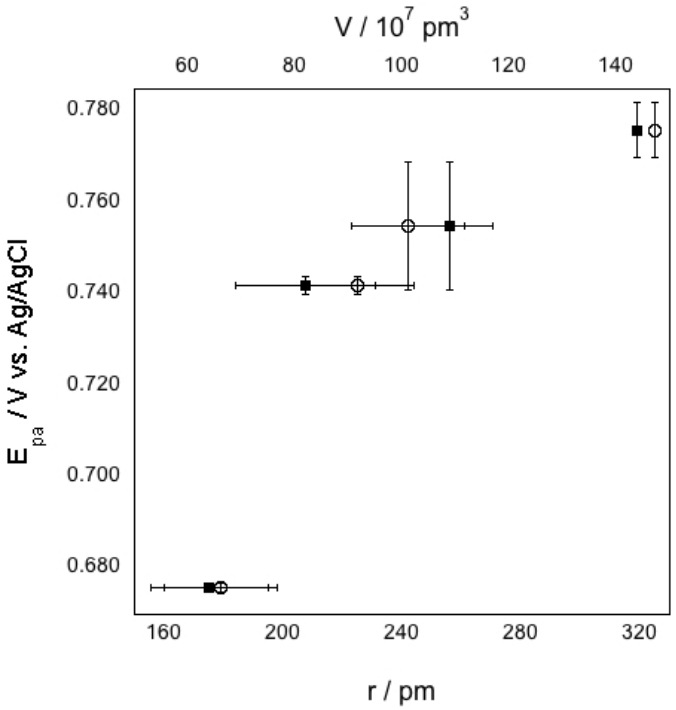


**Figure A10.** $E_{pa}$ (V vs. Ag/AgCl) vs. anionic radii (O, pm) and volumes (■, $10^7$ pm$^3$). Data in Table A2.

solvents form porous three-dimensional networks with molecular-sized cavities between the rigid polyether chains.[31] Along this line, the data presented in Table A2 and Figure

A10 suggest that the size and the structure of the free volume elements within the polymer must swell and/or rearrange to accommodate the larger anions. Solvent swelling of polymer films has been shown to influence their electrochemical behavior,[32] which underscores the necessity for a 4:1 NMP:$H_2O$ solvent mixture. The polymer must be swollen with NMP for the ionic transport processes to be facile; however, in electrolyte where NMP is the only solvent, the polymer films rapidly desorb from the electrode.

Cyclic voltammograms of **1** when the solvent is 2:1, 1:1, and 0:1 NMP:H2O—0.1 M NaNO3 are shown in Figure A11. The positive shift of $E_{pa}$ and the decrease in $i_{pa}$ indicate that PPO–Fc is very hydrophobic, and that in addition to swelling there may a significant contribution to the increase in $E_{pa}$ from the free energy of dehydration. That is, in order for the anions to enter the hydrophobic polymer it is first necessary to shed their hydration shell either in whole or in part, or the free energy of hydration must be

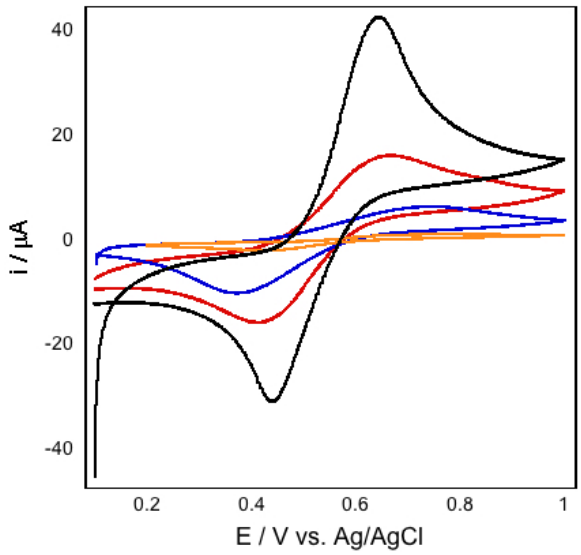


**Figure A11.** Cyclic voltammograms recorded with a glassy carbon disk electrode with films of **1** at 25 mV $s^{-1}$ in oxygen-free 0.1 M $NaNO_3$ 4:1 NMP:$H_2O$ (black), 2:1 NMP:$H_2O$ (red), 1:1 NMP:$H_2O$ (blue), 0:1 NMP:$H_2O$ (orange). Pt counter electrode, Ag/AgCl reference electrode.

overcome by electromigration to effectively pull the anion into the polymer network. This would be especially true in the case of $NO_3^-$, which has the largest free energy of hydration ($\Delta G_{hyd}$).[33] However, since the $\Delta G_{hyd}$ of $ClO_4^-$, $PF_6^-$, and $N(SO_2CF_3)_2^-$ are all less than that of the $\Delta G_{hyd}$ for $NO_3^-$ (Table A2), it is clear that this contribution to the increase in $E_{pa}$ is secondary to the size of the anion in the electrolyte of choice.

*3.4. Electrochromism*

Shown in Figure A12 are images of ITO electrodes coated with **1** pre- and post-electrolysis at 1.0 V vs. Ag/AgCl in 4:1 NMP:H2O–0.1 M $NaNO_3$. Note the blue–green veins in the oxidized polymer showing that there are distinct regions of functionalized and non-functionalized polymer that appear to self-segregate when cast from methylene chloride solution. Previous studies of PPO have shown that the polymer structure can be controlled by casting the polymer from different organic solvents as well as by controlling the relative humidity in the casting environment.[31b, 31c] We are presently seeking to adjust the casting procedure to obtain a more homogeneous polymer.

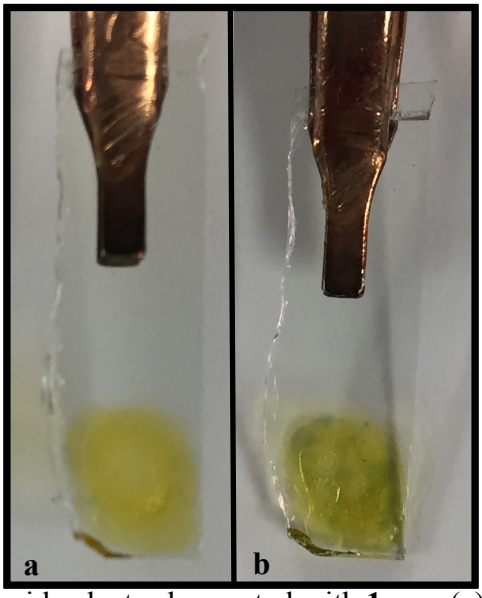


**Figure A12.** Indium tin oxide electrodes coated with **1** pre- (a) and post-electrolysis (b) at +1.0 V vs. Ag/AgCl in 4:1 NMP:$H_2O$–0.1 M $NaNO_3$. Pt counter electrode.

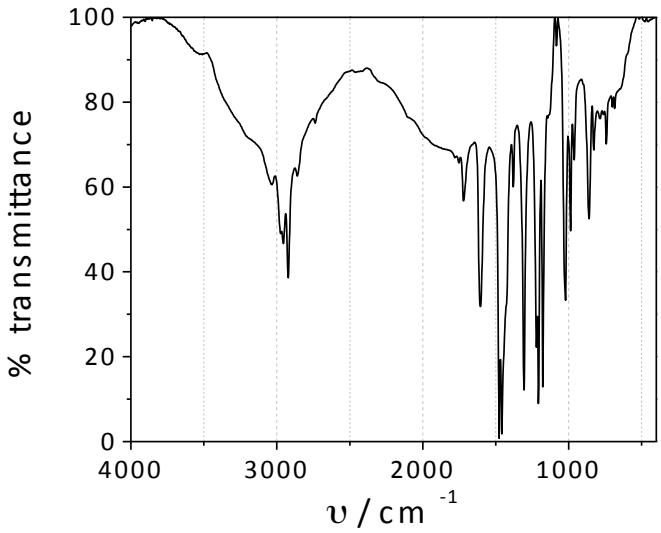


**Figure A13.** FTIR of PPO–Br

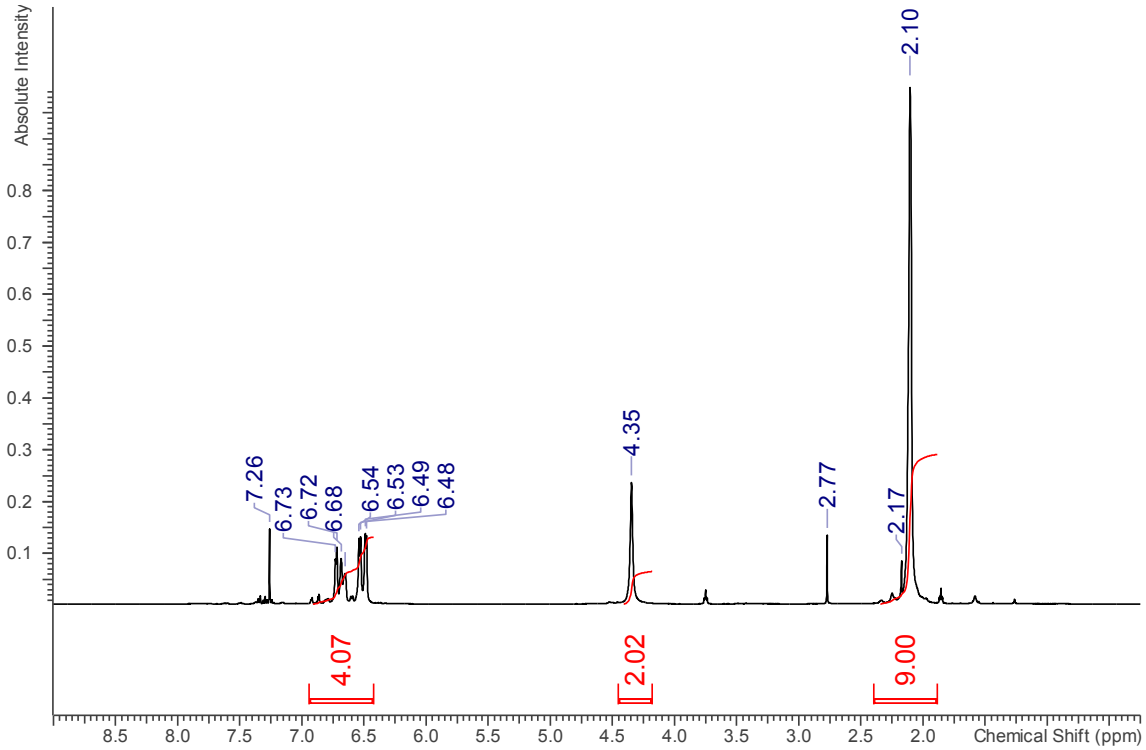

**Figure A14.** $^{1}H$ NMR of PPO–Br

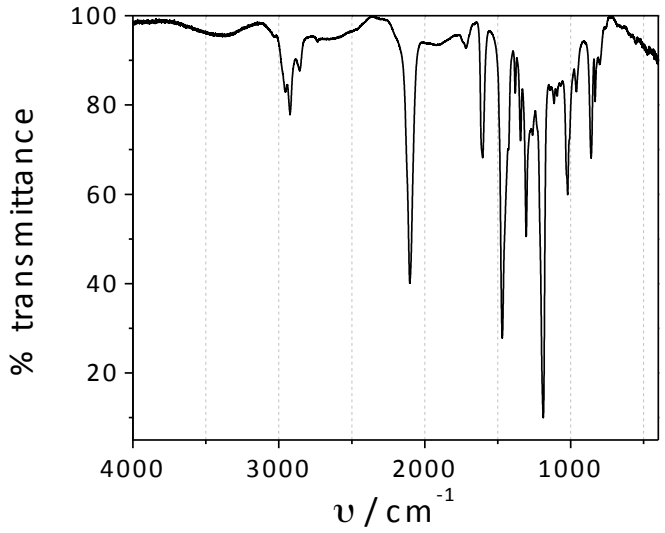


**Figure A15.** FTIR of PPO–$N_3$

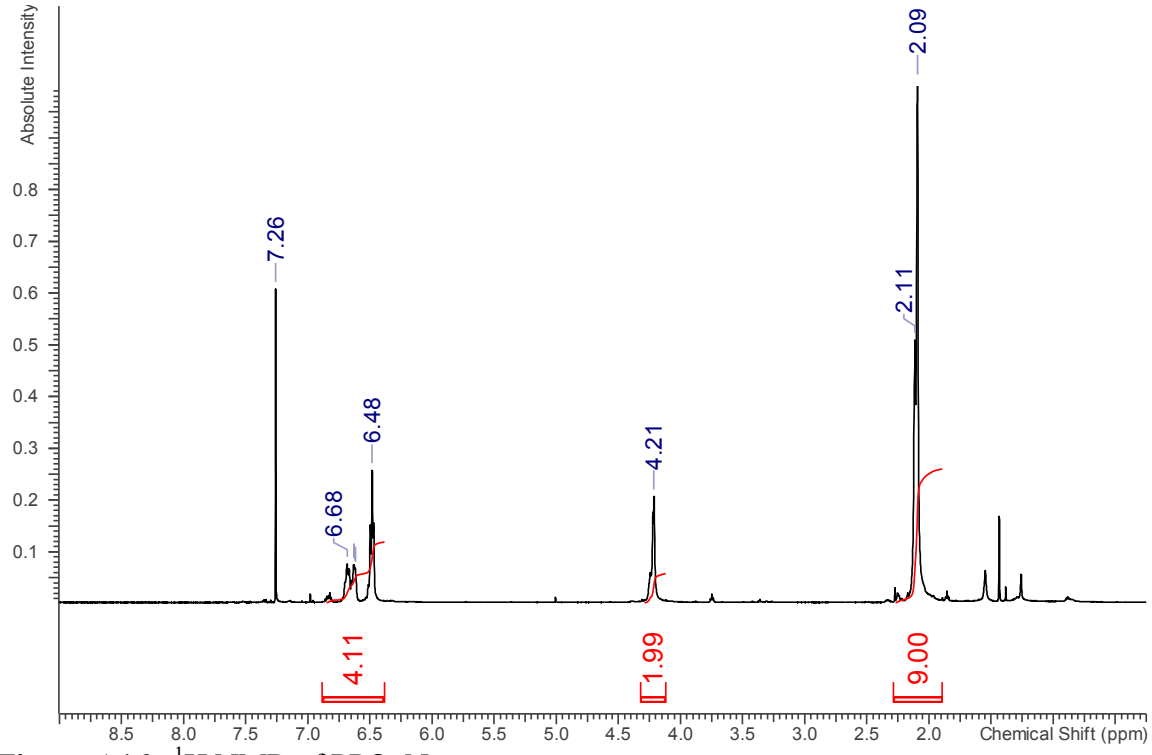


**Figure A16.** $^{1}H$ NMR of PPO–$N_3$

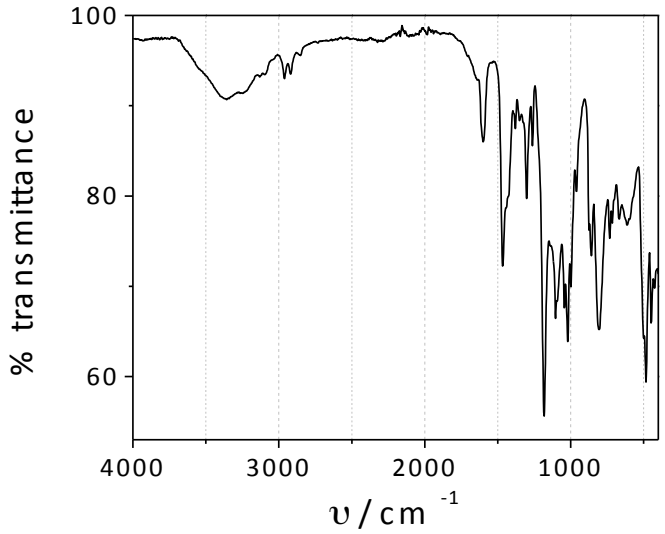


**Figure A17.** FTIR of **1**

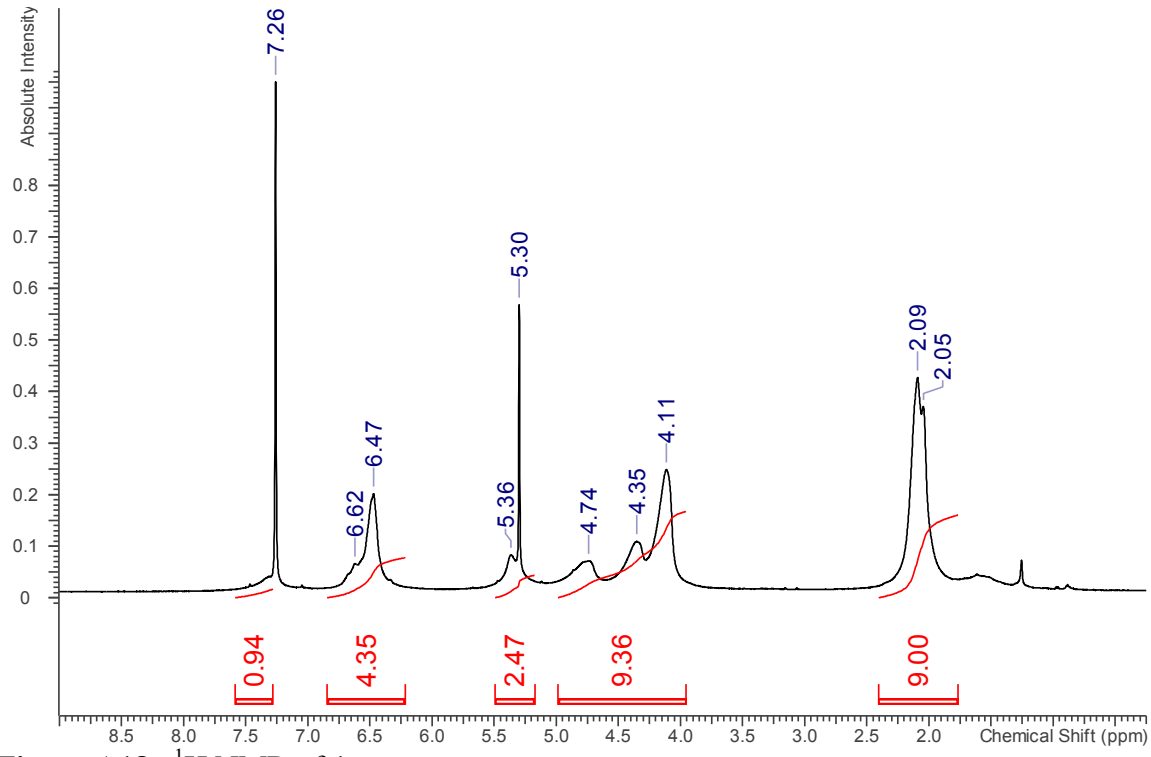


**Figure A18.** $^{1}$H NMR of **1**

## APPENDIX A REFERENCES


1. (a) Song, H. K.; Palmore, G. T. R., Redox-Active Polypyrrole: Toward Polymer-Based Batteries. *Advanced Materials* **2006,** *18* (13), 1764-1768; (b) Tamura, K.; Akutagawa, N.; Satoh, M.; Wada, J.; Masuda, T., Charge/Discharge Properties of Organometallic Batteries Fabricated with Ferrocene-Containing Polymers. *Macromolecular Rapid Communications* **2008,** *29* (24), 1944-1949; (c) Montoto, E. C.; Nagarjuna, G.; Moore, J. S.; Rodríguez-López, J., Redox Active Polymers for Non-Aqueous Redox Flow Batteries: Validation of the Size-Exclusion Approach. *Journal of The Electrochemical Society* **2017,** *164* (7), A1688-A1694.

2. (a) Lange, U.; Roznyatovskaya, N. V.; Mirsky, V. M., Conducting polymers in chemical sensors and arrays. *Analytica chimica acta* **2008,** *614* (1), 1-26; (b) Joshi, P. P.; Merchant, S. A.; Wang, Y.; Schmidtke, D. W., *Anal. Chem.* **2005,** *77*, 3183-3188; (c) Gallaway, J. W.; Barton, S. A. C., *J. Am. Chem. Soc.* **2008,** *130*, 8527-8536; (d) Tsiafoulis, C. G.; Florou, A. B.; Trikalitis, P. N.; Bakas, T.; Prodromidis, M. I., Electrochemical study of ferrocene intercalated vanadium pentoxide xerogel/polyvinyl alcohol composite films: Application in the development of amperometric biosensors. *Electrochemistry Communications* **2005,** *7* (7), 781-788.

3. (a) Cyr, P. W.; Tzolov, M.; Manners, I.; Sargent, E. H., *Macromol. Chem. Phys.* **2003,** *204*, 915-921; (b) Holcombe, T. W.; Woo, C. H.; Kavulak, D. F. J.; Thompson, B. C.; Fréchet, J. M. J., *J. Am. Chem. Soc.* **2009,** *131*, 14160-14161; (c) Li, G.; Zhu, R.; Yang, Y., *Nat. Photonics* **2012,** *6*, 155-161.

4. (a) Zeng, Q.; McNally, A.; Keyes, T. E.; Forster, R. J., Three colour electrochromic metallopolymer based on a ruthenium phenolate complex bound to poly(4-vinyl)pyridine. *Electrochemistry Communications* **2008,** *10* (3), 466-470; (b) Bao, X.; Zhao, Q.; Wang, H.; Liu, K.; Qiu, D., Metallopolymer electrochromic film prepared by oxidative electropolymerization of a Fe(II) complex with arylamine functionalized terpyridine ligand. *Inorganic Chemistry Communications* **2013,** *38*, 88-91.

5. (a) Zhang, J.; Yan, J.; Pageni, P.; Yan, Y.; Wirth, A.; Chen, Y. P.; Qiao, Y.; Wang, Q.; Decho, A. W.; Tang, C., Anion-Responsive Metallopolymer Hydrogels for Healthcare Applications. *Scientific reports* **2015,** *5*, 11914; (b) Zhang, K.; Feng, X.; Sui, X.; Hempenius, M. A.; Vancso, G. J., Breathing pores on command: redox-responsive spongy membranes from poly(ferrocenylsilane)s. *Angewandte Chemie* **2014,** *53* (50), 13789-93; (c) Zhang, K. Y.; Liu, S.; Zhao, Q.; Huang, W., Stimuli–responsive metallopolymers. *Coordination Chemistry Reviews* **2016,** *319*, 180-195.

6. (a) Valincius, G.; Niaura, G.; Kazakevičienė, B.; Talaikytė, Z.; Kažemėkaitė, M.; Butkus, E.; Razumas, V., *Langmuir* **2004,** *20* (6631-6638); (b) Tong, R.; Zhao, Y.; Wang, L.; Yu, H.; Ren, F.; Saleem, M.; Amer, W. A., *J. Organomet. Chem.* **2014,** *755*, 16-32; (c) Amer, W. A.; Wang, L.; Amin, A. M.; Ma, L.; Yu, H., *J. Inorg. Organomet. Polym.* **2010,** *20*, 605-615; (d) Guven, N.; Camurlu, P.; Desde, M.; Yucel, B., Post Polymerization Functionalization of a Soluble Poly(2,5-dithienylpyrrole) Derivative via Click Chemistry. *Journal of The Electrochemical Society* **2017,** *164* (7), H430-H436; (e) Calvo-Muñoz, M. L.; Bile, B. E.-A.; Billon, M.; Bidan, G., Electrochemical study by a redox probe of the chemical post-functionalization of N-substituted polypyrrole films: Application of a new approach to immobilization of biotinylated molecules. *Journal of Electroanalytical Chemistry* **2005,** *578* (2), 301-313; (f) Camurlu, P.; Guven, N.; Bicil, Z., Ferrocene clicked polypyrrole derivatives: effect of spacer group on electrochemical properties and post-polymerization functionalization. *Designed Monomers and Polymers* **2016,** *19* (3), 212-221; (g) Li, J. H.; Wang, L.; Yu, H. J.; Tan, Q. H.; Deng, L. B.; Huo, J., *Designed Monomers and Polymers* **2007,** *10*, 193-205; (h) Pietschnig, R., Polymers with pendant ferrocenes. *Chemical Society reviews* **2016,** *45* (19), 5216-31; (i) Hudson, R. D. A., *J. Organomet. Chem.* **2001,** *637-639*, 47-69; (j) Gallei, M., The Renaissance of Side-Chain Ferrocene-Containing Polymers: Scope and Limitations of Vinylferrocene and Ferrocenyl Methacrylates. *Macromolecular Chemistry and Physics* **2014,** *215* (8), 699-704.

7. Inzelt, G.; Szabo, L., The Effect of the Nature and the Concentration of Couter Ions on the Electrochemistry of Poly(VinylFerrocene) Polymer Film Electrodes. *Electrochimica Acta* **1986,** *31* (11), 1381-1387.

8. Rowe, G. K.; Creager, S. E., Redox and Ion-Pairing Thermodynamics in Self-Assembled Monolayers. *Langmuir* **1991,** *7*, 2307-2312.

9. Uosaki, K.; SSato, Y.; Kita, H., Electrochemical Characteristics of a Gold Electrode Modified with a Self-Assembled Monolayer of Ferrocenylalkanethiols. *Langmuir* **1991,** *7*, 1510-1514.

10. Kondo, T.; Okamura, M.; Uosaki, K., Anion effect on the electrochemical characteristics of a gold electrode modified with a self-assembled monolayer of ferrocenylhexanethiol in aqueous and dichloromethane solutions. *J. Organomet. Chem.* **2001,** *637-639*, 841-844.

11. (a) Gale, P. A.; Hursthouse, M. B.; Light, M. E.; Sessler, J. L.; Warriner, C. N.; Zimmerman, R. S., *Tetrahedron Lett.* **2001,** *42*, 6759-6762; (b) Tomapatanaget, B.; Tuntulani, T., *Tetrahedron Lett.* **2001,** *42*, 8105-8109; (c) Stone, D. L.; Smith, D. K., *Polyhedron* **2003,** *22*, 763-768; (d) Molina, P.; Zapata, F.; Caballero, A., Anion Recognition Strategies Based on Combined Noncovalent Interactions. *Chemical reviews* **2017,** *117* (15), 9907-9972; (e) Scherer, M.; Sessler, J. L.; Gebauer, A.; Lynch, V., *Chem. Commun.* **1998**, 85-86; (f) Boulas, P. L.; Gómez-Kaifer, M.; LEchegoyen, L., *Angew. Chem. Int. Ed.* **1998,** *37*, 216-247; (g) Beer, P. D., *Acc. Chem. Res.* **1998,** *31*, 71-80; (h) Beer, P. D., Sykes, A. G., Ed. Academic Press, Inc.: San Diego, 1992; Vol. 39, pp 79-157; (i) Beer, P. D.; Gale, P. A., *Angew. Chem. Int. Ed.* **2001,** *40*, 486-516.

12. Armarego, W. L. F.; Chai, C. L. L., *Purificaiton of Laboratory Chemicals*. Fifth ed.; Butterworth-Heinemann: New York, 2005.

13. Fulmer, G. R.; Miller, A. J. M.; Sherden, N. H.; Gottlieb, H. E.; Nudelman, A.; Stoltz, B. M.; Bercaw, J. E.; Goldberg, K. I., NMR Chemical Shifts of Trace Impurities: Common Laboratory Solvents, Organics, and Gases in Deuterated Solvents Relevant to the Organometallic Chemist. *Organometallics* **2010,** *29* (9), 2176-2179.

14. Becke, A. D., *J. Chem. Phys.* **1993,** *98*, 5848-5652.

15. Lee, C. T.; Yang, W. T.; Parr, R. G., *Phys. Rev. B* **1988,** *37*, 785-789.

16. Frisch, M. J.; Trucks, G. W.; Schlegel, H. B.; Scuseria, G. E.; Robb, M. A.; Cheeseman, J. R.; Scalmani, G.; Barone, V.; Mennucci, B.; Petersson, G. A.; Nakatsuji, H.; Caricato, M.; Li, X.; Hratchian, H. P.; Izmaylov, A. F.; Bloino, J.; Zheng, G.; Sonnenberg, J. L.; Hada, M.; Ehara, M.; Toyota, K.; Fukuda, R.; Hasegawa, J.; Ishida, M.; Nakajima, T.; Honda, Y.; Kitao, O.; Nakai, H.; Vreven, T.; J. A. Montgomery, J.; Peralta, J. E.; Ogliaro, F.; Bearpark, M.; Heyd, J. J.; Brothers, E.; Kudin, K. N.; Staroverov, V. N.; Kobayashi, R.; Normand, J.; Raghavachari, K.; Rendell, A.; Burant, J. C.; Iyengar, S. S.; Tomasi, J.; Cossi, M.; Rega, N.; Millam, J. M.; Klene, M.; Knox, J. E.; Cross, J. B.; Bakken, V.; Adamo, C.; Jaramillo, J.; Gomperts, R.; Stratmann, R. E.; Yazyev, O.; Austin, A. J.; Cammi, R.; Pomelli, C.; Ochterski, J. W.; Martin, R. L.; Morokuma, K.; Zakrzewski, V. G.; Voth, G. A.; Salvador, P.; Dannenberg, J. J.;

Dapprich, S.; Daniels, A. D.; Farkas, O.; Foresma, J. B.; Ortiz, J. V.; Cioslowski, J.; Fox, D. J. *Gaussian 09, Revision A.02*, Wallingford, CT, 2009.

17. Aziz, S. G.; Elroby, S. A.; Alyoubi, A.; Osman, O. I.; Hilal, R., *J. Mol. Model* **2014,** *20*, 2078.

18. (a) Chang, H. I.; Yang, M. S.; Liang, M., *Reactive & Functional Polymers* **2010,** *70*, 944-950; (b) Li, N.; Guiver, M. D.; Binder, W. H., *ChemSusChem.* **2013,** *6*, 1376-1383.

19. Scates, B. A.; Lashbrook, B. L.; Chastain, B. C.; Tominaga, K.; Elliott, B. T.; Theising, N. J., *Bioorganic Med. Chem.* **2008,** *16*, 10295-10300.

20. Doran, S.; Yilmaz, G.; Yagci, Y., *Macromolecules* **2015,** *48*, 7446-7452.

21. (a) Cheng, R.-R.; Wu, Z.-L.; Hou, Y.-L.; Dong, J.; Cui, J.-Z.; Zhao, B., Three Cu(II) coordination polymers with novel bi-triazole ligand: Synthesis, structure and EPR properties. *Inorganic Chemistry Communications* **2015,** *51*, 95-98; (b) Cohen, A.; Yang, Y.; Yan, Q.-L.; Shlomovich, A.; Petrutik, N.; Burstein, L.; Pang, S.-P.; Gozin, M., Highly Thermostable and Insensitive Energetic Hybrid Coordination Polymers Based on Graphene Oxide–Cu(II) Complex. *Chemistry of Materials* **2016,** *28* (17), 6118-6126; (c) Gómez, V.; Benet-Buchholz, J.; Martin, E.; Galán-Mascarós, J. R., Architectures in Copper Metal-Organic Frameworks from 4-Substituted Anionic 1,2,4-Triazoles. *European Journal of Inorganic Chemistry* **2014,** *2014* (19), 3125-3132; (d) Guo, H.-M.; He, X.; Liu, J.-J.; Han, J.; Li, M.-X., Syntheses, structures and properties of five copper coordination polymers constructed by the triazole ligand. *Polyhedron* **2011,** *30* (12), 1982-1989; (e) Liu, L.; Wu, D.; Zhao, B.; Han, X.; Wu, J.; Hou, H.; Fan, Y., Copper(II) coordination polymers: tunable structures and a different activation effect of hydrogen peroxide for the degradation of methyl orange under visible light irradiation. *Dalton transactions* **2015,** *44* (3), 1406-11; (f) Liu, S.; Gao, H.-L.; Cui, J.-Z., Substituent effect of R-phthalates (R = –CH 3 , –NO 2 ) on the construction of two novel 2D Cu II coordination polymers: Syntheses, crystal structures and magnetic properties. *Inorganic Chemistry Communications* **2014,** *48*, 99-102; (g) Lv, Z.-J.; Jin, P.-N.; Wang, Y.-H.; Wei, X.-B.; Yang, G., Synthesis, Structures and Luminescent Properties of 3D Copper(I) 1,2,4-Triazolates Containing Cubic Cu4X4 Clusters (X = Cl, Br). *Journal of Cluster Science* **2014,** *26* (4), 1389-1401; (h) Wang, P.-N.; Yeh, C.-W.; Tsou, C.-H.; Ho, Y.-W.; Lee, H.-T.; Suen, M.-C., Structural diversity in Cu(II) and Cd(II) coordination complexes with 4-amino-1,2,4-triazole ligand. *Inorganic Chemistry Communications* **2014,** *43*, 70-74; (i) Wang, X.; Zhao, W.; Zhang, J.; Lu, Q.; Luan, J.; Liu, G.; Lin, H.; Tian, A., Three isomeric copper(II) coordination polymers based on a bis-triazole-bis-amide ligand: Assembly, structures, and luminescent properties. *Journal of Coordination Chemistry* **2013,** *66* (20), 3561-3571; (j) Yang, E. C.; Zhang, Y. Y.; Liu, Z. Y.; Zhao, X. J., Diverse self-assembly from predesigned conformationally flexible pentanuclear clusters observed in a ternary copper(II)-triazolate-sulfoisophthalate system: synthesis, structure, and magnetism. *Inorganic chemistry* **2014,** *53* (1), 327-35; (k) Yang, Y.; Yang, J.; Du, P.; Liu, Y.-Y.; Ma, J.-F., A series of coordination polymers

constructed by the semi-rigid bifunctional ligand 5-((1H-1,2,4-triazol-1-yl)methoxy) isophthalic acid: syntheses, structures and the role of solvents. *CrystEngComm* **2014,** *16* (6), 1136-1148; (l) Zaydoun, S.; Guedira, F.; Zrineh, A.; Garrigoulagrange, C.; Lorriaux-Rubbens, A.; Saidi Idrissi, M., *J. Mar. Cheim. Heterocycl.* **2006,** *5*, 12-22.

22. (a) Bock, V. D.; Hiemstra, H.; van Maarseveen, J. H., CuI-Catalyzed Alkyne-Azide "Click" Cycloadditions from a Mechanistic and Synthetic Perspective. *European Journal of Organic Chemistry* **2006,** *2006* (1), 51-68; (b) Rodionov, V. O.; Presolski, S. I.; Dı´az Dı´az, D.; Fokin, V.; Finn, M. G., *J. Am. Chem. Soc.* **2007,** *129*, 12705-12712; (c) Huisgen, R., *Angew. Chem. Int. Ed.* **1963,** *2* (565-598); (d) Meldal, M.; Tornøe, C. W., *Chem. Rev.* **2008,** *108*, 2952-3015.

23. Kim, J. D.; Ghil, L. J.; Jun, M. S.; Choi, J. K.; Chang, H. J.; Kim, Y. C.; Rhee, H. W., Nafion-Propyl-1,2,3-Triazole Composite Membrane for Fuel Cells. *Journal of the Electrochemical Society* **2014,** *161* (6), F724-F728.

24. (a) Borello, E.; Zecchina, A., *Spectrochim. Acta* **1963,** *19*, 1703-1715; (b) Hannant, J.; Hedley, J. H.; Pate, J.; Walli, A.; Farha Al-Said, S. A.; Galindo, M. A.; Connolly, B. A.; Horrocks, B. R.; Houlton, A.; Pike, A. R., Modification of DNA-templated conductive polymer nanowires via click chemistry. *Chemical communications* **2010,** *46* (32), 5870-2.

25. Bard, A. J.; Faulkner, L. R., *Electrochemical Methods Fundamentals and Applications*. Second ed.; John Wiley & Sons, Inc.: New York, 2001.

26. (a) Xue, C.; Chen, Z.; Wen.Y.; T., L. F.; J., C.; Liu, H., *Langmuir* **2005,** *21*, 7860-7865; (b) Alzharani, A.; Ault, C.; Allehyani, E.; Hance, C. S.; Westby, R. B.; Tayo, B. O.; Neef, C. J., *J. Electroanal. Chem.* **2017,** *786*, 129-134; (c) Camurlu, P.; Karagoren, N., *Reactive & Functional Polymers* **2013,** *73*, 847-853; (d) Akhoury, A.; Bromberg, L.; Hatton, T. A., *J. Phys. Chem. B* **2013,** *117*, 333-342; (e) Zu, X.; Rusling, J. F., *Langmuir* **1997,** *13*, 3693-3699; (f) Oyama, N.; Tatsuma, T.; Takahashi, K., *J. Chem. Phys.* **1993,** *97* (10504-10508); (g) Nowak, R. J.; Schultz, F. A.; Umana, M.; Lam, R.; Murray, R. W., *Anal. Chem.* **1980,** *52*, 315-321; (h) Nagel, B.; Warsinke, A.; Katterle, M., *Langmuir* **2007,** *23*, 6807-6811; (i) Datwani, S. S.; Truskett, V. N.; Rosslee, D. A.; Abbott, N. L.; Stebe, K. J., *Langmuir* **2003,** *19*, 8292-8301.

27. Tamaki, T.; Yamaguchi, T., *Ind. Eng. Chem. Res.* **2006,** *45*, 3050-3058.

28. Hofmeister, F., *Arch. Exp. Pathol. Pharmakol.* **1888,** *24*, 247-260.

29. Ju, H.; Leech, D., *J. Chem. Soc., Faraday Trans.* **1997,** *93* (7), 1371-1375.

30. (a) Ue, M., *J. Electrochem. Soc.* **1994,** *141*, 3336-3342; (b) Roobottom, H. K.; Jenkins, H. D. B.; Passmore, J.; Glasser, L., *J. Chem. Educ.* **1999,** *76*, 1570-1573; (c) Jenkins, H. D. B.; Roobottom, H. K.; Passmore, J.; Glasser, L., *Inorg. Chem.* **1999,** *38*, 3609-3620.

31. (a) Ghosal, K.; Chern, R. T., *J. Membr. Sci.* **1992,** *72*, 91-97; (b) Ilinitch, O. M.; Fenelonov, V. B.; Lapkin, A. A.; Okkel, L. G.; Terskikh, V. V.; Zamaraev, K. I., *Microporous Mesoporous Mater.* **1999,** *31*, 97-110; (c) Tian, Y.; Jiao, Q.; IDing, H.; Shi, Y.; Liu, B., *Polymer Journal* **2006,** *47*, 3866-3873; (d) Hamad, F.; Chowdhury, G.; Matsuura, T., *J. Membr. Sci.* **2001,** *191*, 71-83.

32. (a) Borjas, R.; Buttry, D. A., *J. Electroanal. Chem.* **1990,** *280*, 73-90; (b) Ostrom, G. S.; Buttry, D. A., *J. Phys. Chem.* **1995,** *99*, 15236-15240.

33. (a) Andersson, M. P.; Stipp, S. L., Predicting hydration energies for multivalent ions. *Journal of computational chemistry* **2014,** *35* (28), 2070-5; (b) Marcus, Y., *J. Chem. Soc., Faraday Trans.* **1991,** *87*, 2995-2999; (c) Marcus, Y., *Biophysical Chemistry* **1994,** *51*, 111-127.